Adhesive Joint and Composites Modeling in SIERRA

Daniel C. Hammerand, Robert S. Chambers, Arthur A. Brown, James W. Foulk,
Douglas B. Adolf and Yuki Ohashi

Sandia National Laboratories
P.O. Box 5800
Albuquerque, NM 87185-0893

Abstract

Polymers and fiber-reinforced polymer matrix composites play an important role in many Defense Program applications. Recently an advanced nonlinear viscoelastic model for polymers has been developed and incorporated into ADAGIO, Sandia's SIERRA-based quasi-static analysis code. Standard linear elastic shell and continuum models for fiber-reinforced polymer-matrix composites have also been added to ADAGIO. This report details the use of these models for advanced adhesive joint and composites simulations carried out as part of an Advanced Simulation and Computing Advanced Deployment (ASC AD) project. More specifically, the thermo-mechanical response of an adhesive joint when loaded during repeated thermal cycling is simulated, the response of some composite rings under internal pressurization is calculated, and the performance of a composite container subjected to internal pressurization, thermal loading, and distributed mechanical loading is determined. Finally, general comparisons between the continuum and shell element approaches for modeling composites using ADAGIO are given.

Contents

List of Figures

List of Tables

1 Introduction

Polymers play an important role in many different Defense Program applications. They provide structural integrity, environmental damping, moisture and voltage isolation and are employed as encapsulants, adhesives and coatings in a variety of weapon components. Polymers are attractive for their low cost, ease of manufacturing, and the ability of their material properties to be tailored through the addition of fillers. However, their thermo-mechanical behavior can be extremely complex. Since polymers are viscoelastic materials, they undergo a glass transition that radically alters the perceived physical properties of the material (varying from the rubbery state above Tg to the glassy state below). Stress and volume relaxation rates are quite sensitive to temperature, and glassy materials can actually yield under loading. The richness of the material behavior makes it important to understand how these materials react to their operational environment. This understanding can aid in the design process, helping to avoid cohesive cracking within the polymer or delamination at key material interfaces.

For this ASC AD project, we are specifically interested in being able to analyze two kinds of material behavior:

1. the thermo-mechanical response of an adhesive joint when loaded during repeated thermal cycling, and

2. the performance of an anisotropic elastic (glassy) structure subjected to internal pressurization, thermal loading, and distributed mechanical loading

Item one calls for a nonlinear viscoelastic model of the adhesive to predict the stresses and strains generated during thermal cycling and loading through glass transition. The polymer constitutive model was developed in past years through collaboration between the Engineering and Materials Sciences Centers and has been implemented in the ADAGIO finite element code. The problem we will be analyzing consists of two concentric metal cylinders bonded together with an adhesive layer. The outer cylinder is shorter and serves as a stiffener that is sealed at both ends to the longer inner cylinder (case). The combined structure is then axially loaded and thermally cycled. Of particular interest is the design and loading of the end seal. This problem will

be among the first major applications to benefit from nonlinear viscoelastic modeling. Moreover, it will afford critical opportunities to evaluate computational performance in a large problem setting while also introducing the DP customer to the benefits of being able to make higher fidelity predictions.

The second item involves new material models and associated code enhancements to accommodate orthotropic/anisotropic elastic materials with thermal strains. For many years, Sandia has had to resort to commercial software (ABAQUS) in order to perform such analyses. Recent and ongoing ADAGIO code development has provided both orthotropic hex elements and anisotropic shell elements complete with thermal strains giving us new in-house capabilities to fulfill this need. A general capability for initializing material orientations has been incorporated into ADAGIO as well. The problem chosen for study is a composite structural container under pressure, thermal, and mechanical loadings. Preliminary results from a purely continuum element approach and a combined shell/continuum element approach will be given. However, to better understand the differences between shell and continuum modeling approaches, comparisons will be made first for rings under internal pressure. The importance of using true cyclic periodic boundary conditions in place of axisymmetric cyclic boundary conditions for composite structures also will be demonstrated. Moreover, general observations will be made about the differences between shell and continuum approaches for modeling composite structures.

2 Adhesively Bonded Joint

The nonlinear viscoelastic (NLVE) analysis of adhesives lends itself to staged calculations where the epoxy first undergoes solidification (curing) at elevated temperatures followed by a thermal cool-down and any subsequent structural modifications and loading. Although a theory for NLVE curing exists, the requisite material characterization and validation are not yet complete and the SIERRA infrastructure is still under construction (e.g., material model library and material interface wrapper for incompressibility). Hence, chemistry (e.g., cure shrinkage effects) is neglected in all subsequent computations.

2.1 Problem Definition

The proposed problem consists of two concentric cylinders that are adhesively bonded together and sealed at the ends. A schematic of the geometry is shown in Figure 1. During manufacturing, the outer cylinder is glued to the inner cylinder at an elevated temperature. The joined cylinders then are cooled to room temperature where the end of the adhesive joint is sealed metallically. Following this, the inner cylinder is axially loaded by 18000 lbs (80067 N) producing a nominal end stress of about 8127 psi (56 MPa). The entire assembly is then thermally cycled between 70 °C and 55 °C at 3 °C/min. During the temperature ramps the axial loading is linearly increased to 30000 lbs at the upper temperature and decreased to 5000 lbs at 55 °C. At 70 °C, the temperature is held constant for 2 hours.

For viscoelastic materials, the analysis must begin from a well-defined reference (equilibrium) state. In a curing epoxy, this naturally would correspond to the elevated cure temperature where the solidification reaction occurs as the material transitions from a liquid to a solid. However, since polymerization is being neglected, the analysis was initiated from the reference temperature (Tref=85 °C) defined for the fully cured material as Tref=Tg + 10 °C. Although this was somewhat higher than the actual curing temperature of 60 °C, it produces a rubbery thermal shrinkage in the direction of what would have been realized by cure shrinkage during polymerization. The temperature was decreased at 1 °C/min from 85 °C to 60 °C (approximate cure temperature) and then cooled at 5 °C/min to 20 °C for the end sealing operation.
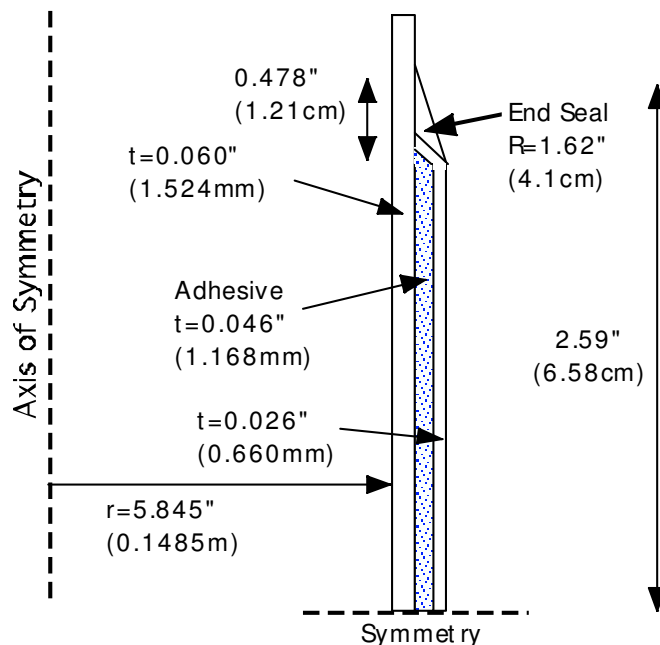
Figure 2.1: Schematic of bonded cylinder geometry.

Notice that during the adhesive bonding and initial cool-down stage, the end seal is not actually present. Geometrically, it is undesirable to birth finite elements onto a deformed geometry. Hence, for modeling purposes only, the end seal was included in the initial mesh, but it was assigned a low modulus. This allowed the material to deform freely under low load during the initial cooling and then structurally enter the problem with a stiffer modulus in the next stage of the analysis after the seal is formally applied at room temperature.

The analysis was performed with SIERRA. Since this is a quasi-static response, ADAGIO was the code of choice. However, to execute the staged analyses allowing the material properties of the metallic seal to be initially low and then increased partway through the analysis, the TEMPO code had to be employed linking two separate ADAGIO analyses. The annotated material model input deck is included in Appendix A. Note that fixed contact was used to tie the corners of the mesh at the top end under the metallic seal. Since the actual geometry of the outer cylinder tapers into the inner cylinder at the seal end, a fixed contact condition was assumed at this interface realizing that adhesive was likely to fill the void and bond the two surfaces

together.

The problem was meshed as a 90-degree sector of the cylinders with symmetry boundary conditions applied along the bottom end of the mesh perpendicular to the axis as shown in Figure 2.1. The total model consisted of 68490 elements and 81328 nodes. Although the mesh size is small by comparison to many models, it must be remembered that the computational expense involved in nonlinear viscoelastic analyses is much greater than elasticity or plasticity. Moreover, the solution required 460 time steps to track the staged solution history. This is more than sufficient to shake out the workings of SIERRA code and demonstrate capability to a customer. A detailed view of the finite element mesh in the vicinity of the end seal is shown in Figure 2.2. Here all three materials are visible. The inner and outer cylinders are made of 6061T6 aluminum and the metallic seal is made from an 1100 aluminum alloy. The aluminum cylinders and seal are assumed to have the same properties: Young's modulus=69 GPa, Poisson's ratio=0.33, and CTE=23.4 ppm/C. A definition of the nonlinear viscoelastic material properties for the adhesive is provided through the ADAGIO input deck in APPENDIX A. Because of its length, it is not reproduced here. The analysis was performed on "Rogue", a 407-node Linux cluster. Rogue is divided into two parts. Jobs run in the "Serial" queue are performed using 2.4 GHz Xeon compute nodes, whereas jobs performed in the "Scico" queue are run using 3.06 GHz Xeon compute nodes. Note that parallel jobs can be run in either queue. Using 16 processors in the Scico queue, the execution time was just over 10 hours.

2.2 Thermo-mechanical Response

In the first stage of the analysis, residual stresses are generated as the adhesively bonded cylinders are cooled to 20 °C. These stresses arise from the mismatch between the thermal strains in the aluminum and adhesive. Because the adhesive originally is at a temperature higher than its glass transition temperature (Tg), it first exhibits a rubbery response and then becomes glassy below Tg. Figure 2.3 contains a color plot of the maximum principal stresses in the adhesive at T=20 °C after cooling just prior to adding the metallic seal. The adhesive shear stresses are an order of magnitude lower. Figure 2.4 illustrates the corresponding Von Mises stress in the outer aluminum cylinder. The stresses in the inner cylinder are less than half the magnitude of those
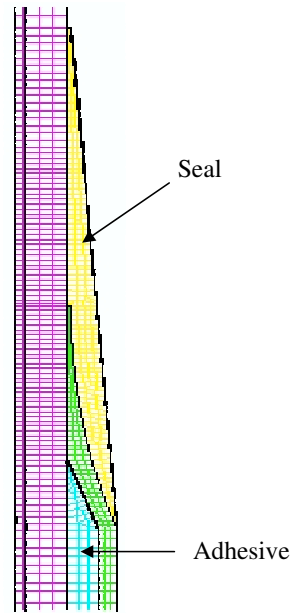
Figure 2.2: View of finite element mesh at end seal.

in Figure 2.4.

No attempt was made to analyze any manufacturing stresses induced by the end sealing operation at room temperature. Rather the Young's modulus of the metallic seal was increased from the fictitiously low value of 1 MPa to 69 GPa effectively giving birth to the joint for the remainder of the analyses. This provided a realistic stiffness to resist subsequent loading. Note also there is the implicit assumption that the interface between the inner and outer cylinders (underneath the metallic seal) is adhesively bonded together. This is achieved by a fixed contact.

Once the end seal is in place the inner cylinder is axial pre-loaded in tension under 18000 lbs (80067 N). A plot of the Von Mises element stresses is shown in Figure 2.5 just after application of the pre-load. The magnitude of the maximum stress in the inner cylinder, outer cylinder, and metallic seal are 61 MPa (8.85 ksi), 69 MPa (10 ksi), and 51 MPa (7.4 ksi), respectively. The highest stress in the metallic seal during the entire thermo- mechanical history was recorded at the 70 °C temperature where the axial load was increased to 30000 lbs. A plot of these Von Mises stresses is provided in Figure 2.6. Here the maximum stress is seen to reach 85 MPa and is located along the thin top end of the seal. The stress in the area of the cylinder overlap
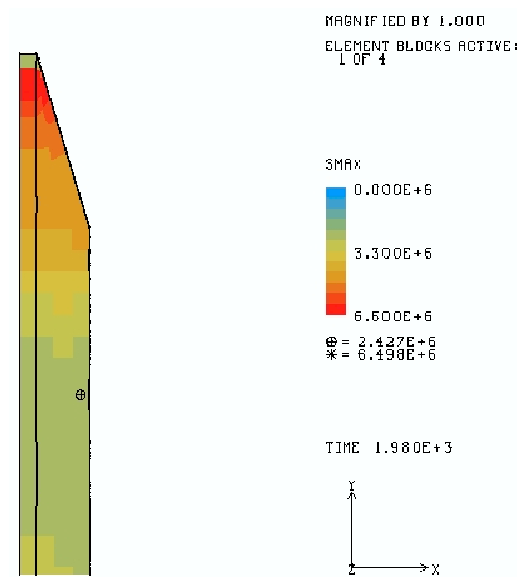
Figure 2.3: Maximum principal stresses (Pa) in adhesive at T=20 °C prior to sealing.
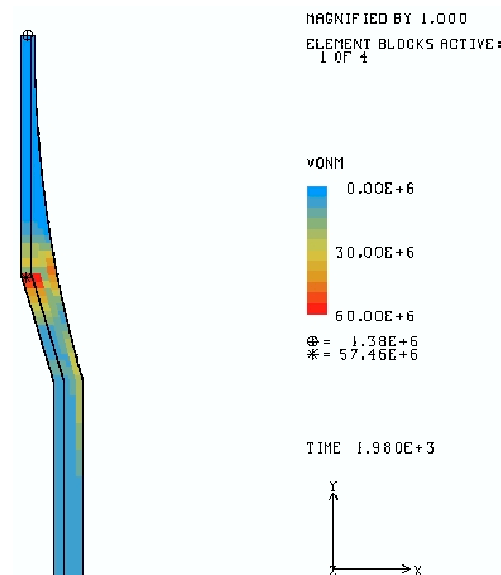
Figure 2.4: von Mises stresses (Pa) in outer cylinder at T=20 °C prior to sealing.
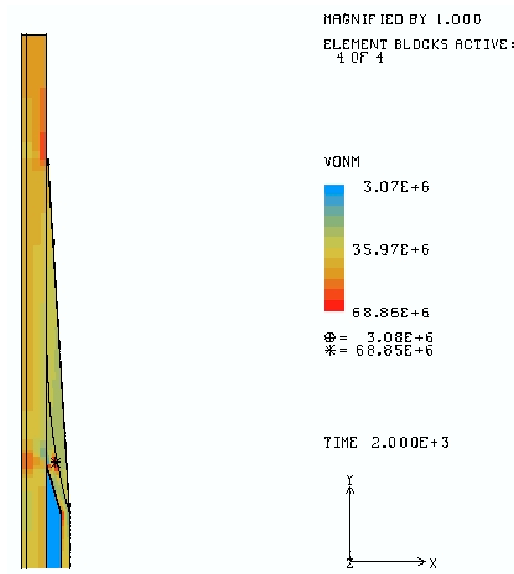
Figure 2.5: von Mises element stresses (Pa) after application of pre-load.

is between 45 and 55 MPa. The seal stresses at the lower temperature (T=-55 °C) are actually reduced somewhat due to the fact that the axial pre-load is only 5000 lbs. These stresses are plotted in Figure 2.7. However, the location of the maximum stress does shift towards the opposite end of the seal. The maximum principal stresses in the adhesive are greatest at the lower temperature due to the increased mismatch in thermal strains under the geometric constraint between cylinders. These stresses are plotted in Figure 2.8.
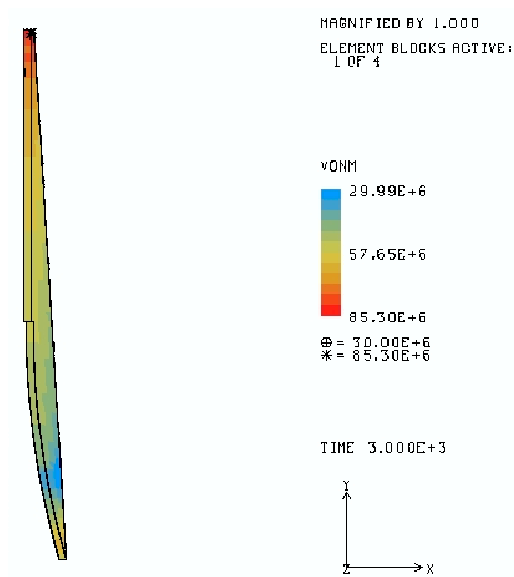
Figure 2.6: von Mises stresses (Pa) in seal at T=70 °C under 30000 lb load.
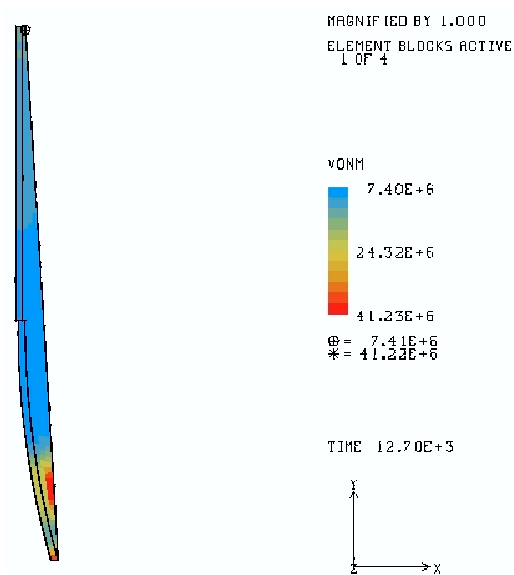
Figure 2.7: von Mises stresses (Pa) in seal at T=-55 °C under 5000 lb load.
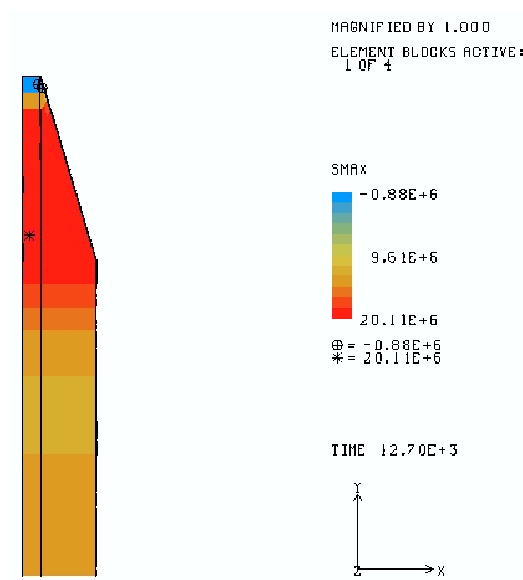
Figure 2.8: Maximum principal stresses in adhesive at T=-55 °C under 5000lb load.

3   Isotropic and Composite Circular Rings Under Internal Pressure

3.1   Composite Modeling Overview

Laminated fiber-reinforced composite structures can be classified as plate or shells in almost all cases. Recall that plates refer to flat structures which are thin in their thickness direction compared to their inplane dimensions, whereas shells refer to similar structures which are curved. Due to this small thickness, certain kinematic assumptions can usually be applied in analyzing such structures. If a plate or shell is thin enough, the usual Kirchhoff bending constraints of normals to the midplane remaining straight and normal to the midplane under the application of load can be applied. That is, if thin enough, the plate or shell will not exhibit any transverse shear response. However, if a structure is sufficiently thick, this condition needs to be relaxed to allow the transverse shear response of the structure to be captured. In such cases, Mindlin theory is typically applied. In a majority of cases, using a plate/shell theory in modeling a composite structure is usually sufficient. However, using such a theory is not a requirement. That is, such composites can be analyzed using an appropriate continuum approach. Such a continuum approach does not involve enforcing any kinematic conditions likely to result for a given structure a *priori* beyond the usual selection of a suitable strain measure.

Regardless of whether a shell or continuum approach is used, it is usually necessary to use a numerical method to determine the structural response of a composite structure for most cases beyond a simple few for which analytical results can be determined. In structural mechanics, the favored approach is, of course, finite element analysis. The pertinent questions are then when can shell elements be used accurately and efficiently? and when will it be necessary to use continuum elements? ADAGIO and PRESTO already have the necessary constitutive laws for models using either approach.[1] The continuum material law that can be used for an individual layer is given by the inverse of Eq. (1.1) in Reference 1, whereas the laminate material model that can be used for an entire lay-up is given by Eqs. (1.27) and (1.28) in Reference 1.

When analyzing composite structures, much of the intuition acquired from analysis of isotropic structures cannot be used. For instance, in the case of an isotropic

structure possessing axisymmetric geometry under axisymmetric loads, no circumferential displacements will occur. Rather, in such a case, the structure can only expand/contract along the radial and axial directions. Hence, such a situation can be modeled by considering only a small sector (pie cut) and applying boundary conditions on the circumferential edges specifying that no circumferential displacements occur. However, in the case of a laminated composite structure possessing axisymmetric geometry under axisymmetric loads, circumferential displacements may or may not occur depending on the laminate stacking sequence. Thus, when a small sector is modeled for a composite structure, it is not correct to simply apply a condition of no circumferential displacements along the sector circumferential edges. Rather, true cyclic periodic boundary conditions must be used such that the sector modeled deforms in a way that the periodicity is preserved in the response. That is, the response is still axisymmetric in that it is independent of the angular position when expressed using an appropriate cylindrical coordinate system, even though it may involve circumferential displacements. For example, if a $10°$ sector is modeled, the deformations must be such that taking 36 of these deformed $10°$ sectors, the ends would still fit together to form a complete $360°$ ring with no gaps.

In order to demonstrate these concepts clearly, various isotropic and composite rings under internal pressure will be examined. Two different ring geometries will be considered. The first ring geometry to be presented corresponds to a smaller radius, larger thickness, and a longer axial dimension than that for the second ring geometry which will be examined. Each ring is analyzed for various layer properties and stacking sequences. One goal of this ASC AD project has been to understand the differences between modeling thin structures using continuum and shell approaches in terms of the types of behavior that can be captured and in terms of computational cost. Hence, the rings will be analyzed using both continuum and shell element approaches. The linear elastic orthotropic shell and continuum models in ADAGIO/PRESTO have been verified with numerous orthotropic regression tests. Nevertheless, each modeling approach has its advantages and disadvantages/limitations. These differences will be explored presently.

R$_o$ = 4.1" (10.414 cm)

R$_i$ = 4.0" (10.160 cm)
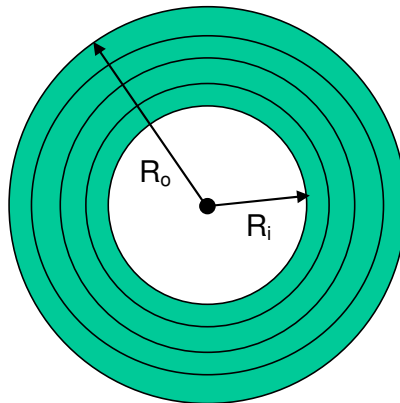
Figure 3.1: Ring A geometry.

3.2 Ring A Problem Definition

The "Ring A" geometry is as shown in Figure 3.1. Four layers each having a thickness of 0.025" (0.0635 cm) are used with an inner ring radius of 4.0" (10.16 cm). The ring has an axial length of 0.25" (0.0635cm). Each lamina has the following orthotropic properties:

$$E_{11} = 64.03 \text{ GPa} \tag{3.1}$$

$$E_{22} = 55.50 \text{ GPa} \tag{3.2}$$

$$E_{33} = 9.78 \text{ GPa} \tag{3.3}$$

$$\nu_{12} = 0.081 \tag{3.4}$$

$$\nu_{23} = 0.303 \tag{3.5}$$

$$\nu_{31} = 0.0462805 \tag{3.6}$$

$$G_{12} = G_{23} = G_{31} = 4.45 \text{ GPa} \tag{3.7}$$

Three composite laminate stacking sequences are considered: a symmetric cross-ply stacking sequence of [0/90/90/0], a uniform stacking sequence of [30/30/30/30], and a non-symmetric stacking sequence of [10/50/60/30]. Here the first layer in each stacking sequence corresponds to the outermost ring. A fiber angle of 0° corresponds to the circumferential direction, while a fiber angle of 90° corresponds to the axial direction.

Other fiber angles are established by the appropriate rotation in the plane defined by the 0° and 90° fiber directions.

In order to demonstrate the validity of the cyclic periodic boundary conditions in ADAGIO, only a 10° sector of each ring is modeled. The cyclic periodic boundary conditions applied on each circumferential edge allow for circumferential displacements. However, as previously noted, the circumferential displacements of the two circumferential edges must be compatible such that 36 of these 10° sectors could be fit together to create a complete ring without any gaps in the deformed configuration. The composite rings for this ring geometry are modeled only using a continuum approach with solid brick elements.

3.3   Ring A Results

Each ring is subjected to an internal pressure of 100 psi. For the [0/90/90/0] cross-ply, the deformed shape is as shown in Figure 3.2. Such a symmetric cross-ply stacking sequence does not lead to any coupling between shear and normal behaviors or membrane and bending behaviors. Furthermore for this stacking sequence, the cross-ply stacking sequence is aligned with the cylindrical geometry such that the fibers are aligned in the circumferential and axial directions only. Hence, the deformations involve only radial and axial displacements. In such a case as this, explicitly constraining the circumferential displacements to be zero would not affect the solution.

The deformed mesh for the [30/30/30/30] composite ring is shown in Figures 3.3 and 3.4. Here, although there is no coupling between membrane and bending behaviors because the lay-up is symmetric about the middle surface, the shear and normal behaviors are coupled when viewed using the cylindrical coordinate system aligned naturally with the cylindrical ring geometry. That is, the membrane and bending normal stresses are coupled to the membrane and bending shear strains, respectively. Likewise, the membrane and bending shear stresses are coupled to the membrane and bending normal strains. It is precisely these couplings which lead to the shear behavior which is evident in the deformed geometry. Here is a case where if no circumferential displacements were applied to the circumferential edges of the 10° wedge, the solution that would result would not correspond to the solution determined by modeling the entire ring. That is, applying no circumferential displacements to the 10° wedge would
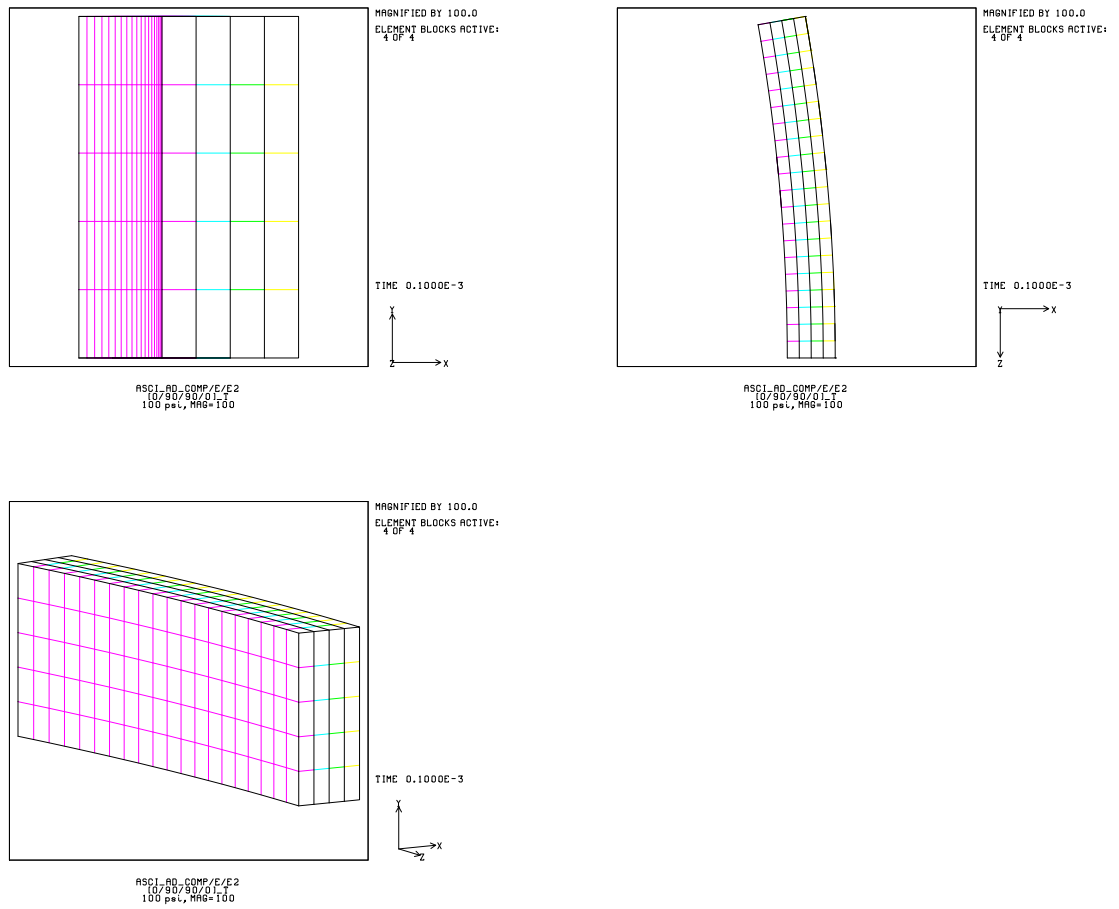
Figure 3.2: Deformed [0/90/90/0] composite Ring A (100X mag. of displacements).
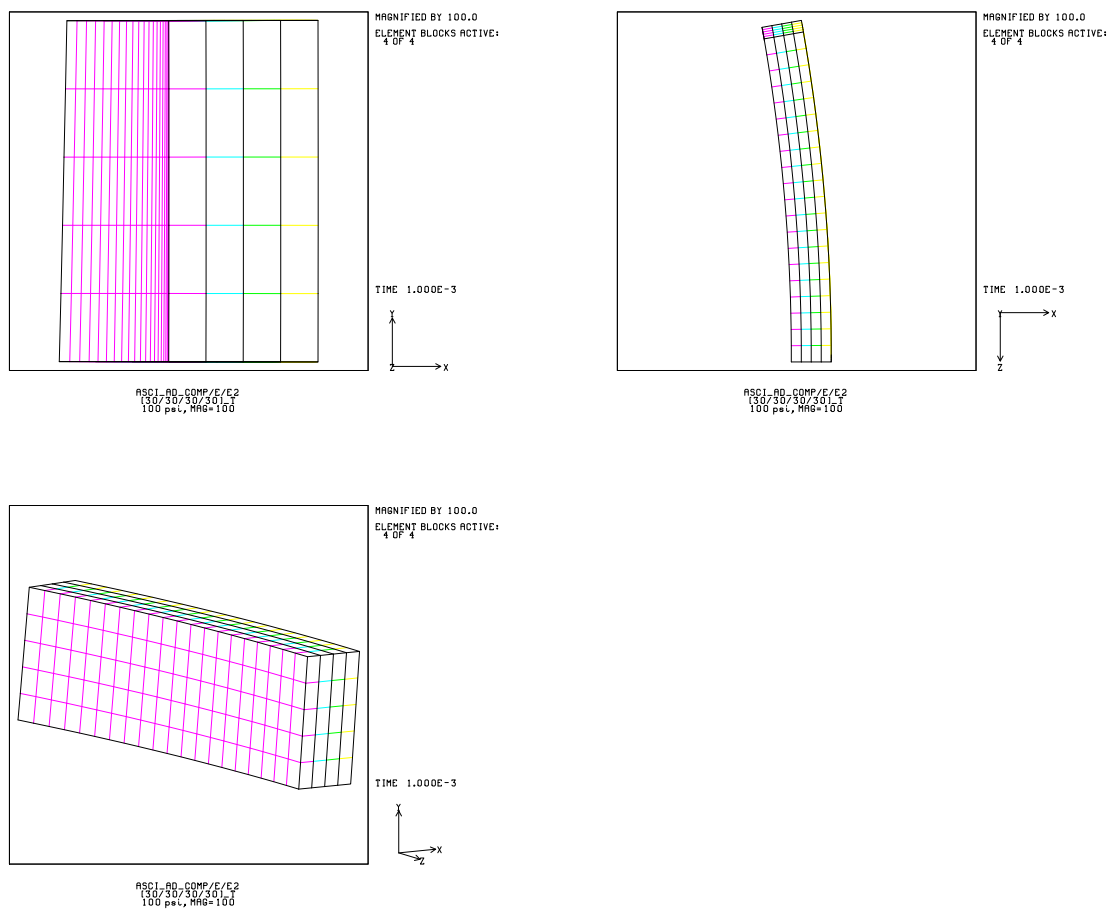
Figure 3.3: Deformed [30/30/30/30] composite Ring A (100X mag. of displacements).

overconstrain the solution.

Finally, the deformed mesh for the [10/50/60/30] stacking sequence is shown in Figures 3.5 and 3.6. This stacking sequence involves coupling both between normal and shear behaviors and membrane and bending behaviors. The coupling between membrane and bending behaviors arises from the non-symmetric lay-up and links the membrane stresses to the bending strains as well as connecting the bending stresses to the membrane strains. Clearly, the deformed shape in this case is the most complex owing to its stacking sequence which has all possible couplings present.
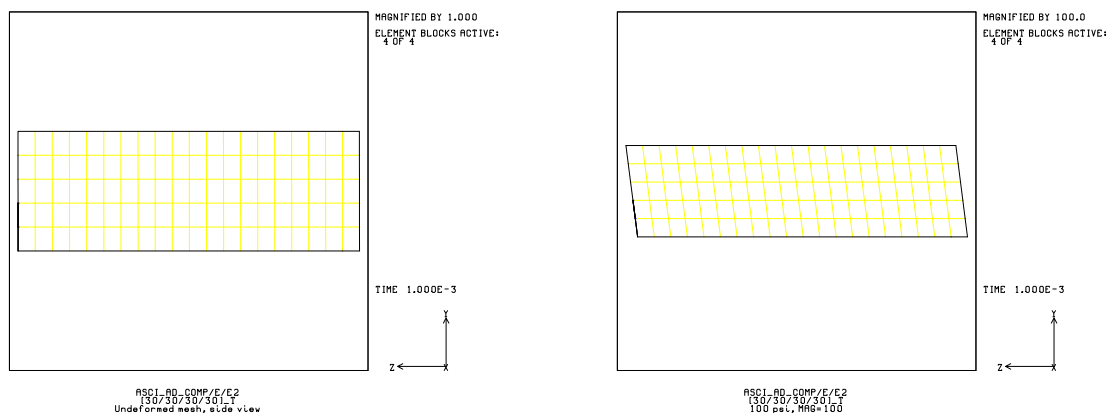
Figure 3.4: Undeformed and deformed side views of [30/30/30/30] composite Ring A (100X mag. of displacements).

3.4 Ring B Problem Definition

Like the Ring A problems just presented, the "Ring B" problems involve a 4-layer composite ring under internal pressure. However, Ring B has a larger internal radius of 7.908" and a smaller total thickness of 0.01". Stacking sequences of [0/90/90/0], [30/45/45/30], [30/−30/30/−30], and [30/60/50/10] are analyzed. In each case, the stacking sequence is given with the first angle corresponding to the outer layer with the remaining angles for the remaining layers working inward. The base material properties for each layer when viewed from a local coordinate system aligned with the
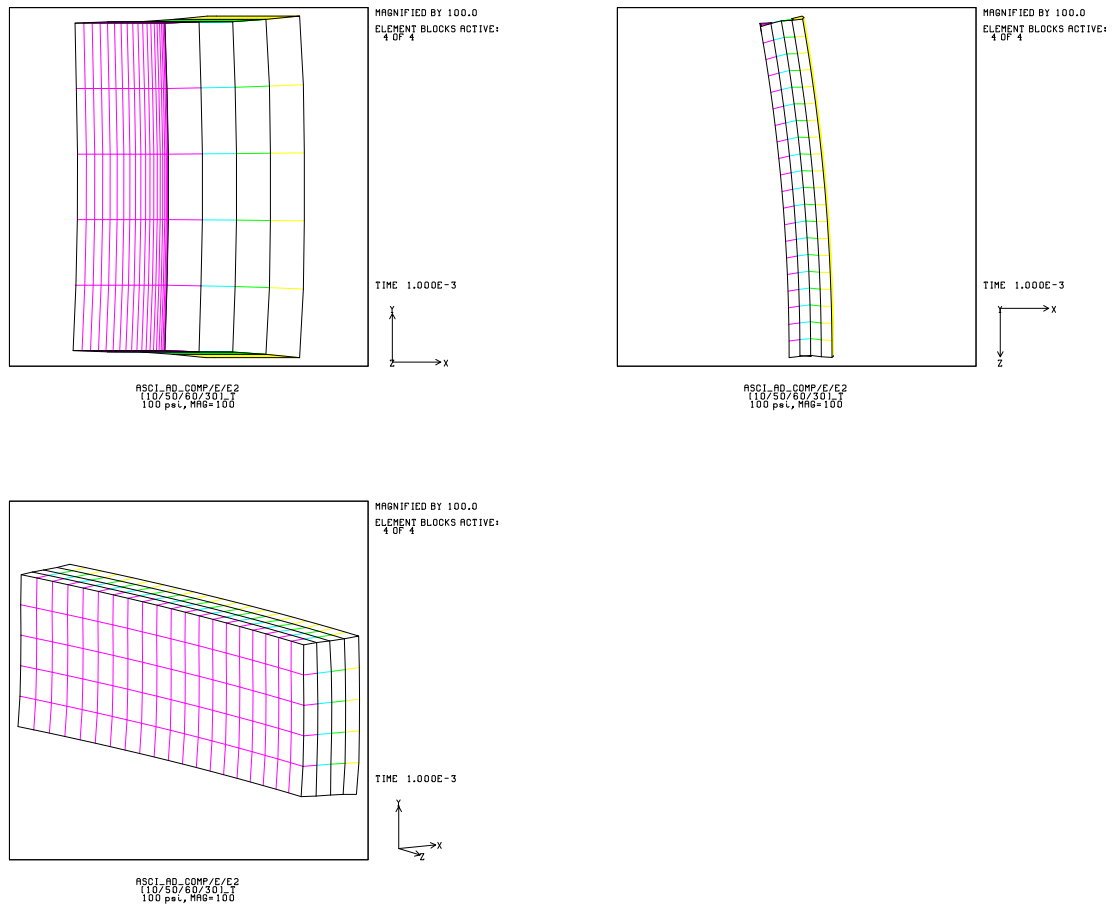
Figure 3.5: Deformed [10/50/60/30] composite Ring A (100X mag. of displacements).
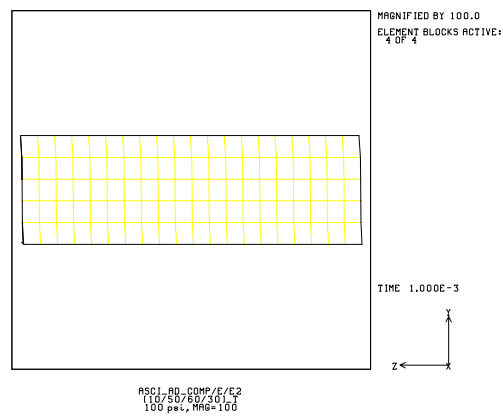
Figure 3.6: Deformed side view of [10/50/60/30] composite Ring A (100X mag. of displacements).

principal material directions are

$$E_{11} = 9.28691 \text{ Msi} \qquad (3.8)$$

$$E_{22} = 8.04972 \text{ Msi} \qquad (3.9)$$

$$E_{33} = 1.41849 \text{ Msi} \qquad (3.10)$$

$$\nu_{12} = 0.081 \qquad (3.11)$$

$$\nu_{23} = 0.303 \qquad (3.12)$$

$$\nu_{31} = 0.0462805 \qquad (3.13)$$

$$G_{12} = 0.645428 \text{ Msi} \qquad (3.14)$$

$$G_{23} = 0.645428 \text{ Msi} \qquad (3.15)$$

$$G_{31} = 0.645428 \text{ Msi} \qquad (3.16)$$

$$\rho = 0.000140426 \, \frac{\text{lb} \cdot \text{s}^2}{\text{in}^4} \qquad (3.17)$$

In addition to studying actual composite rings, an isotropic ring with the following material properties is also studied:

$$E = 9.28691 \text{ Msi} \qquad (3.18)$$

$$\nu = 0.303 \qquad (3.19)$$

$$\rho = 0.000140426 \, \frac{\text{lb} \cdot \text{s}^2}{\text{in}^4} \qquad (3.20)$$

For each stacking sequence including the isotropic ring, the ring has a height of 0.1". In a further demonstration example, a [30/45/45/30] ring with a height of 0.01" is presented as a special case where the shell theory kinematic assumptions do not lead to high accuracy for some of the stress results. In all cases, the applied pressure magnitude is 1 psi and the ring is free on all other edges. The ADAGIO input decks for the continuum and shell models corresponding to the [30/60/50/10] stacking sequence case are given in Appendices B and C, respectively.

In the case of an isotropic ring, simple results for the circumferential stress and expansion can be determined. Straightforward equilibrium calculations lead to the following equation for the hoop stress:

$$\sigma_{\theta\theta} = \frac{pR}{t} \qquad (3.21)$$

where θ is the circumferential coordinate of the natural r-θ-z cylindrical coordinate

system, p is the applied pressure, R is the nominal ring radius, and t is the ring thickness. Because the only nonzero stress is the circumferential stress, the corresponding circumferential strain can then be determined as

$$\epsilon_{\theta\theta} = \frac{\sigma_{\theta\theta}}{E} \tag{3.22}$$

Finally, the radial deflection required to produce this circumferential strain is

$$v_r = R_{new} - R_{old} \approx \epsilon_{\theta\theta} R_{old} \tag{3.23}$$

For the chosen geometry and isotropic material properties, the following results are obtained:

$$\sigma_{\theta\theta} = 790.8 \text{ psi} \tag{3.24}$$

$$\epsilon_{\theta\theta} = 0.0000851521 \tag{3.25}$$

$$v_r = 0.000673 \text{ in.} \tag{3.26}$$

3.5 Ring B Results

In the following pages, deformation and stress results are presented for all of the chosen rings. Also shown are the deformed geometries for all cases, and plots of strain, stress, or force and force-couple resultants for a few select cases. For all of the rings that are 0.1" tall, a 0.5° sector is modeled with periodic boundary conditions. For the additional [30/45/45/30] ring which is 0.01" tall, a 0.0625° sector is modeled, again with periodic boundary conditions. For the plots of the deformed meshes, only the first column of elements is shown for convenience. Note that which entries are present in the laminate stiffness matrices that describe the laminate material response depend on the specific stacking sequence. A full range of stacking sequences have been chosen all the way from an isotropic case to a random lay-up of [30/60/50/10] which has nonzero values for all entries in $[A]$, $[B]$, and $[D]$.

Results for the various rings are presented in numerous tables and figures in this section. However, only an overview of the many results will be discussed subsequently.

For the isotropic case, the continuum and shell element results match very well. Moreover, the results from each for the radial displacement and circumferential stress match the mechanics of materials solution given by Eqs. (3.21)-(3.23). Similarly, excellent agreement between the two approaches results for the [0/90/90/0] symmetric

cross-ply stacking sequence. Note that the [0/90/90/0] stacking sequence results in the same set of nonzero entries in $[A]$, $[A_{ts}]$, $[B]$, and $[D]$ as the isotropic case, but with, of course, different values. For both of these simple cases, the shell results required both fewer CG iterations and CPU time in ADAGIO.

For the [30/45/45/30] symmetric stacking sequence, the laminate has coupling between normal and shear membrane stresses and strains (nonzero A_{16} and A_{26}), in addition to coupling between normal and shear bending stresses and strains (nonzero D_{16} and D_{26}). For this case, the agreement between the two approaches is reasonable for all results for the 0.1" high ring. Note in Figure 3.11 which shows the deformed continuum model for this ring height, edge effects are quite apparent. However, the corresponding deformed shell model shown in Figure 3.12 does not exhibit such displacement edge effects. Such edge effects should become even more dominant for a smaller height ring. This is, in fact, what is observed for the [30/45/45/30] ring which is only 0.01" in height. For this smaller ring height, reasonable agreement between the continuum and shell approaches result for the radial displacement and circumferential stress, but both the axial stress and the circumferential shear stress results differ significantly. In this particular case, care must be taken to achieve accurate results as demonstrated by the distribution of stresses shown in Figures 3.14 and 3.15. The corresponding force and force-couple resultants for the shell model are shown in Figures 3.17-3.19. Obviously, since only a single element is used in the thickness direction under the assumptions of Mindlin shell theory, it is not possible for the shell model to capture the actual stress variation in the radial direction, or the curving of lines which are originally purely radial in direction.

The antisymmetric angle-ply stacking sequence of [30/−30/30/−30] does not have coupling between normal and shear membrane stresses and strains or coupling between normal and shear bending stresses and strains. However, it does have coupling between the shear bending strains and the normal membrane stresses, the normal bending strains and the shear membrane stresses, the shear membrane strains and the normal bending stresses, and the normal membrane strains and the shear bending stresses (nonzero B_{16} and B_{26}). For this particular case, the agreement between the two approaches for the radial deflection appears to be reasonable. On the other hand, most of the stress results are off. For instance, the circumferential stress results are

very different in nature with the continuum model giving circumferential stresses which are similar in each layer, but the shell model giving values that differ between the inner and outer layers. Moreover, the shell model predicts nonzero axial stresses which sum to zero over the four layers, whereas the continuum model predicts all layers to have zero axial stress. Finally, although the circumferential shear stress results have the same sign for each layer in the two approaches, the shell model predicts a big variation in the value of this stress between the inner and outer layers, whereas the continuum model does not. The variation in layer stresses coming from the shell model is seen to arise from its prediction of a significant bending shear strain as shown in Figure 3.24. In this and most other cases, presumably the continuum model results are to be trusted more than the shell results, because the continuum model is based on less restrictive kinematic assumptions than the shell model. Note that for this particular stacking sequence, the shell and continuum models required comparable computational effort.

Finally, the somewhat contrived [30/60/50/10] lay-up has all terms present in $[A]$, $[B]$, and $[D]$ leading to all possible couplings between membrane and bending stresses and strains. However, the off-diagonal terms in $[A_{ts}]$ are still zero, as the two transverse shear moduli are taken to be equal. For this particular case, reasonable agreement exists between the shell and continuum results for all quantities examined. Note in Figures 3.25 and 3.26 the relatively significant bending that results for this stacking sequence which has a full membrane/bending coupling matrix $[B]$. In this particular case, the shell model required significantly more computational effort than the continuum model.

Table 3.1: Radial displacement at middle of inside surface for isotropic Ring B.

Case	V_r (in.)
Mech. of Mat.	0.000673
Cont. FEM	0.000674161
Shell FEM	0.000673471

Table 3.2: Stress $\sigma_{XX} = \sigma_{rr}$ at ring center for isotropic Ring B.

Case	L1 (psi)	L2 (psi)	L3 (psi)	L4 (psi)
Mech. of Mat.	0.0	0.0	0.0	0.0
Cont. FEM	-1.285492E-01	-3.789259E-01	-6.307772E-01	-8.768584E-01
Shell FEM	-1.322894E-10	-1.322894E-10	-1.322894E-10	-1.322894E-10

Table 3.3: Stress $\sigma_{YY} = \sigma_{zz}$ at ring center for isotropic Ring B.

Case	L1 (psi)	L2 (psi)	L3 (psi)	L4 (psi)
Mech. of Mat.	0.0	0.0	0.0	0.0
Cont. FEM	9.381270E-03	4.009083E-03	-7.445849E-03	-1.784666E-02
Shell FEM	-2.792358E-02	-1.004028E-02	7.873535E-03	2.575684E-02

Table 3.4: Stress $\sigma_{ZZ} = \sigma_{\theta\theta}$ at ring center for isotropic Ring B.

Case	L1 (psi)	L2 (psi)	L3 (psi)	L4 (psi)	AVG (psi)
Mech. of Mat.	790.8000	790.8000	790.8000	790.8000	790.8000
Cont. FEM	790.5351	790.7678	790.9818	791.1935	790.8696
Shell FEM	790.7740	790.8325	790.8911	790.9496	790.8618

Table 3.5: Stress $\sigma_{XY} = \sigma_{zr}$ at ring center for isotropic Ring B.

Case	L1 (psi)	L2 (psi)	L3 (psi)	L4 (psi)
Mech. of Mat.	0.0	0.0	0.0	0.0
Cont. FEM	8.828444E-07	3.358880E-06	2.407217E-06	1.432775E-06
Shell FEM	-4.016570E-05	-4.016575E-05	-4.016580E-05	-4.016585E-05

Table 3.6: Stress $\sigma_{YZ} = -\sigma_{\theta z}$ at ring center for isotropic Ring B.

Case	L1 (psi)	L2 (psi)	L3 (psi)	L4 (psi)
Mech. of Mat.	0.0	0.0	0.0	0.0
Cont. FEM	-6.401723E-05	-6.235721E-05	-6.138064E-05	-6.052429E-05
Shell FEM	7.139375E-06	2.592917E-06	-1.953540E-06	-6.499996E-06

Table 3.7: Stress $\sigma_{ZX} = -\sigma_{r\theta}$ at ring center for isotropic Ring B.

Case	L1 (psi)	L2 (psi)	L3 (psi)	L4 (psi)
Mech. of Mat.	0.0	0.0	0.0	0.0
Cont. FEM	3.224001E-03	-8.411866E-03	-2.593525E-03	1.459236E-02
Shell FEM	3.944047E-03	3.944046E-03	3.944045E-03	3.944044E-03

Table 3.8: Computational cost for isotropic Ring B.

Case	Model	Elements	Nodes	DOF w/o BC	Iterations	CPU (sec)
Cont. FEM	0.5 deg	800	1155	3465	518	5.779
Shell FEM	0.5 deg	200	231	1386	230	2.290
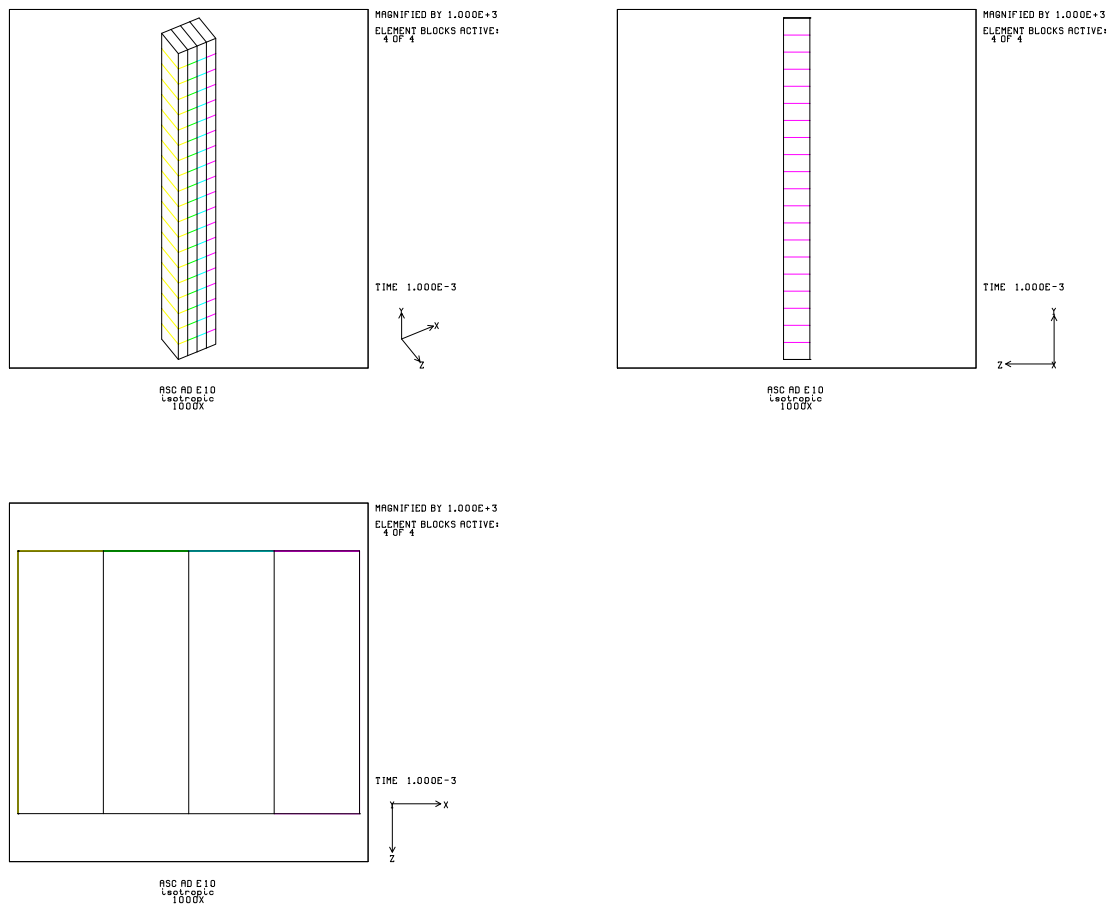
Figure 3.7: Deformed isotropic Ring B continuum model showing 1 element in circumferential direction. Deformations magnified by 1000.
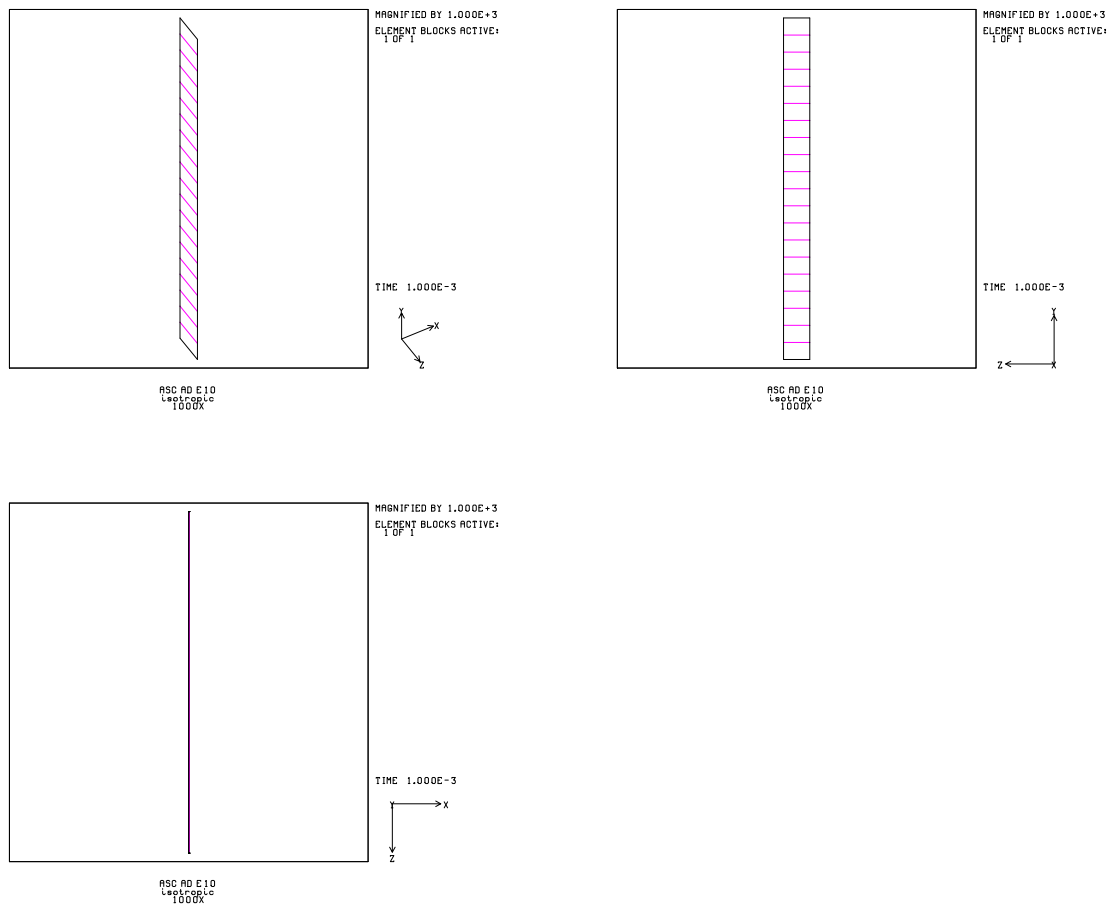
Figure 3.8: Deformed isotropic Ring B shell model showing 1 element in circumferential direction. Deformations magnified by 1000.

Table 3.9: Radial displacement at middle of inside surface for [0/90/90/0] Ring B.

Case	V_r (in.)
Cont. FEM	0.00072226
Shell FEM	0.000721516

Table 3.10: Stress $\sigma_{XX} = \sigma_{rr}$ at ring center for [0/90/90/0] Ring B.

Case	L1 (psi)	L2 (psi)	L3 (psi)	L4 (psi)
Cont. FEM	-1.340192E-01	-3.844722E-01	-6.194120E-01	-8.685544E-01
Shell FEM	-1.033863E-10	-1.034079E-10	-1.034079E-10	-1.033864E-10

Table 3.11: Stress $\sigma_{YY} = \sigma_{zz}$ at ring center for [0/90/90/0] Ring B.

Case	L1 (psi)	L2 (psi)	L3 (psi)	L4 (psi)
Cont. FEM	4.265626E+00	-4.262483E+00	-4.255891E+00	4.250383E+00
Shell FEM	4.275406E+00	-4.267586E+00	-4.271603E+00	4.263306E+00

Table 3.12: Stress $\sigma_{ZZ} = \sigma_{\theta\theta}$ at ring center for [0/90/90/0] Ring B.

Case	L1 (psi)	L2 (psi)	L3 (psi)	L4 (psi)	AVG (psi)
Cont. FEM	847.2699	734.0089	734.2285	848.0016	790.8772
Shell FEM	847.7199	734.1360	734.0841	847.5402	790.8701

Table 3.13: Stress $\sigma_{XY} = \sigma_{zr}$ at ring center for [0/90/90/0] Ring B.

Case	L1 (psi)	L2 (psi)	L3 (psi)	L4 (psi)
Cont. FEM	-1.181300E-05	-1.513988E-05	8.299375E-06	8.985447E-06
Shell FEM	-1.835007E-05	-1.834918E-05	-1.834918E-05	-1.835007E-05

Table 3.14: Stress $\sigma_{YZ} = -\sigma_{\theta z}$ at ring center for [0/90/90/0] Ring B.

Case	L1 (psi)	L2 (psi)	L3 (psi)	L4 (psi)
Cont. FEM	-2.408314E-05	7.427691E-06	6.961428E-06	-2.420312E-05
Shell FEM	4.575826E-06	1.429134E-06	-1.717616E-06	-4.864422E-06

Table 3.15: Stress $\sigma_{ZX} = -\sigma_{r\theta}$ at ring center for [0/90/90/0] Ring B.

Case	L1 (psi)	L2 (psi)	L3 (psi)	L4 (psi)
Cont. FEM	7.271318E-04	-5.612549E-03	-2.052617E-03	1.376524E-02
Shell FEM	3.746277E-03	3.747842E-03	3.747843E-03	3.746279E-03

Table 3.16: Computational cost for [0/90/90/0] Ring B.

Case	Model	Elements	Nodes	DOF w/o BC	Iterations	CPU (sec)
Cont. FEM	0.5 deg	800	1155	3465	643	8.859
Shell FEM	0.5 deg	200	231	1386	369	3.180
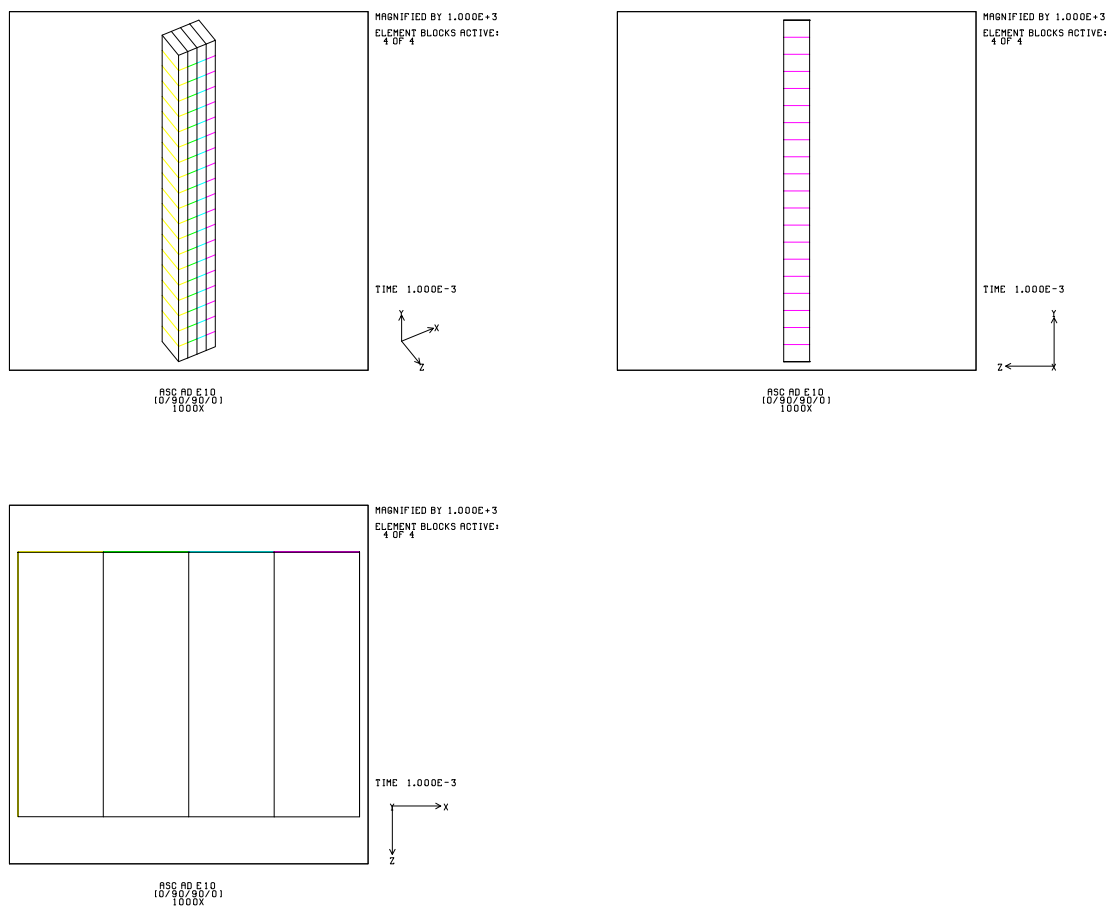
Figure 3.9: Deformed [0/90/90/0] Ring B continuum model showing 1 element in circumferential direction. Deformations magnified by 1000.

MAGNIFIED BY 1.000E+3
ELEMENT BLOCKS ACTIVE:
  1 OF 1

TIME 1.000E-3

ASC AD E10
[0/90/90/0]
1000X

MAGNIFIED BY 1.000E+3
ELEMENT BLOCKS ACTIVE:
  1 OF 1

TIME 1.000E-3

ASC AD E10
[0/90/90/0]
1000X

MAGNIFIED BY 1.000E+3
ELEMENT BLOCKS ACTIVE:
  1 OF 1

TIME 1.000E-3

ASC AD E10
[0/90/90/0]
1000X

Figure 3.10: Deformed [0/90/90/0] Ring B shell model showing 1 element in circumferential direction. Deformations magnified by 1000.

Table 3.17: Radial displacement at middle of inside surface for 0.1" high [30/45/30/30] Ring B.

Case	V_r (in.)
Cont. FEM	0.00204457
Shell FEM	0.00202239

Table 3.18: Stress $\sigma_{XX} = \sigma_{rr}$ at ring center for 0.1" high [30/45/30/30] Ring B.

Case	L1 (psi)	L2 (psi)	L3 (psi)	L4 (psi)
Cont. FEM	-1.518291E-01	-4.006721E-01	-6.055231E-01	-8.550707E-01
Shell FEM	-4.583551E-10	-4.592669E-10	-4.592670E-10	-4.583556E-10

Table 3.19: Stress $\sigma_{YY} = \sigma_{zz}$ at ring center for 0.1" high [30/45/30/30] Ring B.

Case	L1 (psi)	L2 (psi)	L3 (psi)	L4 (psi)
Cont. FEM	-85.04935	84.39281	84.80602	-84.15880
Shell FEM	-83.72532	83.80194	83.76256	-83.83939

Table 3.20: Stress $\sigma_{ZZ} = \sigma_{\theta\theta}$ at ring center for 0.1" high [30/45/30/30] Ring B.

Case	L1 (psi)	L2 (psi)	L3 (psi)	L4 (psi)	AVG (psi)
Cont. FEM	953.9507	642.9663	643.4601	955.7718	799.0372
Shell FEM	945.3959	636.7208	636.6677	945.2206	791.0013

Table 3.21: Stress $\sigma_{XY} = \sigma_{zr}$ at ring center for 0.1" high [30/45/30/30] Ring B.

Case	L1 (psi)	L2 (psi)	L3 (psi)	L4 (psi)
Cont. FEM	-4.364775E-03	1.234140E-02	1.218694E-02	-8.669811E-03
Shell FEM	-9.679240E-05	-1.342813E-04	-1.342804E-04	-9.679284E-05

Table 3.22: Stress $\sigma_{YZ} = -\sigma_{\theta z}$ at ring center for 0.1" high [30/45/30/30] Ring B.

Case	L1 (psi)	L2 (psi)	L3 (psi)	L4 (psi)
Cont. FEM	-355.1625	355.5782	355.4099	-355.8285
Shell FEM	-351.9032	351.9069	351.8897	-351.8960

Table 3.23: Stress $\sigma_{ZX} = -\sigma_{r\theta}$ at ring center for 0.1" high [30/45/30/30] Ring B.

Case	L1 (psi)	L2 (psi)	L3 (psi)	L4 (psi)
Cont. FEM	4.623912E-03	-1.053747E-02	-5.237671E-03	1.940667E-02
Shell FEM	4.268043E-03	4.284822E-03	4.284825E-03	4.268053E-03

Table 3.24: Computational cost for 0.1" high [30/45/30/30] Ring B.

Case	Model	Elements	Nodes	DOF w/o BC	Iterations	CPU (sec)
Cont. FEM	0.5 deg	800	1155	3465	1258	16.309
Shell FEM	0.5 deg	200	231	1386	1983	13.509
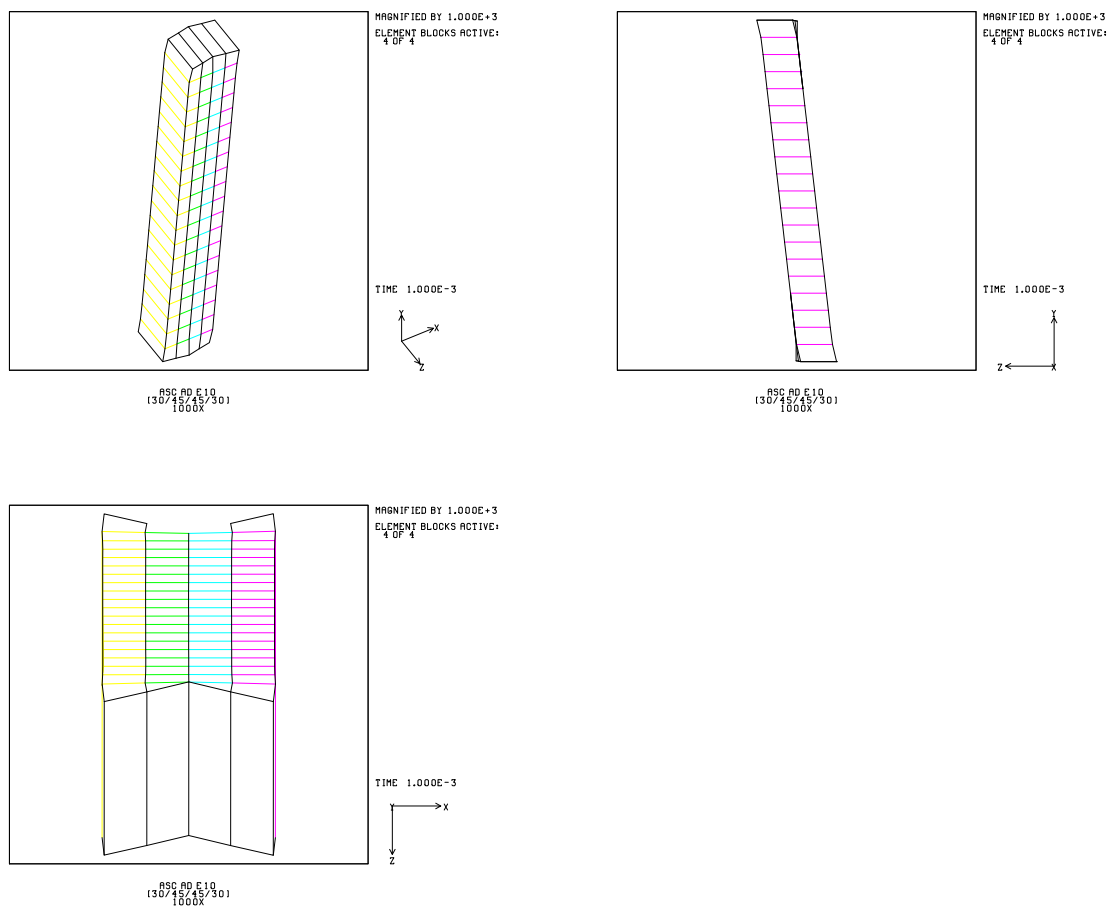
Figure 3.11: Deformed 0.1" high [30/45/45/30] Ring B continuum model showing 1 element in circumferential direction. Deformations magnified by 1000.

MAGNIFIED BY 1.000E+3
ELEMENT BLOCKS ACTIVE:
1 OF 1

TIME 1.000E-3

ASC AD E10
[30/45/45/30]
1000X

MAGNIFIED BY 1.000E+3
ELEMENT BLOCKS ACTIVE:
1 OF 1

TIME 1.000E-3

ASC AD E10
[30/45/45/30]
1000X

MAGNIFIED BY 1.000E+3
ELEMENT BLOCKS ACTIVE:
1 OF 1

TIME 1.000E-3

ASC AD E10
[30/45/45/30]
1000X
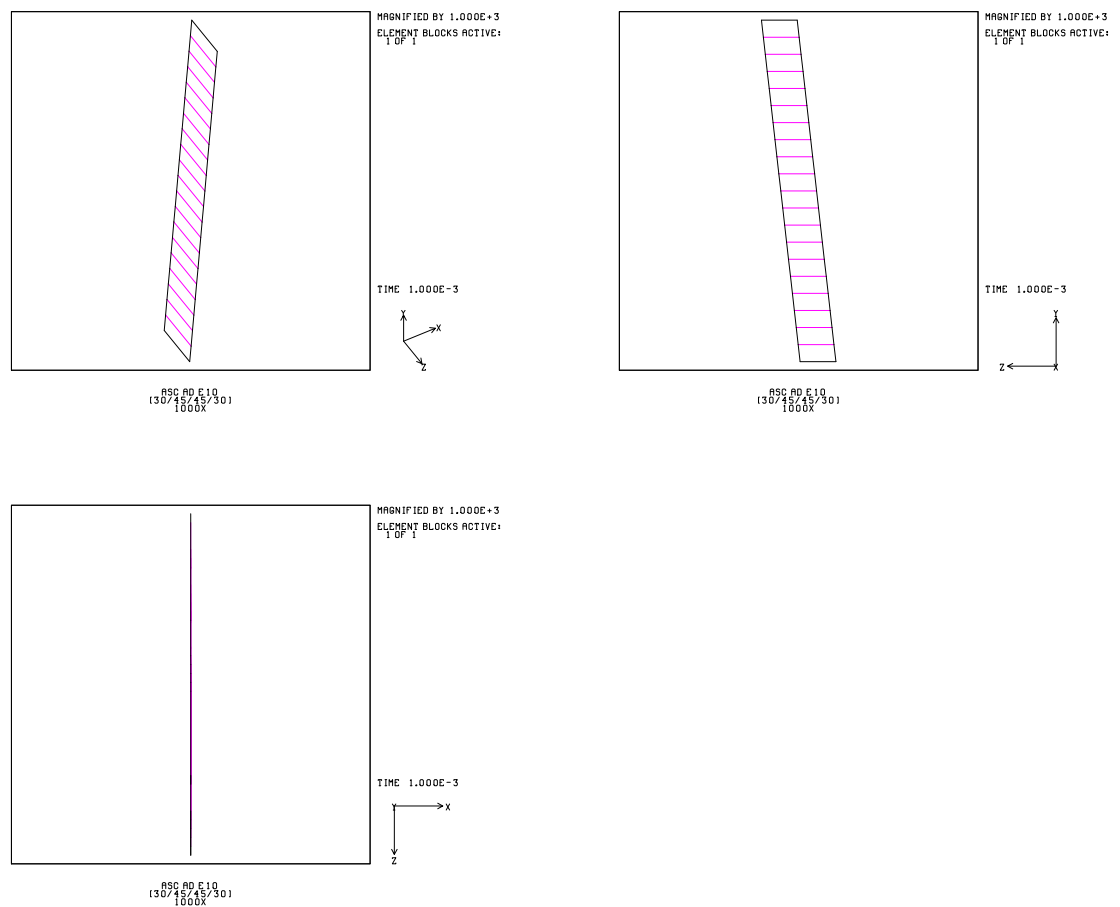
Figure 3.12: Deformed 0.1" high [30/45/45/30] Ring B shell model showing 1 element in circumferential direction. Deformations magnified by 1000.

Table 3.25: Radial Displacement at middle of inside surface for 0.01" high [30/45/30/30] Ring B.

Case	V_r (in.)
Cont. FEM	0.00224834
Shell FEM	0.00202239

Table 3.26: Stress $\sigma_{XX} = \sigma_{rr}$ (average over layer) for 0.01" high [30/45/30/30] Ring B.

Case	L1 (psi)	L2 (psi)	L3 (psi)	L4 (psi)
Cont. FEM	-1.366517E-01	-3.938791E-01	-6.084564E-01	-8.641918E-01
Shell FEM	2.517050E-09	2.515813E-09	2.515813E-09	2.517050E-09

Table 3.27: Stress $\sigma_{YY} = \sigma_{zz}$ (average over layer) for 0.01" high [30/45/30/30] Ring B.

Case	L1 (psi)	L2 (psi)	L3 (psi)	L4 (psi)
Cont. FEM	-19.25563	19.26583	19.28215	-19.26312
Shell FEM	-83.78129	83.78321	83.78173	-83.78320

Table 3.28: Stress $\sigma_{ZZ} = \sigma_{\theta\theta}$ (average over layer) for 0.01" high [30/45/30/30] Ring B.

Case	L1 (psi)	L2 (psi)	L3 (psi)	L4 (psi)	AVG (psi)
Cont. FEM	926.0904	655.4124	655.6328	927.0034	791.0348
Shell FEM	945.3318	636.7004	636.6885	945.2853	791.0015

Table 3.29: Stress $\sigma_{XY} = \sigma_{zr}$ (average over layer) for 0.01" high [30/45/30/30] Ring B.

Case	L1 (psi)	L2 (psi)	L3 (psi)	L4 (psi)
Cont. FEM	-2.939306E-03	5.007919E-03	1.916127E-03	-6.155546E-04
Shell FEM	-1.529511E-05	1.814652E-05	1.814592E-05	-1.529484E-05

Table 3.30: Stress $\sigma_{YZ} = -\sigma_{\theta z}$ (average over layer) for 0.01" high [30/45/30/30] Ring B.

Case	L1 (psi)	L2 (psi)	L3 (psi)	L4 (psi)
Cont. FEM	-174.1657	174.3227	174.3401	-174.3924
Shell FEM	-351.9023	351.9046	351.8919	-351.8970

Table 3.31: Stress $\sigma_{ZX} = -\sigma_{r\theta}$ (average over layer) for 0.01" high [30/45/30/30] Ring B.

Case	L1 (psi)	L2 (psi)	L3 (psi)	L4 (psi)
Cont. FEM	1.423775E-02	5.067150E-02	1.431179E-02	6.711946E-02
Shell FEM	2.623334E-02	2.621714E-02	2.621714E-02	2.623334E-02

Table 3.32: Computational cost for 0.01" high [30/45/30/30] Ring B.

Case	Model	Elements	Nodes	DOF w/o BC	Iterations	CPU (sec)
Cont. FEM	0.0625 deg	576	875	2625	1336	12.450
Shell FEM	0.0625 deg	24	35	210	742	1.099
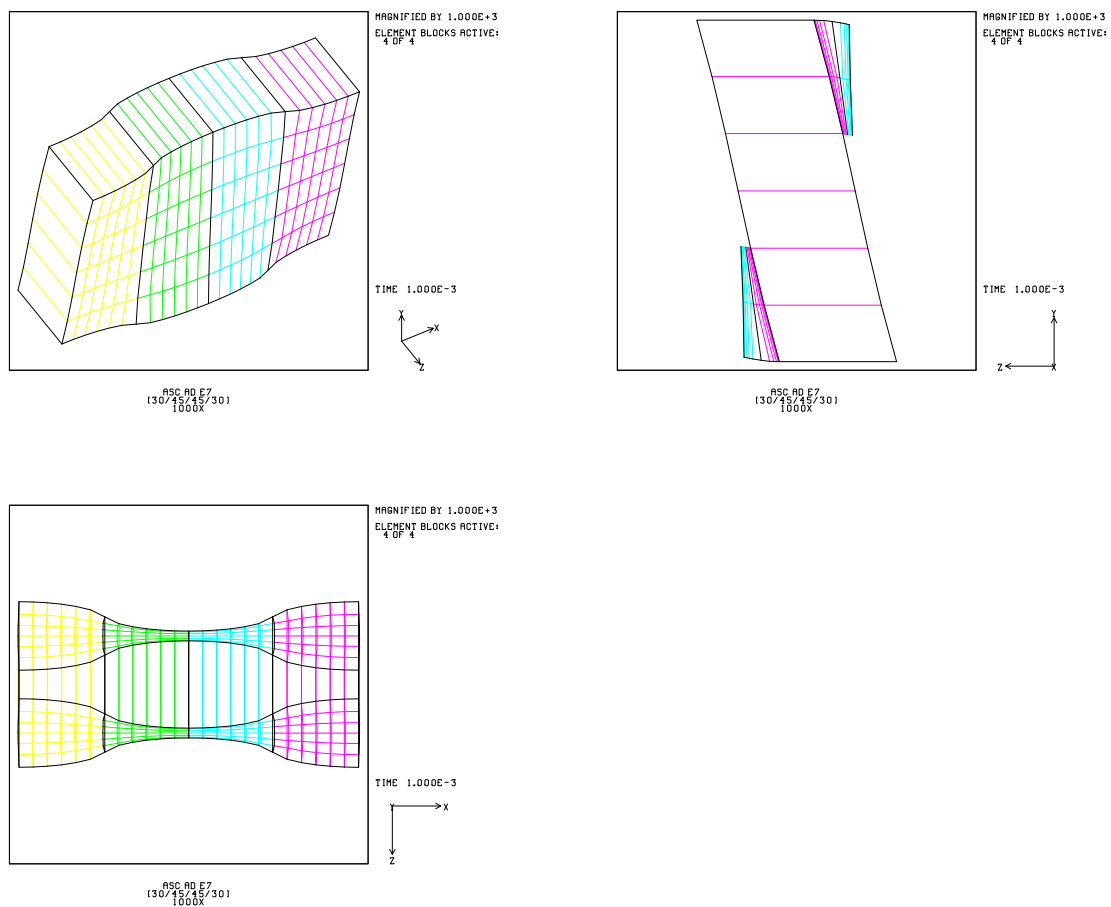
Figure 3.13: Deformed 0.01" high [30/45/45/30] Ring B continuum model showing 1 element in circumferential direction. Deformations magnified by 1000.

(a)

(b)

(c)

Figure 3.14: Stress distribution for deformed 0.01" high [30/45/45/30] Ring B continuum model: (a) $\sigma_{XX} = \sigma_{rr}$; (b) $\sigma_{YY} = \sigma_{zz}$; (c) $\sigma_{ZZ} = \sigma_{\theta\theta}$. Deformations magnified by 1000.

(a)

(b)

(c)
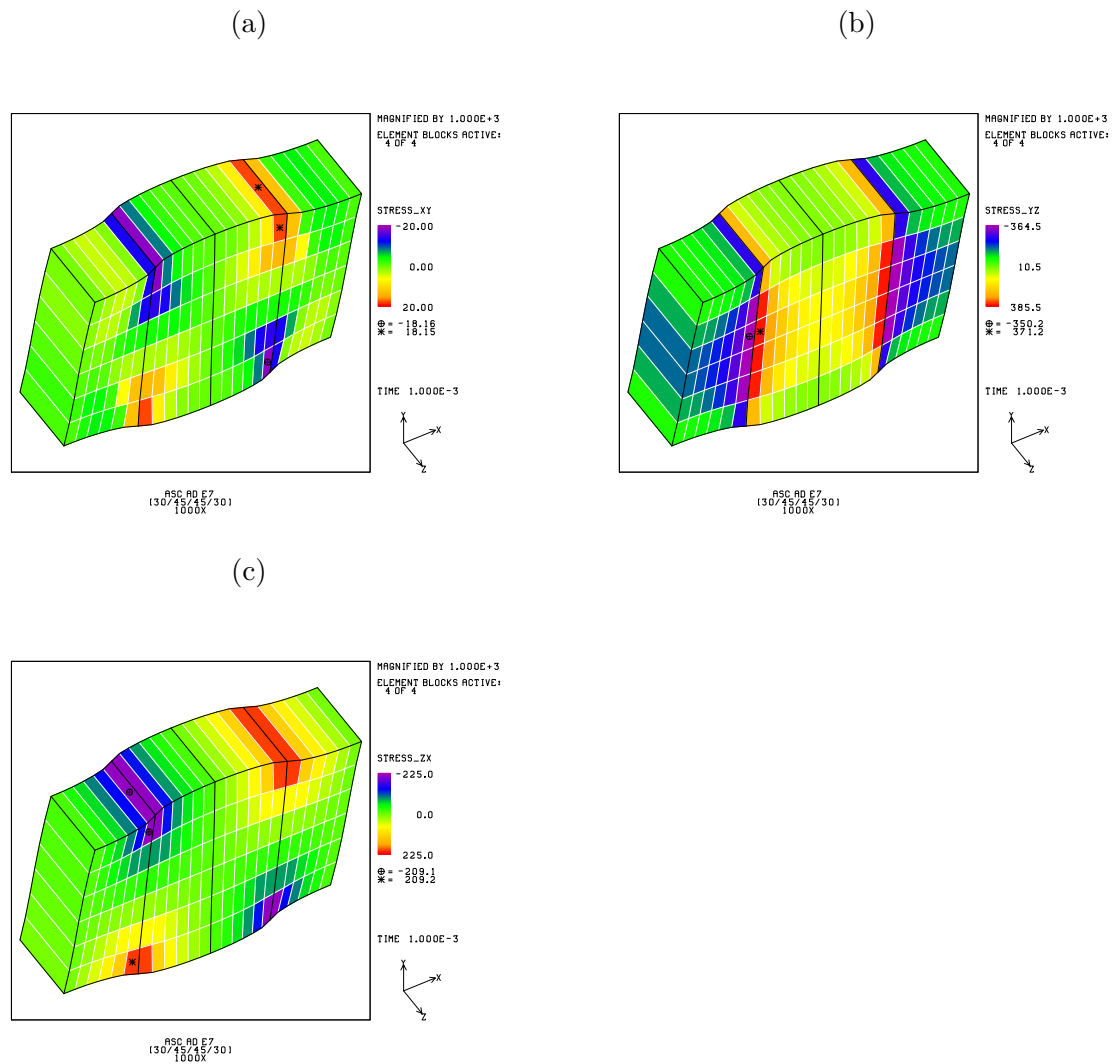
Figure 3.15: Stress distribution for deformed 0.01" high [30/45/45/30] Ring B continuum model: (a) $\sigma_{XY} = \sigma_{zr}$; (b) $\sigma_{YZ} = -\sigma_{\theta z}$; (c) $\sigma_{ZX} = -\sigma_{r\theta}$. Deformations magnified by 1000.
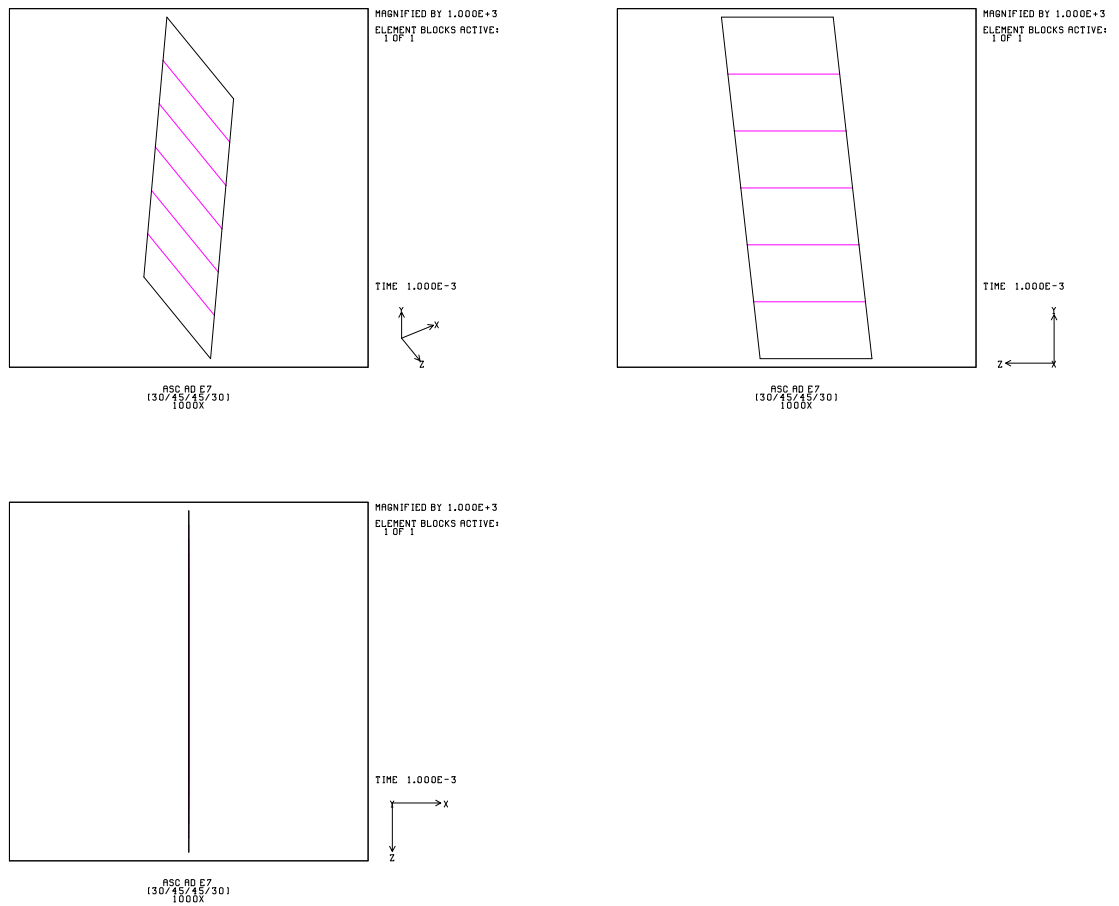
Figure 3.16: Deformed 0.01" high [30/45/45/30] Ring B shell model showing 1 element in circumferential direction. Deformations magnified by 1000.
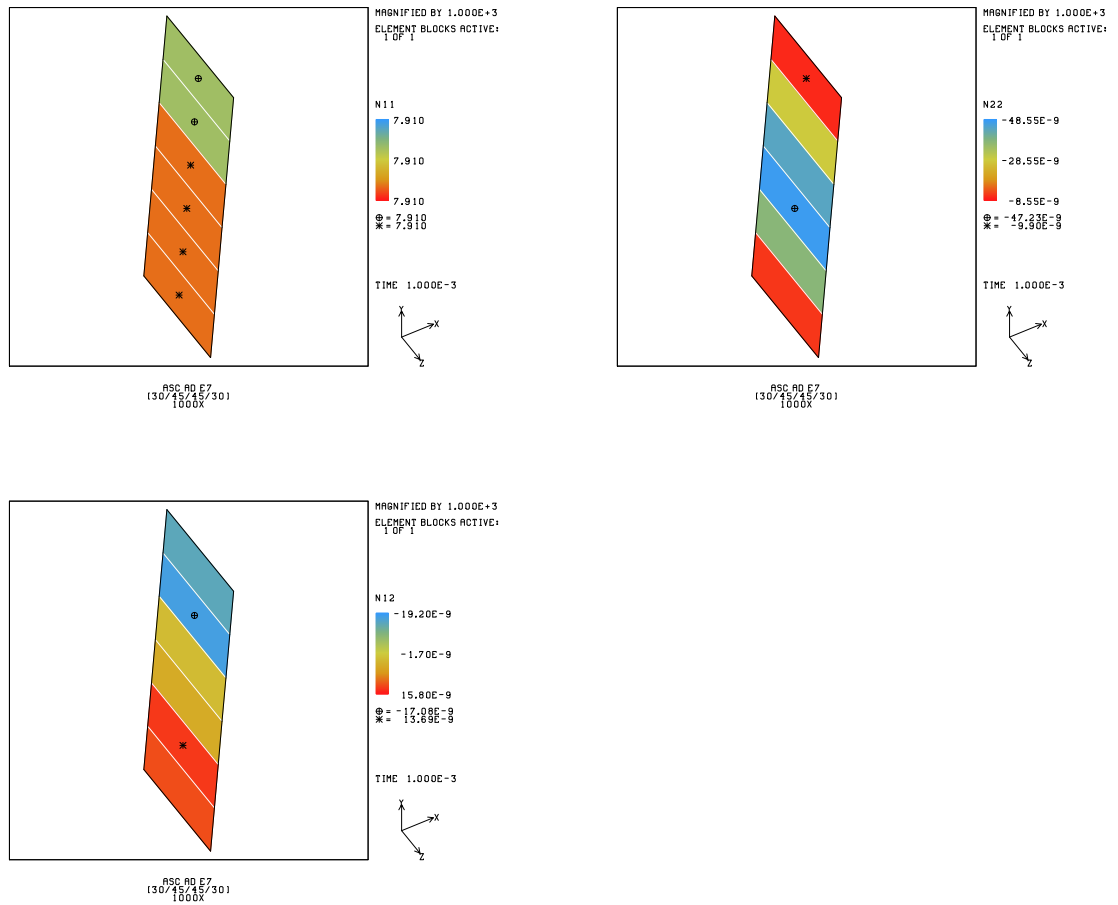
Figure 3.17: Force resultants distribution for deformed 0.01" high [30/45/45/30] Ring B shell model: (a) $N_{11} = N_{\theta\theta}$; (b) $N_{22} = N_{zz}$; (c) $N_{12} = N_{\theta z}$. Deformations magnified by 1000.
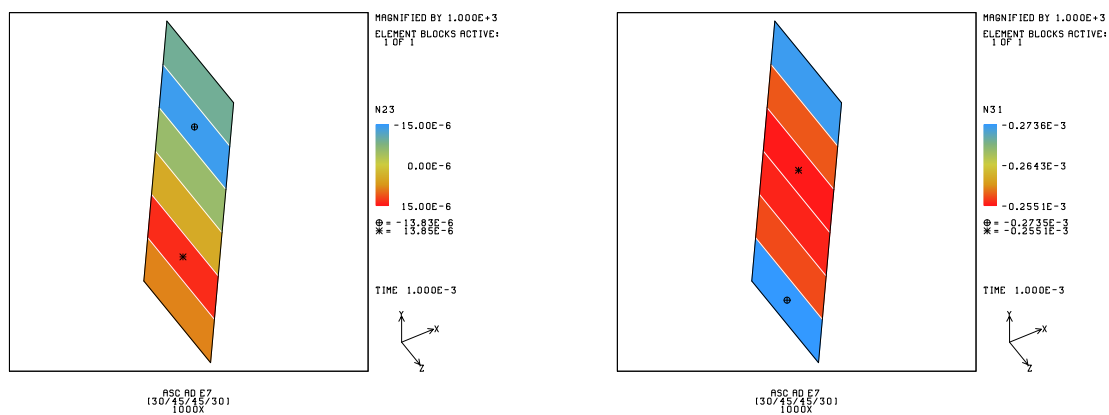
Figure 3.18: Force resultants distribution for deformed 0.01" high [30/45/45/30] Ring B shell model: (a) $N_{23} = N_{zr}$; (b) $N_{31} = N_{r\theta}$. Deformations magnified by 1000.
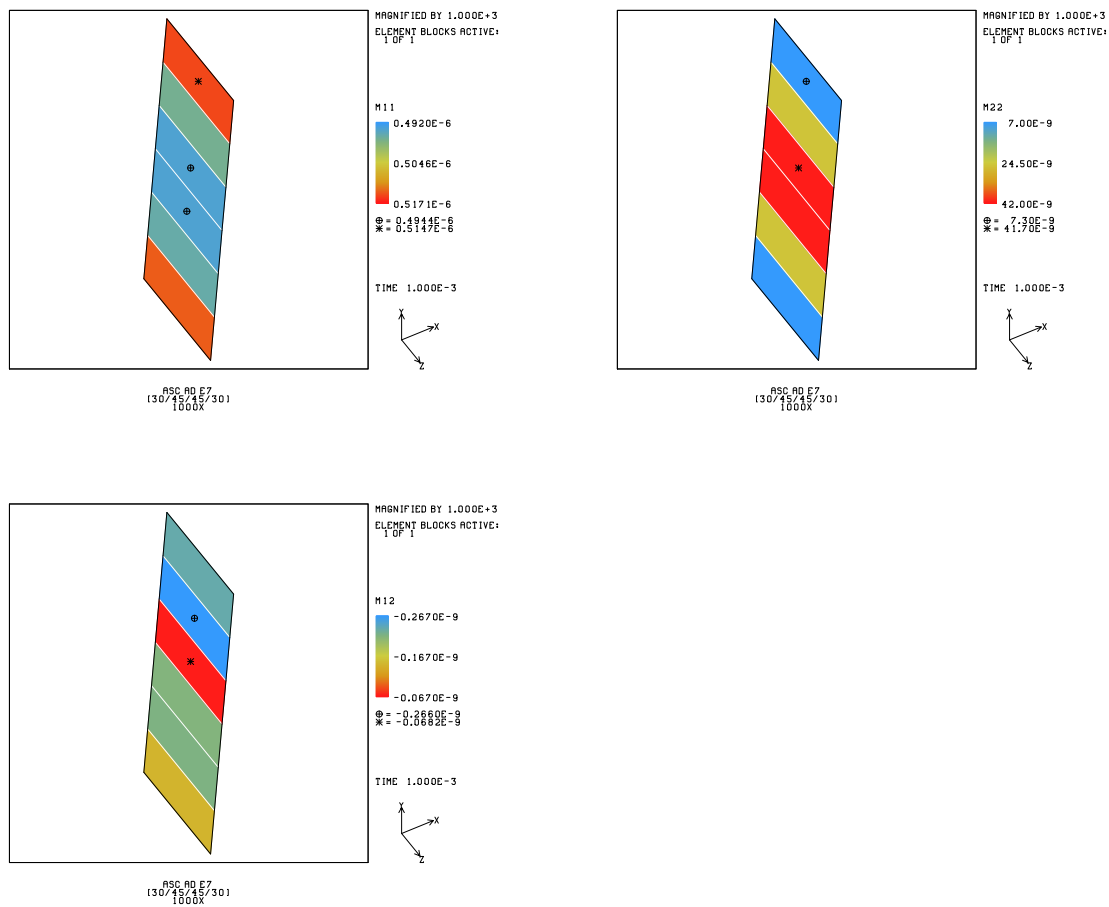
Figure 3.19: Force-couple resultants distribution for deformed 0.01" high [30/45/45/30] Ring B shell model: (a) $M_{11} = M_{\theta\theta}$; (b) $M_{22} = M_{zz}$; (c) $M_{12} = M_{\theta z}$. Deformations magnified by 1000.

Table 3.33: Radial displacement at middle of inside surface for [30/-30/30/-30] Ring B.

Case	V_r (in.)
Cont. FEM	0.00133504
Shell FEM	0.00141851

Table 3.34: Stress $\sigma_{XX} = \sigma_{rr}$ at ring center for [30/-30/30/-30] Ring B.

Case	L1 (psi)	L2 (psi)	L3 (psi)	L4 (psi)
Cont. FEM	-1.234314E-01	-3.684242E-01	-6.204792E-01	-8.742052E-01
Shell FEM	1.607640E-09	1.607727E-09	1.607723E-09	1.607641E-09

Table 3.35: Stress $\sigma_{YY} = \sigma_{zz}$ at ring center for [30/-30/30/-30] Ring B.

Case	L1 (psi)	L2 (psi)	L3 (psi)	L4 (psi)
Cont. FEM	-5.058408E-01	-3.142714E-01	1.706637E-01	6.368898E-01
Shell FEM	61.22946	-61.16712	-61.18947	61.13670

Table 3.36: Stress $\sigma_{ZZ} = \sigma_{\theta\theta}$ at ring center for [30/-30/30/-30] Ring B.

Case	L1 (psi)	L2 (psi)	L3 (psi)	L4 (psi)	AVG (psi)
Cont. FEM	800.2952	801.0306	801.3671	801.7778	801.1177
Shell FEM	702.3005	879.7058	879.6369	702.1315	790.9437

Table 3.37: Stress $\sigma_{XY} = \sigma_{zr}$ at ring center for [30/-30/30/-30] Ring B.

Case	L1 (psi)	L2 (psi)	L3 (psi)	L4 (psi)
Cont. FEM	2.037678E-03	1.994841E-02	-1.885386E-02	7.482109E-03
Shell FEM	-9.842990E-05	-1.138081E-04	-9.132145E-05	-1.067193E-04

Table 3.38: Stress $\sigma_{YZ} = -\sigma_{\theta z}$ at ring center for [30/-30/30/-30] Ring B.

Case	L1 (psi)	L2 (psi)	L3 (psi)	L4 (psi)
Cont. FEM	-402.2333	402.7932	-402.6165	402.5658
Shell FEM	-190.1512	515.7996	-515.7662	190.1199

Table 3.39: Stress $\sigma_{ZX} = -\sigma_{r\theta}$ at ring center for [30/-30/30/-30] Ring B.

Case	L1 (psi)	L2 (psi)	L3 (psi)	L4 (psi)
Cont. FEM	1.904779E-02	2.953888E-02	3.683479E-02	2.801812E-02
Shell FEM	-3.688214E-02	-3.688607E-02	-3.688598E-02	-3.688217E-02

Table 3.40: Computational cost for [30/-30/30/-30] Ring B.

| Case	Model	Elements	Nodes	DOF w/o BC	Iterations	CPU (sec)
Cont. FEM	0.5 deg	800	1155	3465	947	12.589
Shell FEM	0.5 deg	200	231	1386	1961	13.419
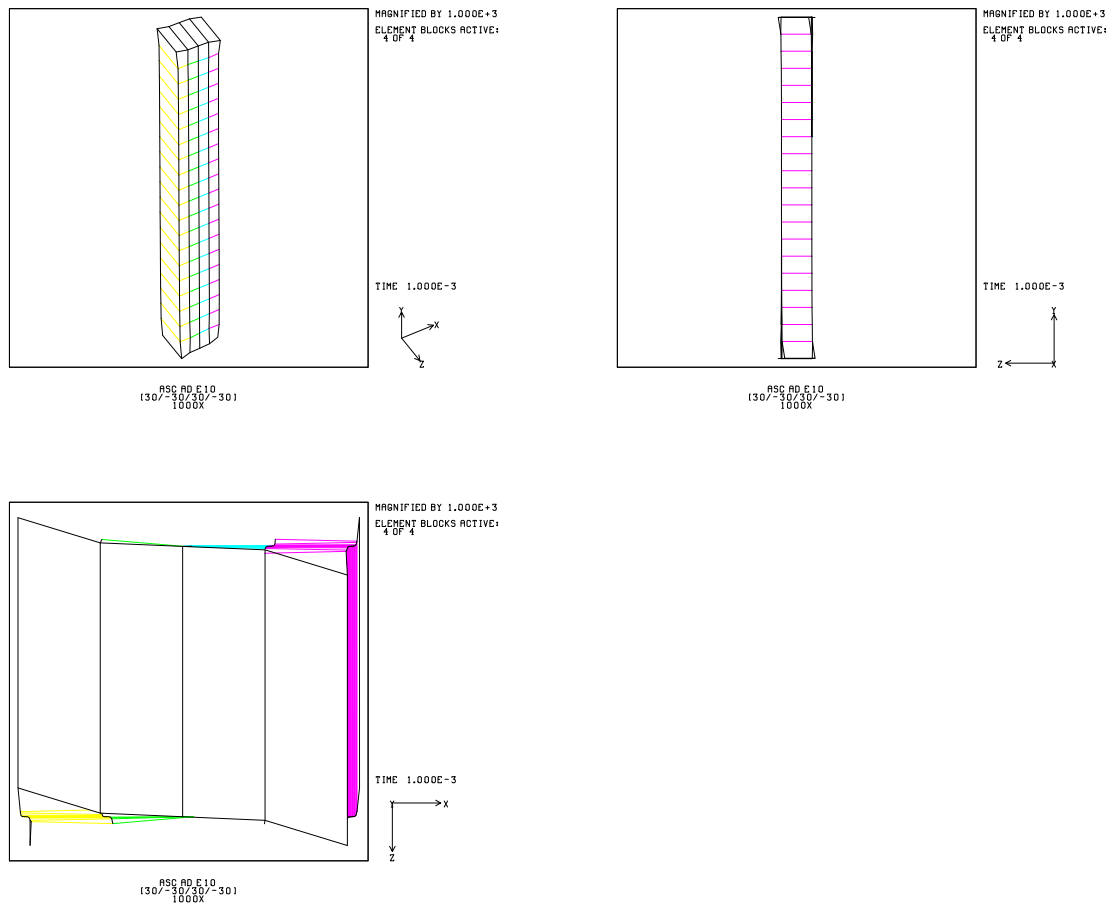
Figure 3.20: Deformed [30/-30/30/-30] Ring B continuum model showing 1 element in circumferential direction. Deformations magnified by 1000.
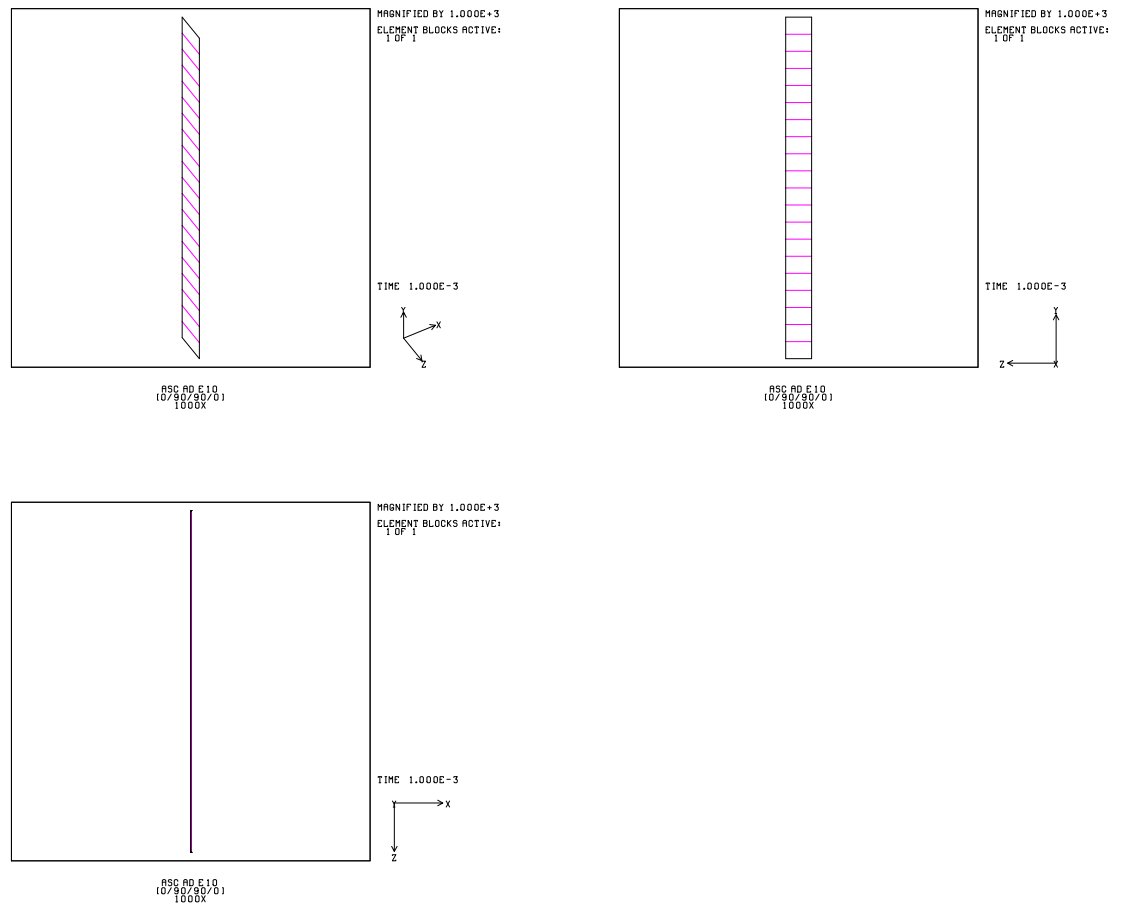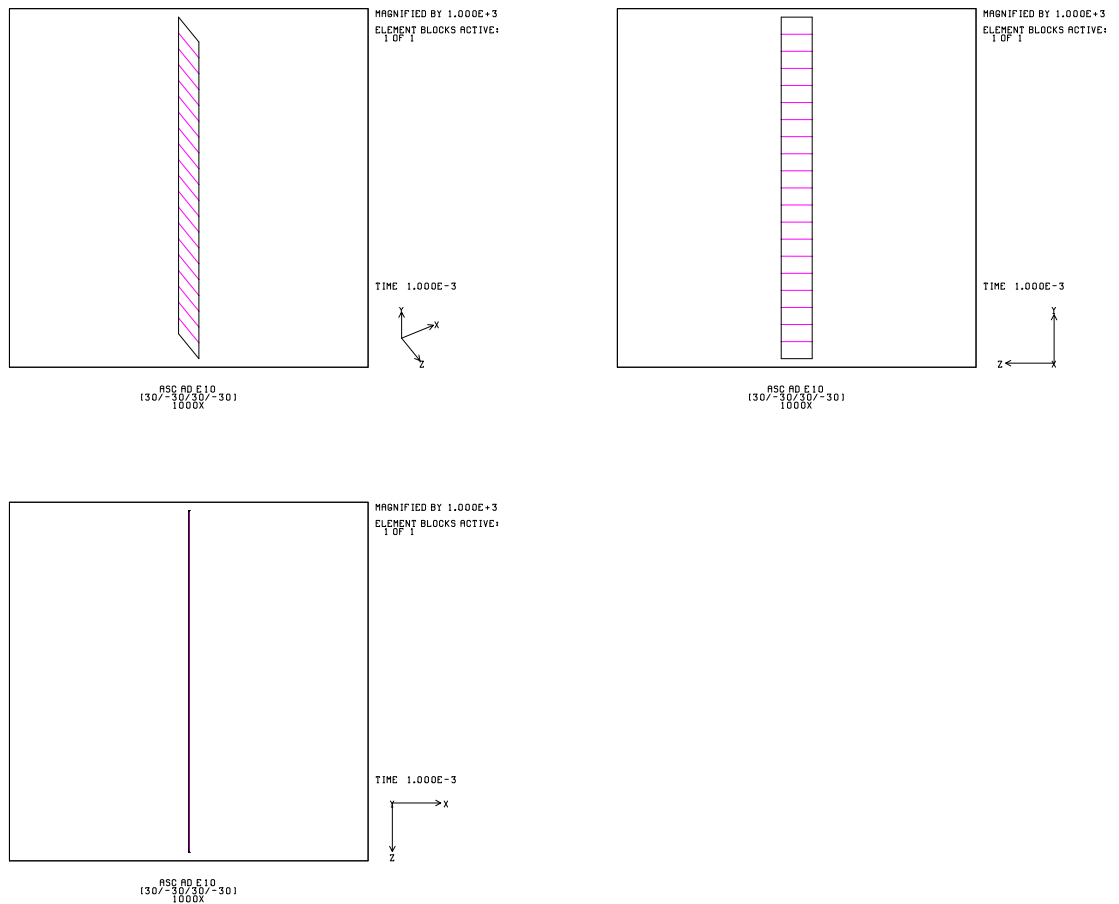
Figure 3.21: Deformed [30/-30/30/-30] Ring B shell model showing 1 element in circumferential direction. Deformations magnified by 1000.
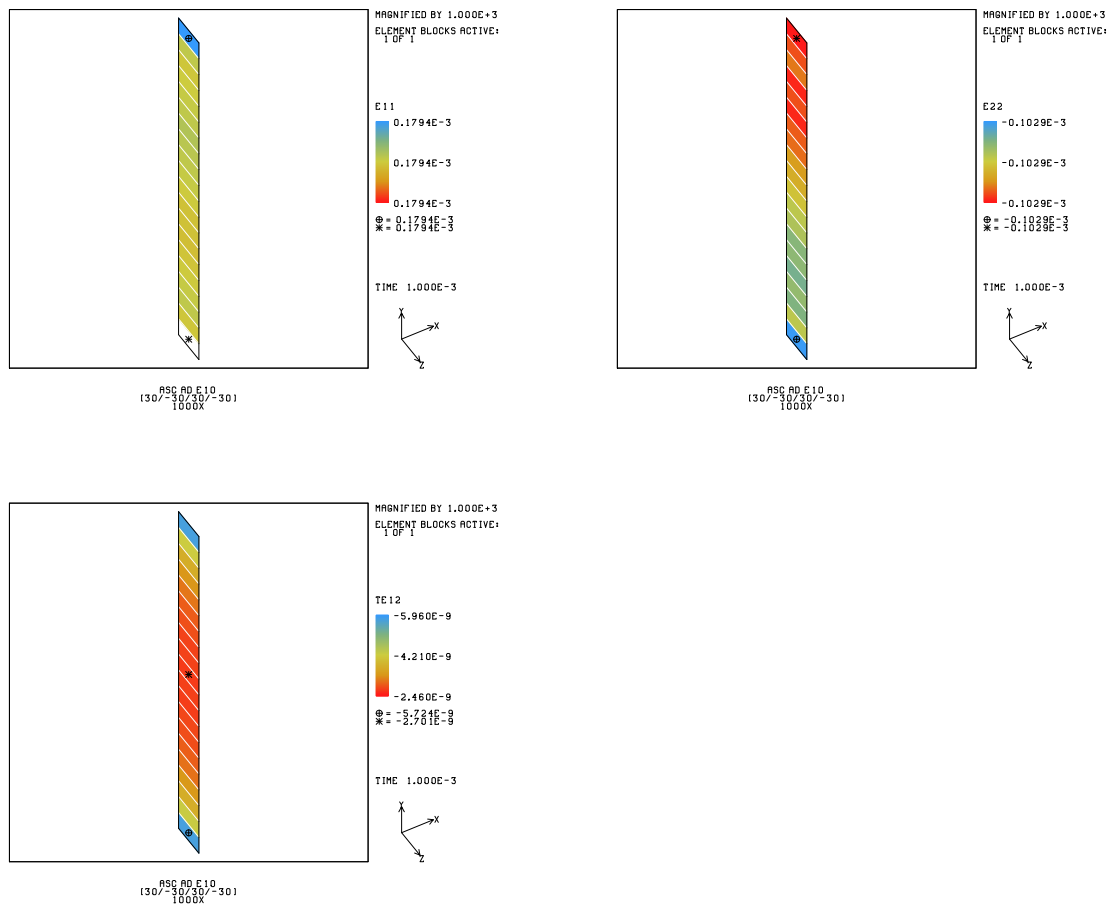
Figure 3.22: Inplane membrane strain distribution for deformed [30/-30/30/-30] Ring B shell model: (a) $e_{11} = e_{\theta\theta}$; (b) $e_{22} = e_{zz}$; (c) $2e_{12} = 2e_{\theta z}$. Deformations magnified by 1000.

MAGNIFIED BY 1.000E+3
ELEMENT BLOCKS ACTIVE:
 1 OF 1

TE23
 -7.755E-9
 -0.005E-9
 7.745E-9
⊕ = -7.509E-9
✳ = 7.494E-9

TIME 1.000E-3

ASC AD E10
[30/-30/30/-30]
1000X

MAGNIFIED BY 1.000E+3
ELEMENT BLOCKS ACTIVE:
 1 OF 1

TE31
 -0.1475E-6
 0.0025E-6
 0.1525E-6
⊕ = -0.1249E-6
✳ = 0.1303E-6

TIME 1.000E-3

ASC AD E10
[30/-30/30/-30]
1000X
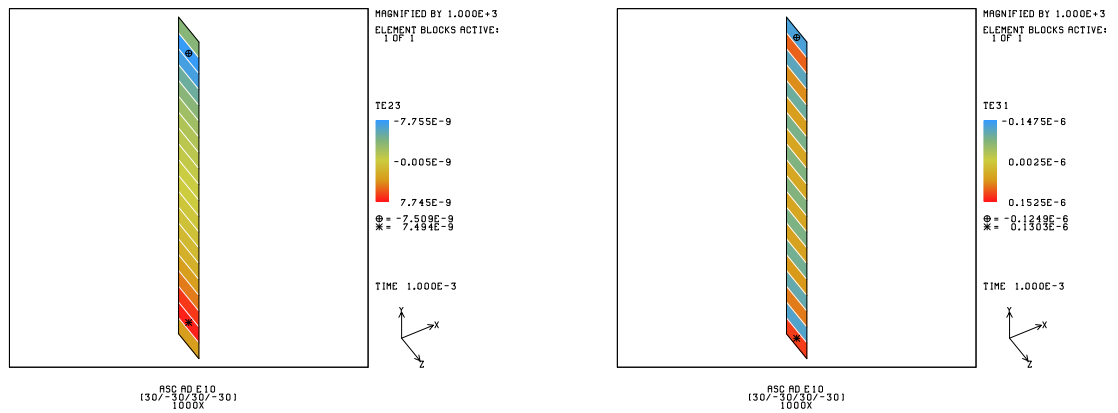
Figure 3.23: Transverse shear strain distribution for deformed [30/-30/30/-30] Ring B shell model: (a) $2e_{23} = 2e_{zr}$; (b) $2e_{31} = 2e_{r\theta}$. Deformations magnified by 1000.
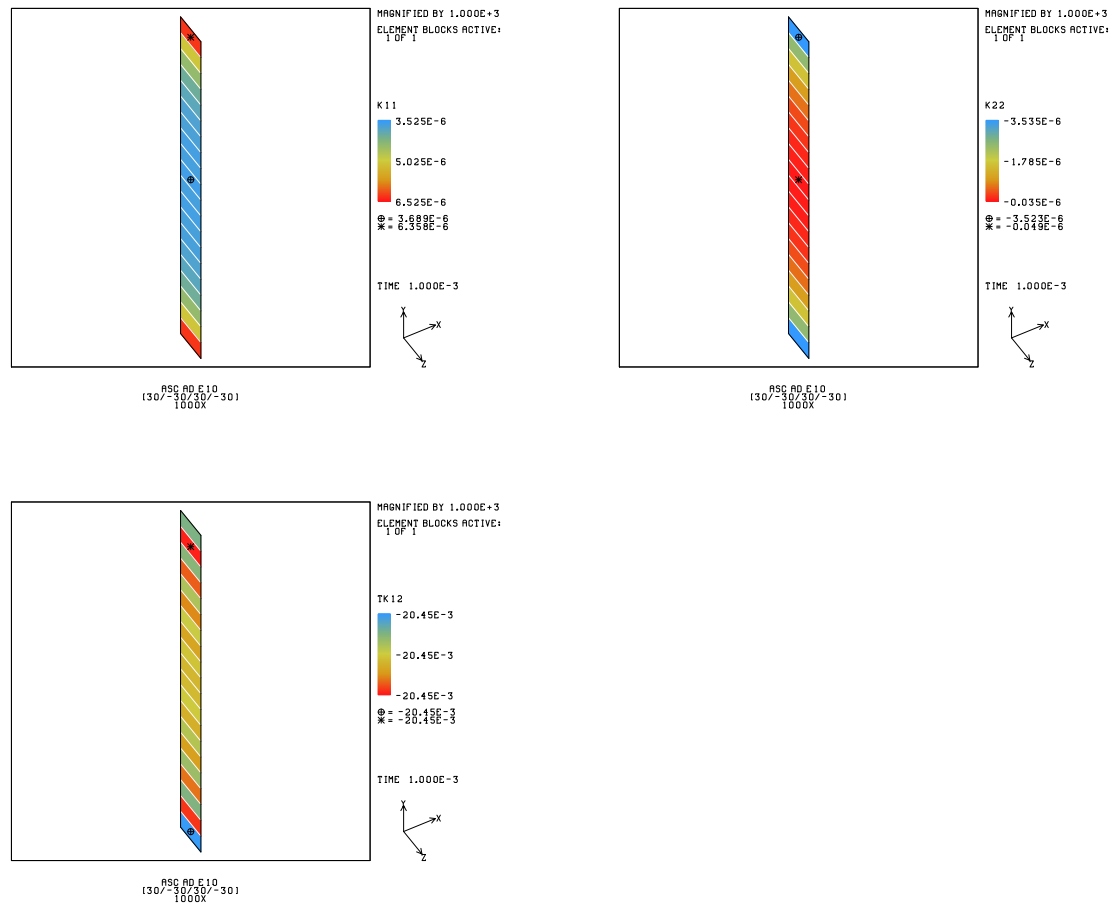
Figure 3.24: Bending strain distribution for deformed [30/-30/30/-30] Ring B shell model: (a) $\kappa_{11} = \kappa_{\theta\theta}$; (b) $\kappa_{22} = \kappa_{zz}$; (c) $2\kappa_{12} = 2\kappa_{\theta z}$. Deformations magnified by 1000.

Table 3.41: Radial Displacement at middle of inside surface for [30/60/50/10] Ring B.

Case	V_r (in.)
Cont. FEM	0.00120676
Shell FEM	0.00119091

Table 3.42: Stress $\sigma_{XX} = \sigma_{rr}$ at ring center for [30/60/50/10] Ring B.

Case	L1 (psi)	L2 (psi)	L3 (psi)	L4 (psi)
Cont. FEM	-1.056251E-01	-3.155246E-01	-5.124476E-01	-8.027225E-01
Shell FEM	-3.145848E-08	-3.403898E-08	4.433894E-08	-6.402386E-08

Table 3.43: Stress $\sigma_{YY} = \sigma_{zz}$ at ring center for [30/60/50/10] Ring B.

Case	L1 (psi)	L2 (psi)	L3 (psi)	L4 (psi)
Cont. FEM	-48.17365	-45.07275	251.1764	-157.8839
Shell FEM	-39.88367	-47.78226	252.3777	-164.6430

Table 3.44: Stress $\sigma_{ZZ} = \sigma_{\theta\theta}$ at ring center for [30/60/50/10] Ring B.

Case	L1 (psi)	L2 (psi)	L3 (psi)	L4 (psi)	AVG (psi)
Cont. FEM	657.5120	666.9631	578.9243	1292.930	799.0824
Shell FEM	635.8290	660.3647	570.6384	1289.375	789.0518

Table 3.45: Stress $\sigma_{XY} = \sigma_{zr}$ at ring center for [30/60/50/10] Ring B.

Case	L1 (psi)	L2 (psi)	L3 (psi)	L4 (psi)
Cont. FEM	-5.734813E-03	8.671496E-03	1.301813E-02	-3.997555E-03
Shell FEM	-1.289170E-03	-1.432853E-03	3.417504E-03	-3.304830E-03

Table 3.46: Stress $\sigma_{YZ} = -\sigma_{\theta z}$ at ring center for [30/60/50/10] Ring B.

Case	L1 (psi)	L2 (psi)	L3 (psi)	L4 (psi)
Cont. FEM	-324.1679	370.4191	161.0073	-207.2136
Shell FEM	-296.3977	370.9121	140.9399	-215.4537

Table 3.47: Stress $\sigma_{ZX} = -\sigma_{r\theta}$ at ring center for [30/60/50/10] Ring B.

Case	L1 (psi)	L2 (psi)	L3 (psi)	L4 (psi)
Cont. FEM	-9.231838E-03	-3.510736E-03	-7.435843E-04	2.587843E-02
Shell FEM	7.039402E-06	1.077726E-02	7.067532E-03	1.297668E-03

Table 3.48: Computational cost for [30/60/50/10] Ring B.

| Case	Model	Elements	Nodes	DOF w/o BC	Iterations	CPU (sec)
Cont. FEM	0.5 deg	800	1155	3465	1341	17.459
Shell FEM	0.5 deg	200	231	1386	50,173	325.040
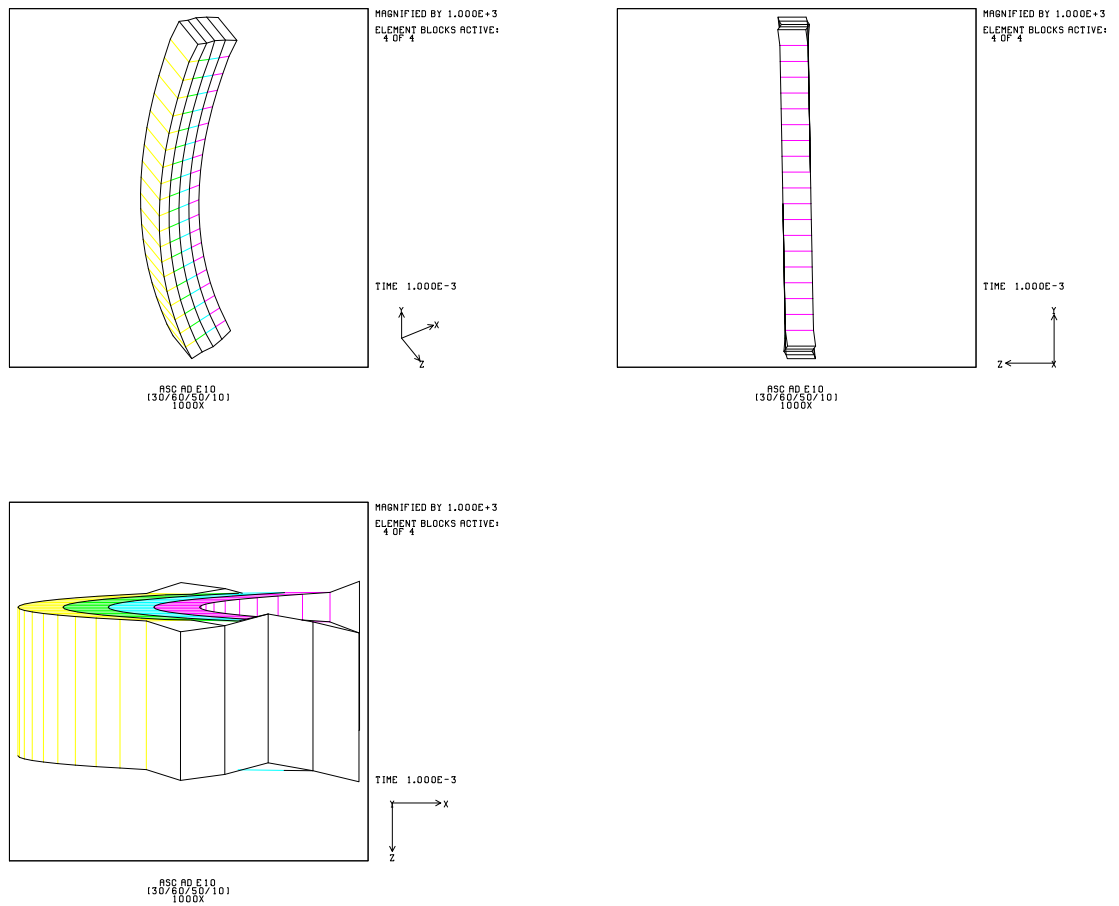
Figure 3.25: Deformed [30/60/50/10] Ring B continuum model showing 1 element in circumferential direction. Deformations magnified by 1000.
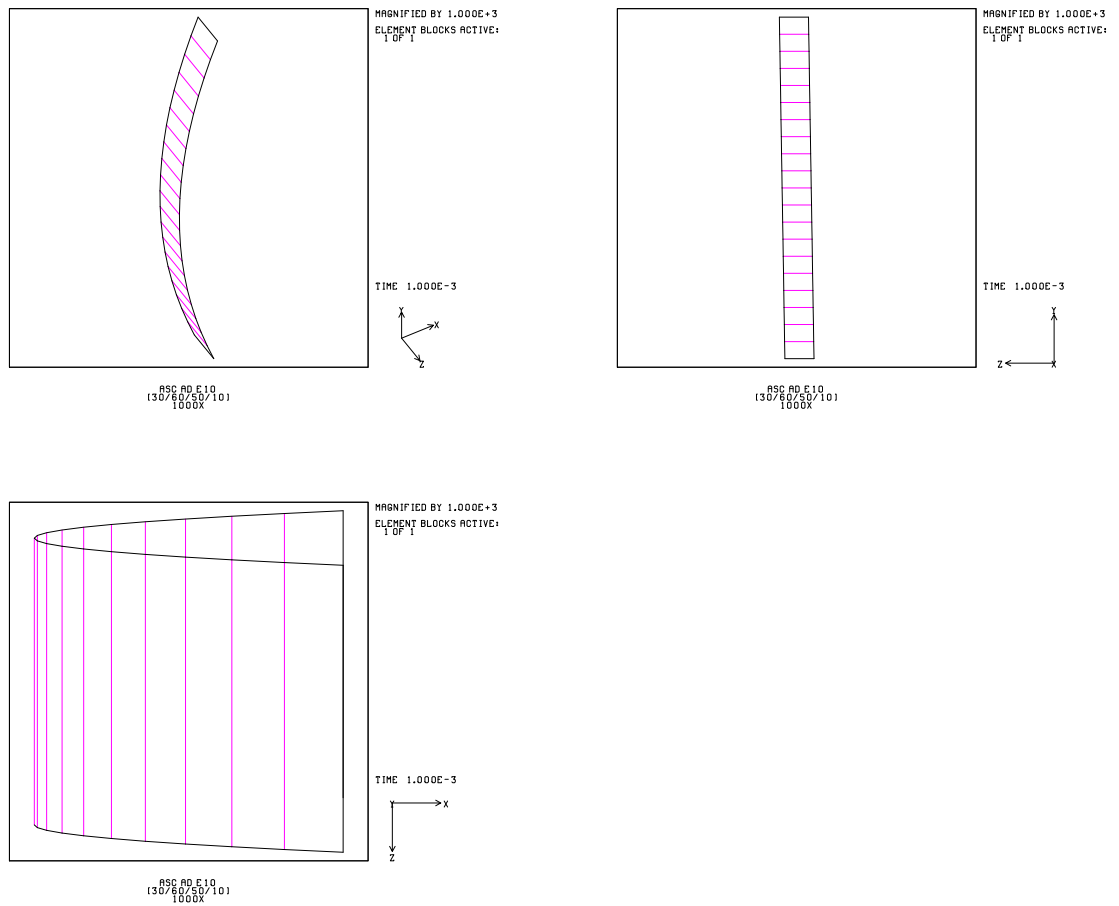
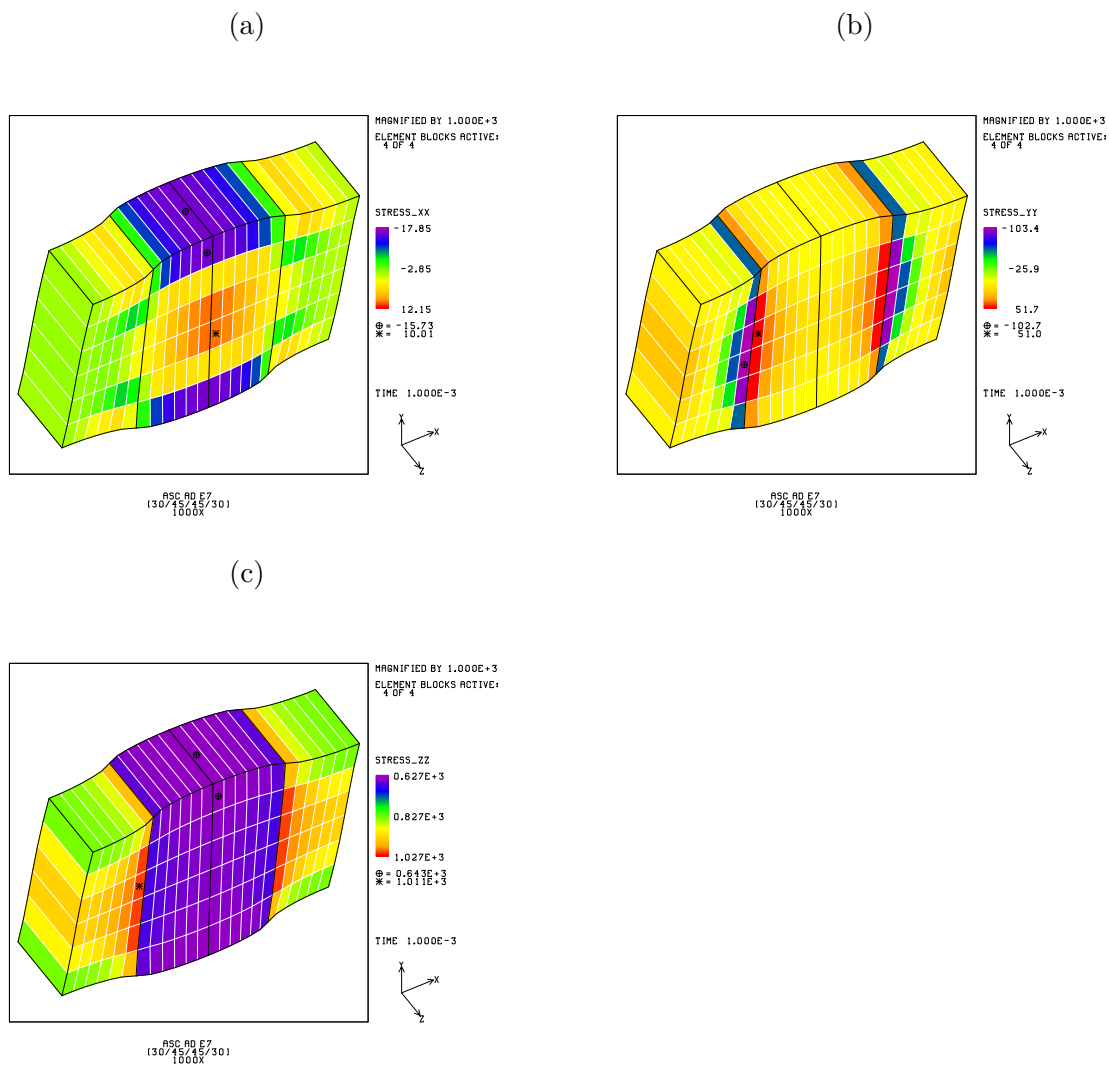Figure 3.26: Deformed [30/60/50/10] Ring B shell model showing 1 element in circumferential direction. Deformations magnified by 1000.

4 Composite Containers

4.1 Problem Definition

In order to demonstrate the ability of ADAGIO to solve large problems involving composites, a composite container will be analyzed under internal pressure, thermal loads, and mechanical loading. The undeformed cylindrical container geometry is shown in Figure 4.1. Although a more realistic composite container would have portions made of metal, the container problem defined here is fully composed of a 4-ply laminated composite, except for the isotropic brackets near the symmetry plane at the center of the structure. Furthermore, a realistic container would also have rounded corners in the end caps instead of the sharp corners modeled here. Nevertheless, the chosen geometry is valid for demonstration purposes.

Each of the four layers in the composite has a thickness of 0.025" (0.0635 cm) for a total thickness of 0.1" (0.254 cm). Similar to the composite rings, the following material properties are chosen for each layer:

$$E_{11} = 64.03 \text{ GPa} \tag{4.1}$$

$$E_{22} = 55.50 \text{ GPa} \tag{4.2}$$

$$E_{33} = 9.78 \text{ GPa} \tag{4.3}$$

$$\nu_{12} = 0.081 \tag{4.4}$$

$$\nu_{23} = 0.303 \tag{4.5}$$

$$\nu_{31} = 0.0462805 \tag{4.6}$$

$$G_{12} = G_{23} = G_{31} = 4.45 \text{ GPa} \tag{4.7}$$

$$\alpha_{11} = \alpha_{22} = 1 \text{ ppm/}^\circ\text{C} \tag{4.8}$$

$$\alpha_{33} = 30 \text{ ppm/}^\circ\text{C} \tag{4.9}$$

The following stacking sequences are used: a symmetric cross-ply sequence of [0/90/90/0], a symmetric lay-up of [30/45/45/30], and an antisymmetric angle-ply arrangement of [30/ − 30/30/ − 30]. Here the first layer is the outermost layer of the structure, whereas the fourth layer is the innermost layer. In the cylindrical side-walls, a 0° fiber angle corresponds to the circumferential direction and a 90° fiber angle corresponds to the axial direction. Likewise, for the end caps, the 0° fiber angle

R = 7.908" (20.086 cm)
L_1 = 1.768" (4.491 cm)
L_2 = 4.175" (10.605 cm)
L_3 = 1.0" (2.54 cm)
H_1 = 15.513" (39.403 cm)
H_2 = 1.175" (2.985 cm)
H_3 = 1" (2.54 cm)
H_4 = 2.04" (5.182 cm)
t_1 = 0.1" (0.254 cm)
t_2 = 0.2" (0.508 cm)
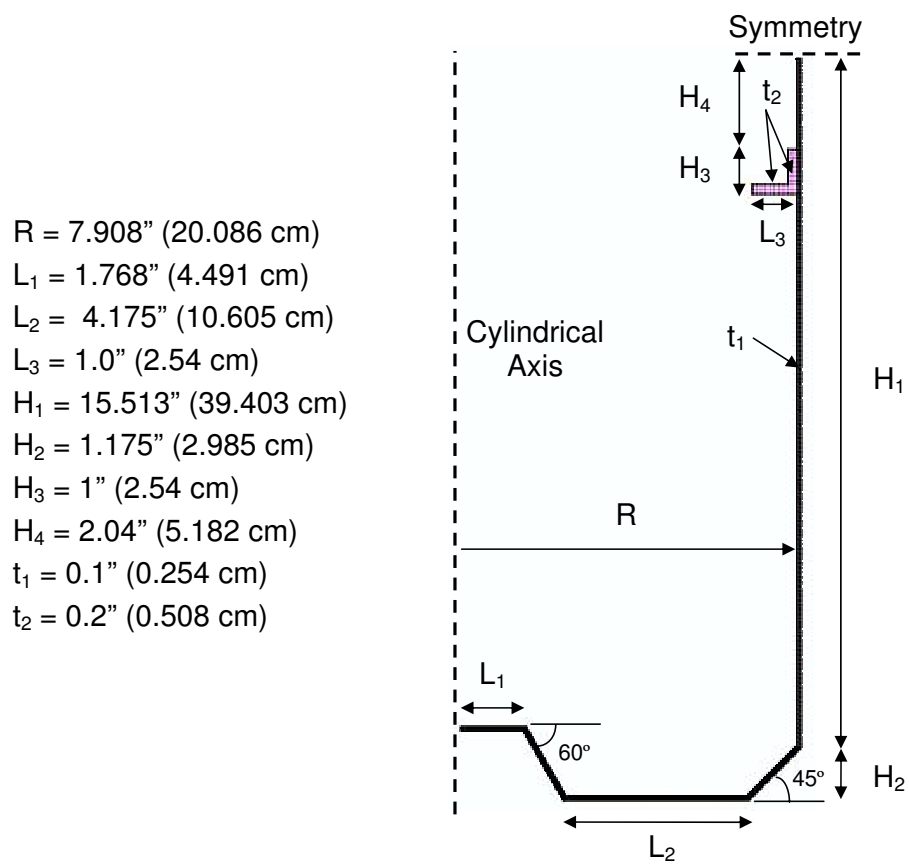
Figure 4.1: Composite container geometry.

corresponds to the circumferential direction. For the horizontal portions of the end caps, a 90° fiber angle gives fiber aligned in the radial direction. Finally, for the non-horizontal portions of the end caps (the -60° and 45° segments), a 90° fiber direction is perpendicular to the circumferential direction, but parallel to the local container surface. Once again, other fiber angles can be determined by a simple rotation in the plane defined by the 0° and 90° fiber directions. The isotropic brackets to which the mechanical load will be applied are taken to have a Youngs modulus of 64.03 GPa, a shear modulus of 24.6 GPa, and a coefficient of thermal expansion of 11.7 ppm/C.

Finally, in order to produce a usable mesh using SEACAS based tools, a small hole is drilled in the center of the end cap. This hole is small and no radial displacements are applied to its edge such that it is equivalent to having a small plug of infinite stiffness in the radial direction. Although other meshing schemes could have been used where this step would have not been required, those schemes are not as straightforward as the one used here where a 2D cross-section is used to sweep out the full 3D geometry.

Both continuum and combined shell/continuum approaches will be used to analyze the composite container response. Because one purpose of this project is to demonstrate the solution of composite problems using parallel processing, the entire 360° structure is modeled, as periodic boundary conditions were not parallel aware in ADAGIO at the time these of analyses. For the purely continuum models, a mesh with a total of 467,520 elements and 585,840 nodes is used. With each continuum node having 3 degrees-of-freedom (DOF), the continuum model possesses a total of 1,757,520 DOF before the application of boundary conditions. The combined shell/continuum approach consists of modeling all of the composite parts (everything but the brackets) with shell elements and using continuum elements for the brackets. The combined continuum/shell approach uses a mesh with 123,360 elements and 126,000 nodes. With each shell node having 6 DOF (three translations and three rotations), a total of 722,742 DOF are used in the combined shell/continuum approach, not counting the reduction in DOF from the application of boundary conditions. Note that when the 4-layer composite is modeled using continuum elements, it is necessary to use a minimum of 4 elements through the thickness (the approach chosen here) with orthotropic properties input for each layer, whereas for the shell modeling, a single element can be used to represent the entire lay-up with the laminate matrices input directly. Although

using 1 element per layer is the minimum requirement for modeling composites using continuum elements, it may be necessary to use more elements to adequately capture all aspects of the composite response, such as bending effects in and around various geometric features.

4.2 Response of Composite Containers to Pressure, Thermal, and Mechanical Loadings

The composite containers are subjected to an internal pressurization of 1 psi (6894 Pa), followed by a 18 °F (10 °C) temperature change, and finally a 0.027 psi (187.69 Pa) distributed loading on the horizontal surface of the load bracket shown in Figure 4.1. The distributed loading of 0.027 psi corresponds to a 1 lb force subjected over the 36.734 in^2 horizontal surface area of the load bracket. Recall that symmetry boundary conditions are used at the top of the geometry shown in Figure 4.1 such that the final results include the effects of loading on a lower bracket (shown) and an upper bracket (not shown). Each of the three types of loads are ramped-up linearly over a specified time range and then held constant for the rest of the analysis. The internal pressurization increases from zero to its final value over the first 0.001 sec, the thermal loading is applied from 0.0001 to 0.0005 sec, and finally the distributed mechanical loading of the bracket is ramped-up over 0.0005 sec to 0.001 sec. A total of 1000 time steps are used for applying the internal pressurization, while 500 time steps are used for applying both the thermal and mechanical loadings for a total of 2000 time steps. It is unknown how close to optimality such a time stepping scenario is to one requiring the least CPU usage. Note that the time variable here is used as the means to control the loadings and that the composite response at any given load level is time independent, as only linear elastic models are being employed.

The parallel finite element runs were performed using Sandia's Rogue Linux cluster. A summary of the number of processors used and the total CPU time expended for each analysis is provided in Table 4.1. Most jobs were run in the slower Serial queue of Rogue. The shell analyses were attempted using the probe nodal preconditioner. For this preconditioner, only the [0/90/90/0] container problem was able to be converged. Additional preliminary attempts to simulate the [30/45/45/30] and [30/-30/30/-30] containers using the full tangent preconditioner with FETI linear solver

Table 4.1: CPU usage for composite container analyses.

Stacking Sequence	Model[+]	Elements	Nodes	DOF	Rogue Queue	No. of CPU	Total CPU Time (hr)
[0/90/90/0]	C	467,520	585,840	1,757,520	Serial	36	2552
[30/45/45/30]	C	467,520	585,840	1,757,520	Scico	36	3460*
[30/−30/30/−30]	C	467,520	585,840	1,757,520	Serial	36	2700
[0/90/90/0]	S/C	123,360	126,000	722,742	Serial	36	1560
[30/45/45/30]	S/C	123,360	126,000	722,742	–	–	–
[30/−30/30/−30]	S/C	123,360	126,000	722,742	–	–	–

[+] C = continuum, S = shell,

  S/C = shell for all composite walls, continuum for load bracket

 *Estimated (some data lost due to restart)

were unsuccessful.

Figures 4.2-4.5 show the deformed cross-sections. Note that the deformations in those figures have been multiplied by ten to aid viewing. Similar deformations result in each case. It can be observed that much of the displacements in the end cap result from bending response at the intersection of the various structural segments. Figures 4.6-4.8 show contour plots of the von Mises stresses for the purely continuum models on a layer-by-layer basis. These von Mises stress distributions are comparable for the stacking sequences considered. However, it is likely that the distribution in the actual tensor components of the stress differ for each stacking sequence.

Figures 4.9-4.14 show the layerwise stress results due only to internal pressurization for the [0/90/90/0] container modeled using solely continuum elements, whereas Figures 4.15-4.20 give the corresponding layerwise stress results when shell elements are used for everything except the load bracket. Note that the load bracket is not shown in any of these figures for convenience. The agreement in the minimum and maximum stresses between the two approaches are better for the outermost and in-
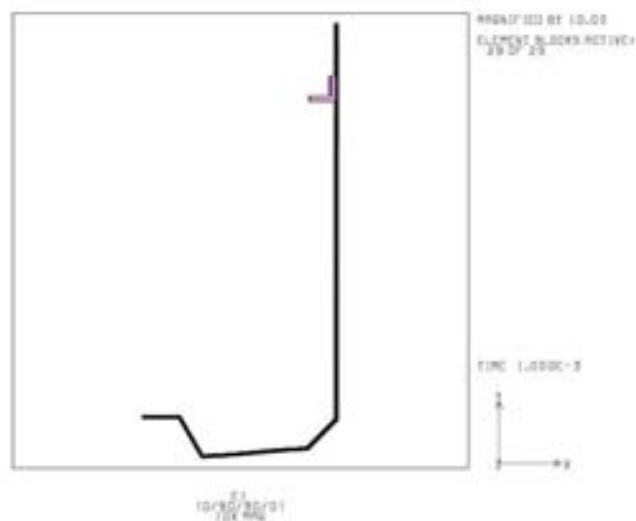
Figure 4.2: Cross sectional view of composite container with [0/90/90/0] lay-up modeled using only continuum elements with 10X mag. of final displacements.

nermost layers than for the inner two layers. These peaks and valleys in the stress distributions occur at the corners between the various container segments where there is significant bending. Hence, one possible explanation for the better agreement in stresses on the outer and inner layers is that bending effects dominate in these regions, the outermost and innermost layers naturally have higher bending strains than the inner two layers, and the shell model is able to capture these bending effects fairly well. A complete explanation requires additional study which was not possible under the time constraints of this project.
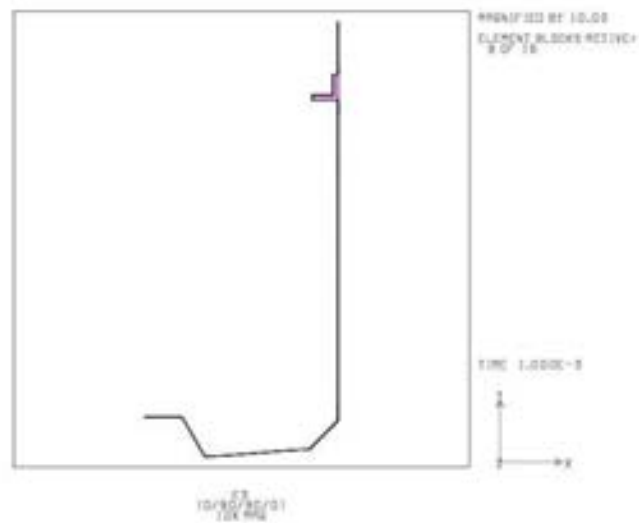
Figure 4.3: Cross sectional view of composite container with [0/90/90/0] lay-up modeled using only primarily shell elements with 10X mag. of final displacements.
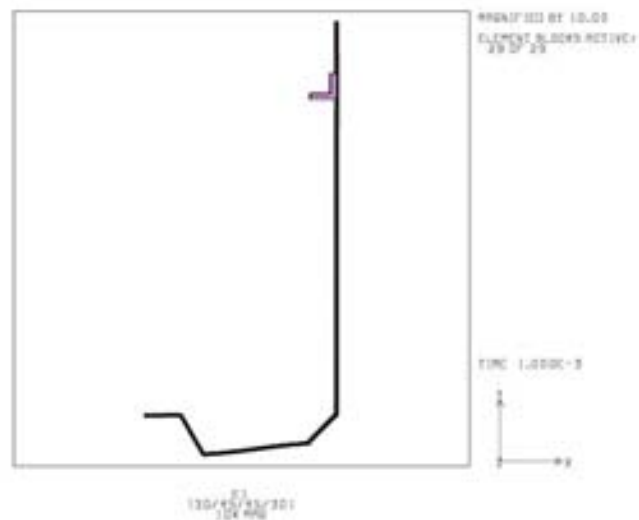
Figure 4.4: Cross sectional view of composite container with [30/45/45/30] lay-up modeled using only continuum elements with 10X mag. of final displacements.
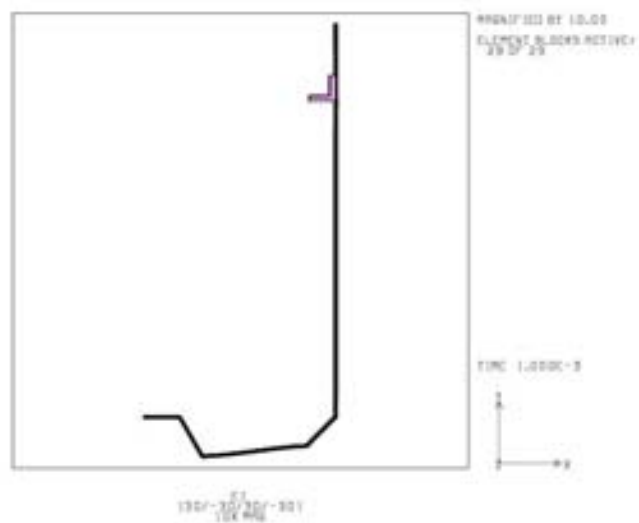
Figure 4.5: Cross sectional view of composite container with [30/-30/30/-30] lay-up modeled using only continuum elements with 10X mag. of final displacements.

74
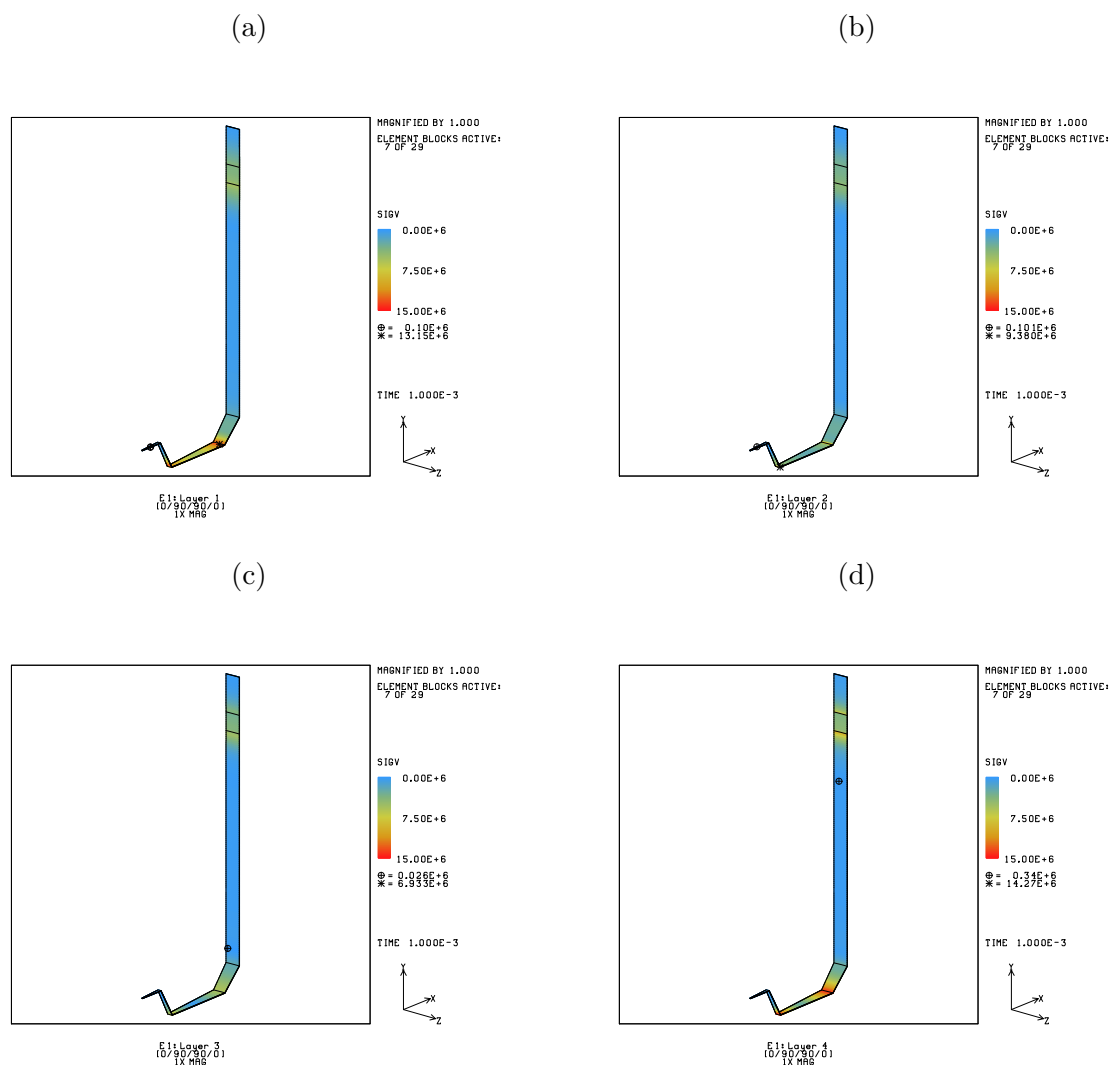
Figure 4.6: von Mises stresses due to internal pressurization, thermal loading, and mechanical loading for the [0/90/90/0] container modeled using only continuum elements: (a) layer 1 (outermost layer); (b) layer 2; (c) layer 3; (d) layer 4 (innermost layer).

(a) (b)

(c) (d)
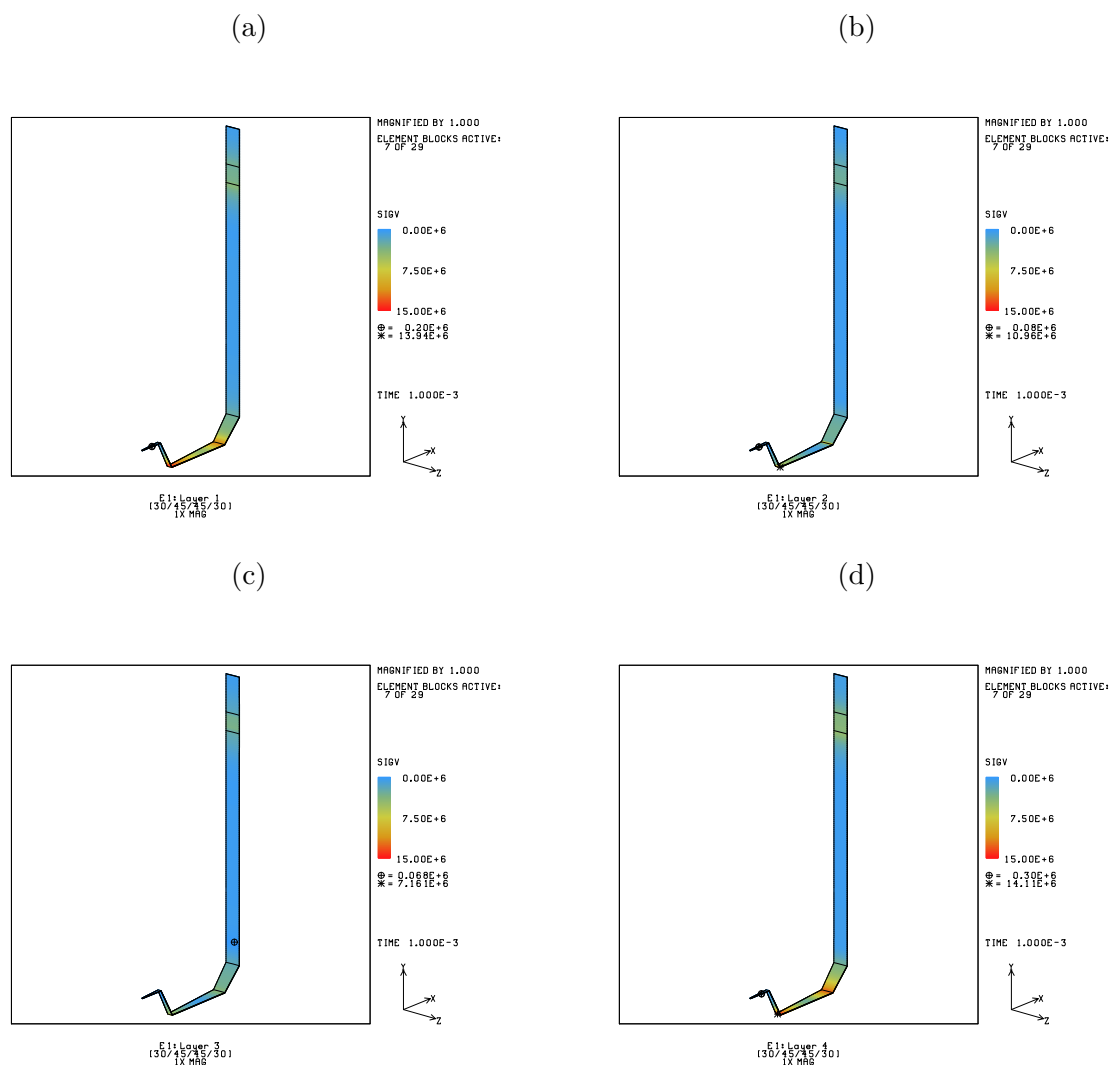
Figure 4.7: von Mises stresses due to internal pressurization, thermal loading, and mechanical loading for the [30/45/45/30] container modeled using only continuum elements: (a) layer 1 (outermost layer); (b) layer 2; (c) layer 3; (d) layer 4 (innermost layer).

(a) (b)

(c) (d)
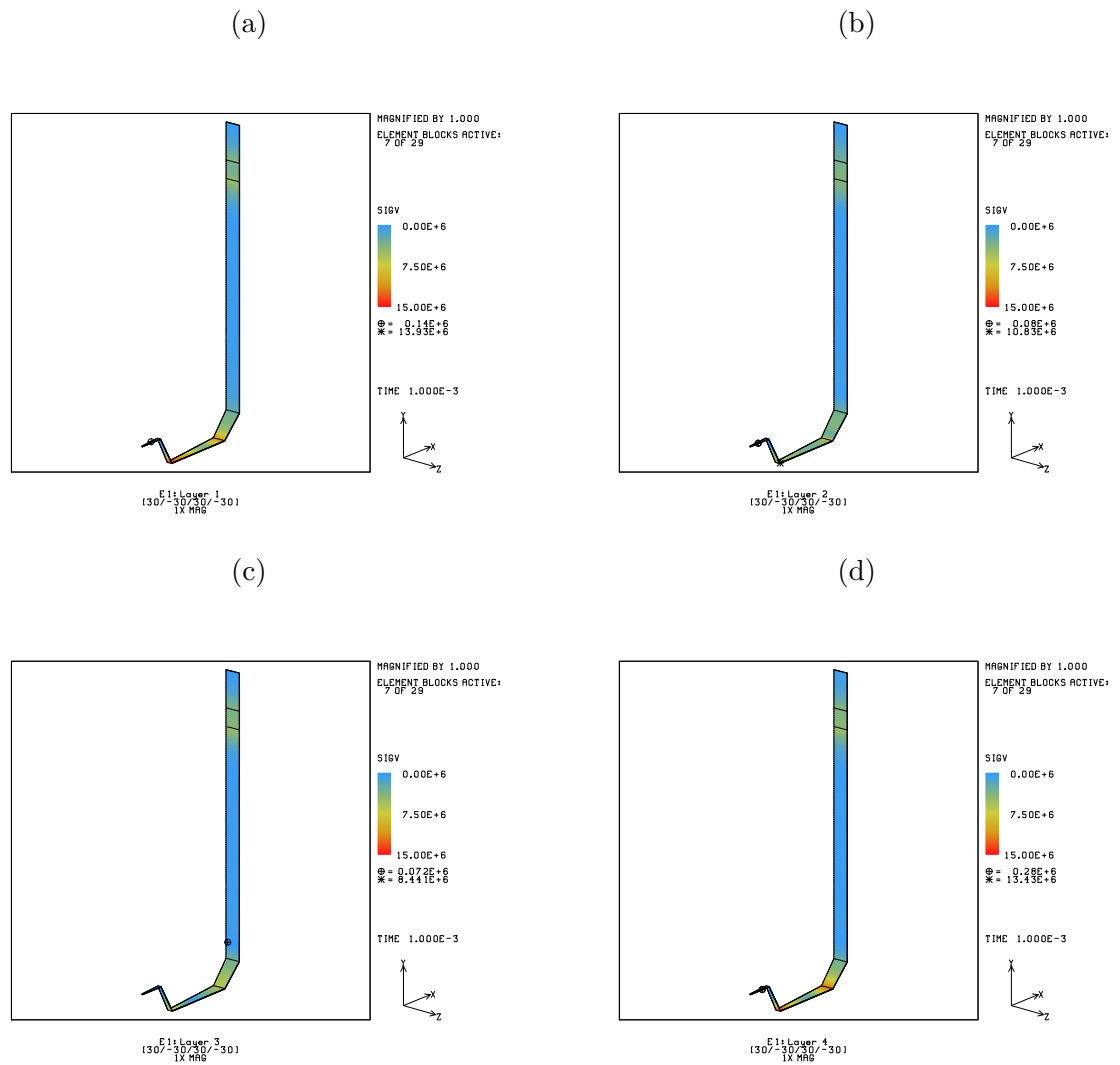
Figure 4.8: von Mises stresses due to internal pressurization, thermal loading, and mechanical loading for the [30/-30/30/-30] container modeled using only continuum elements: (a) layer 1 (outermost layer); (b) layer 2; (c) layer 3; (d) layer 4 (innermost layer).

(a)

(b)

(c)

(d)
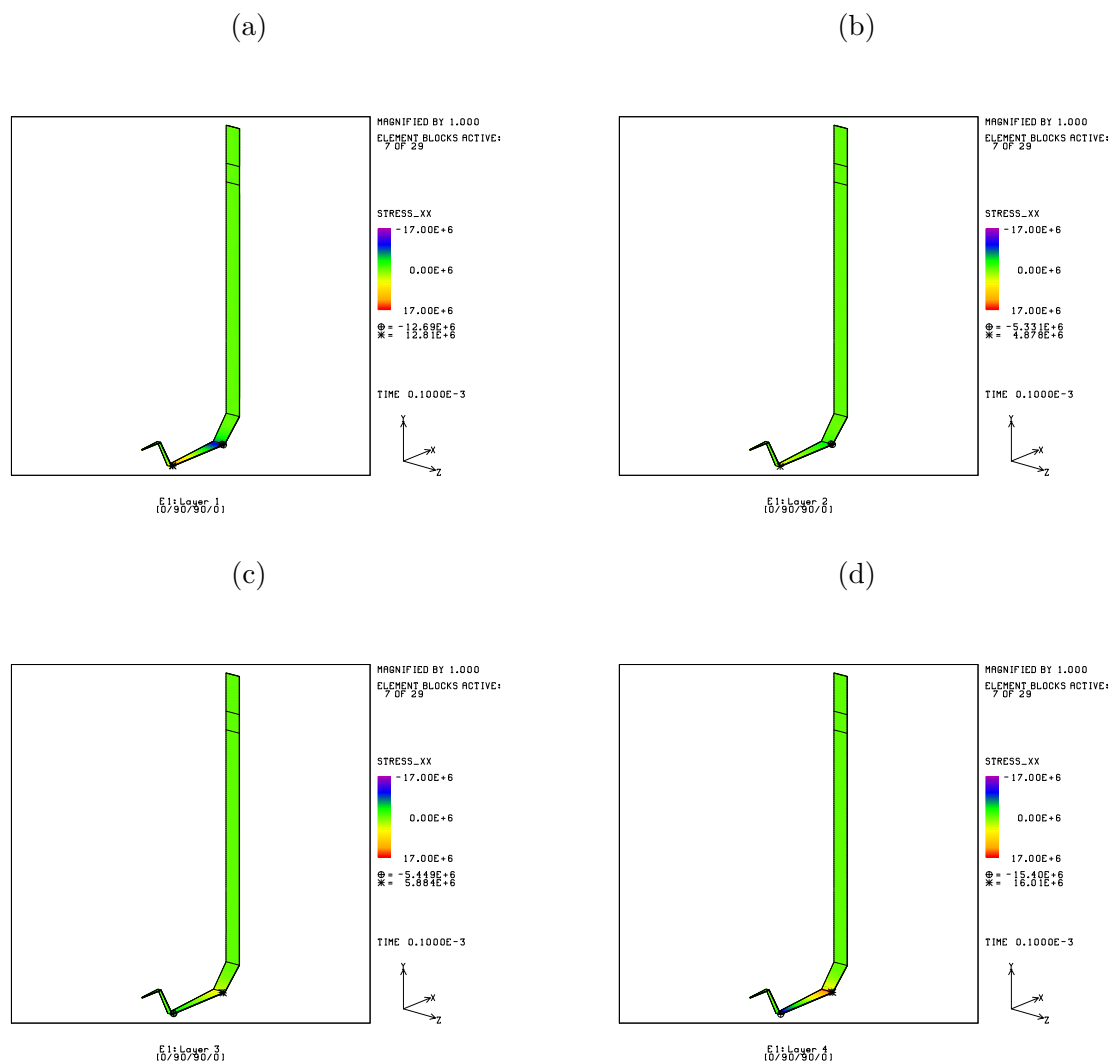
Figure 4.9: Radial stresses due to internal pressurization for the [0/90/90/0] container modeled using only continuum elements: (a) layer 1 (outermost layer); (b) layer 2; (c) layer 3; (d) layer 4 (innermost layer).
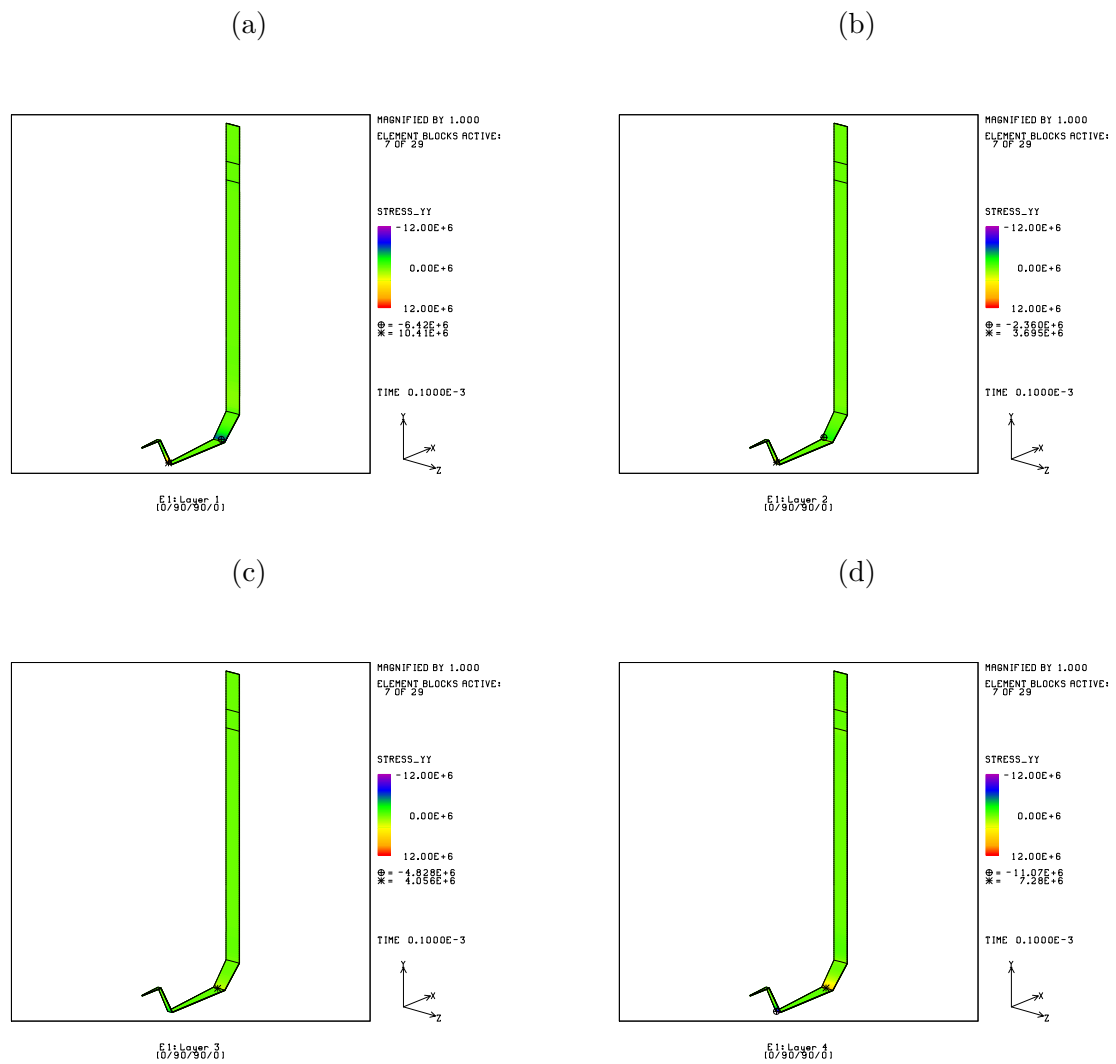
Figure 4.10: Axial stresses due to internal pressurization for the [0/90/90/0] container modeled using only continuum elements: (a) layer 1 (outermost layer); (b) layer 2; (c) layer 3; (d) layer 4 (innermost layer).

(a) (b)

(c) (d)
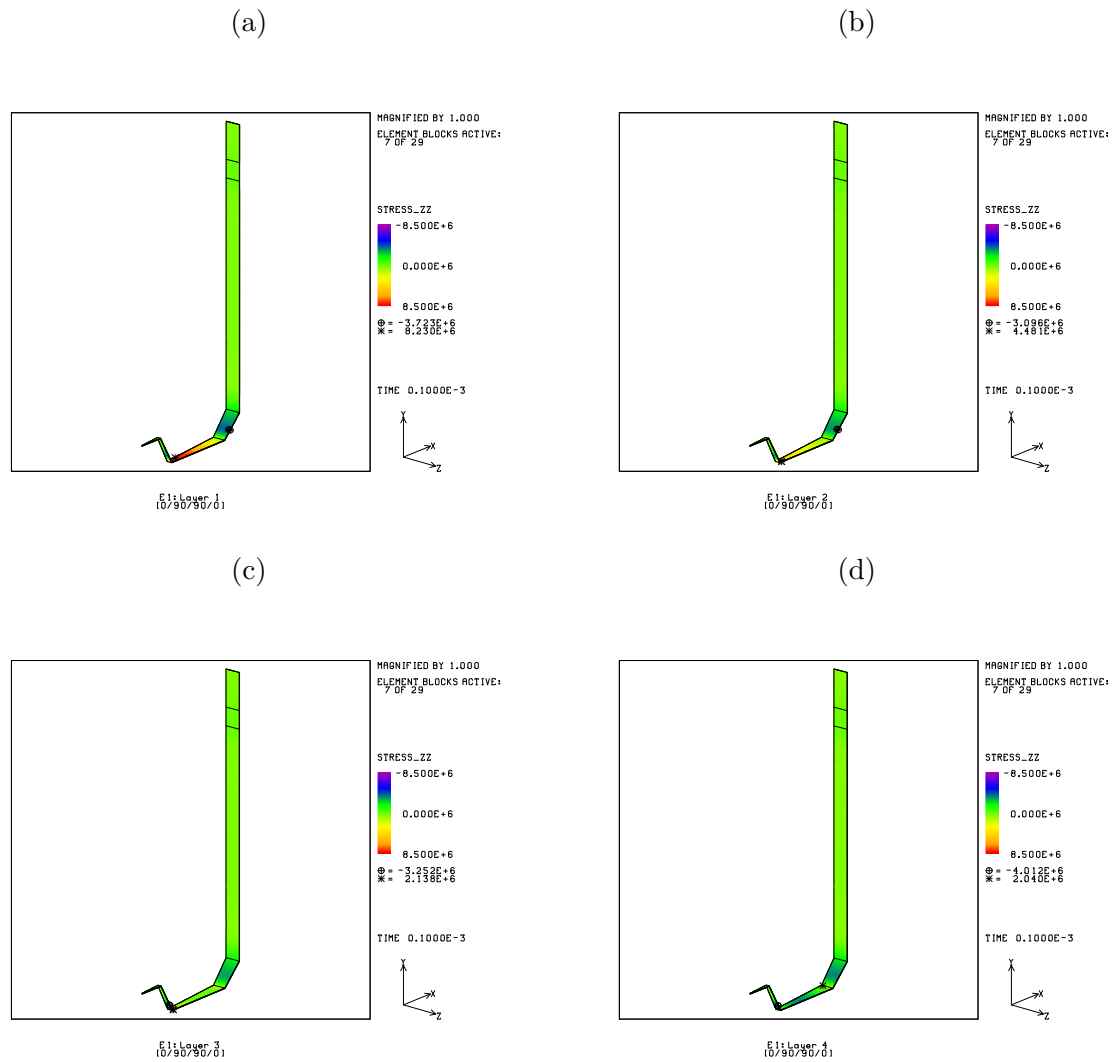
Figure 4.11: Circumferential stresses due to internal pressurization for the [0/90/90/0] container modeled using only continuum elements: (a) layer 1 (outermost layer); (b) layer 2; (c) layer 3; (d) layer 4 (innermost layer).
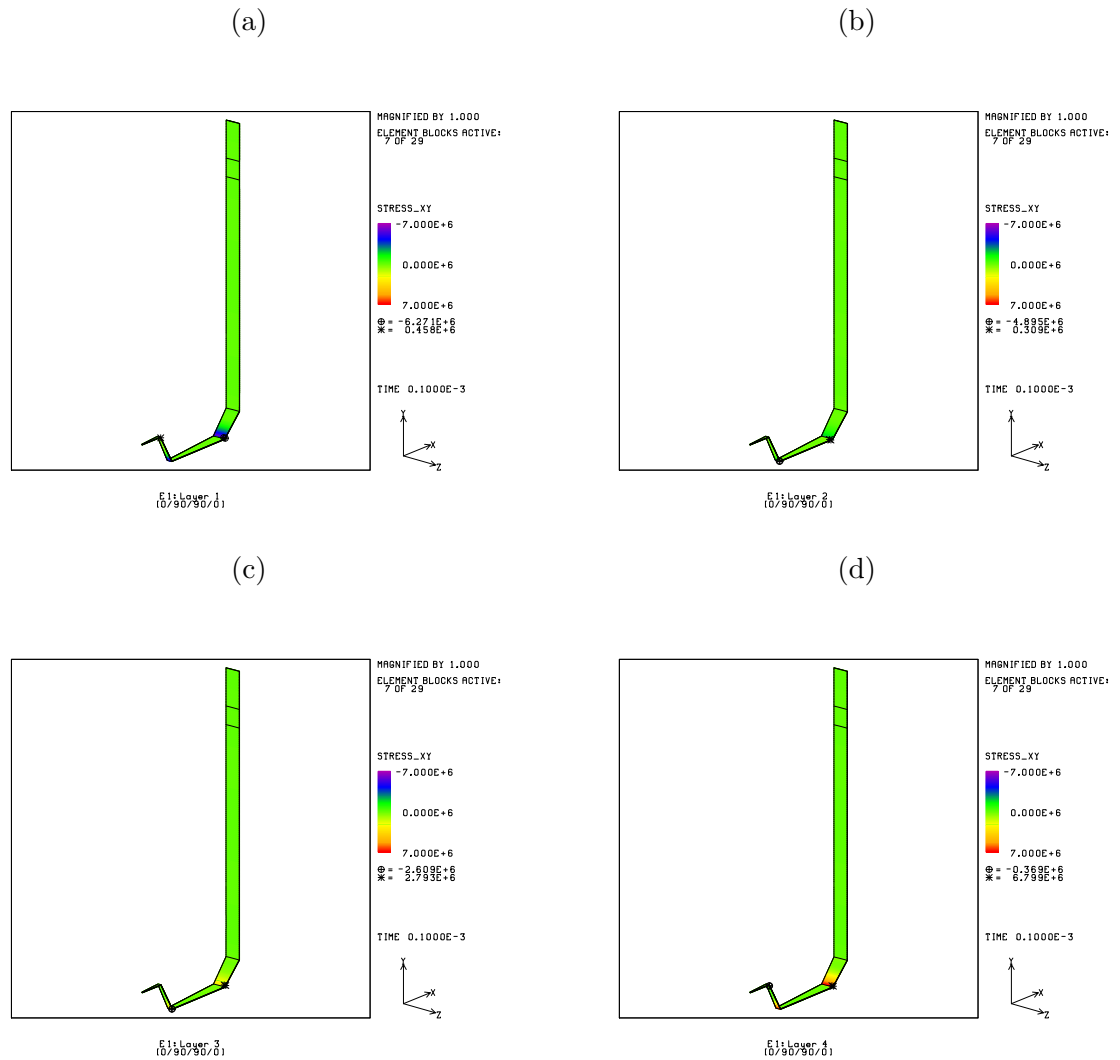
Figure 4.12: Radial-axial shear stresses due to internal pressurization for the [0/90/90/0] container modeled using only continuum elements: (a) layer 1 (outermost layer); (b) layer 2; (c) layer 3; (d) layer 4 (innermost layer).
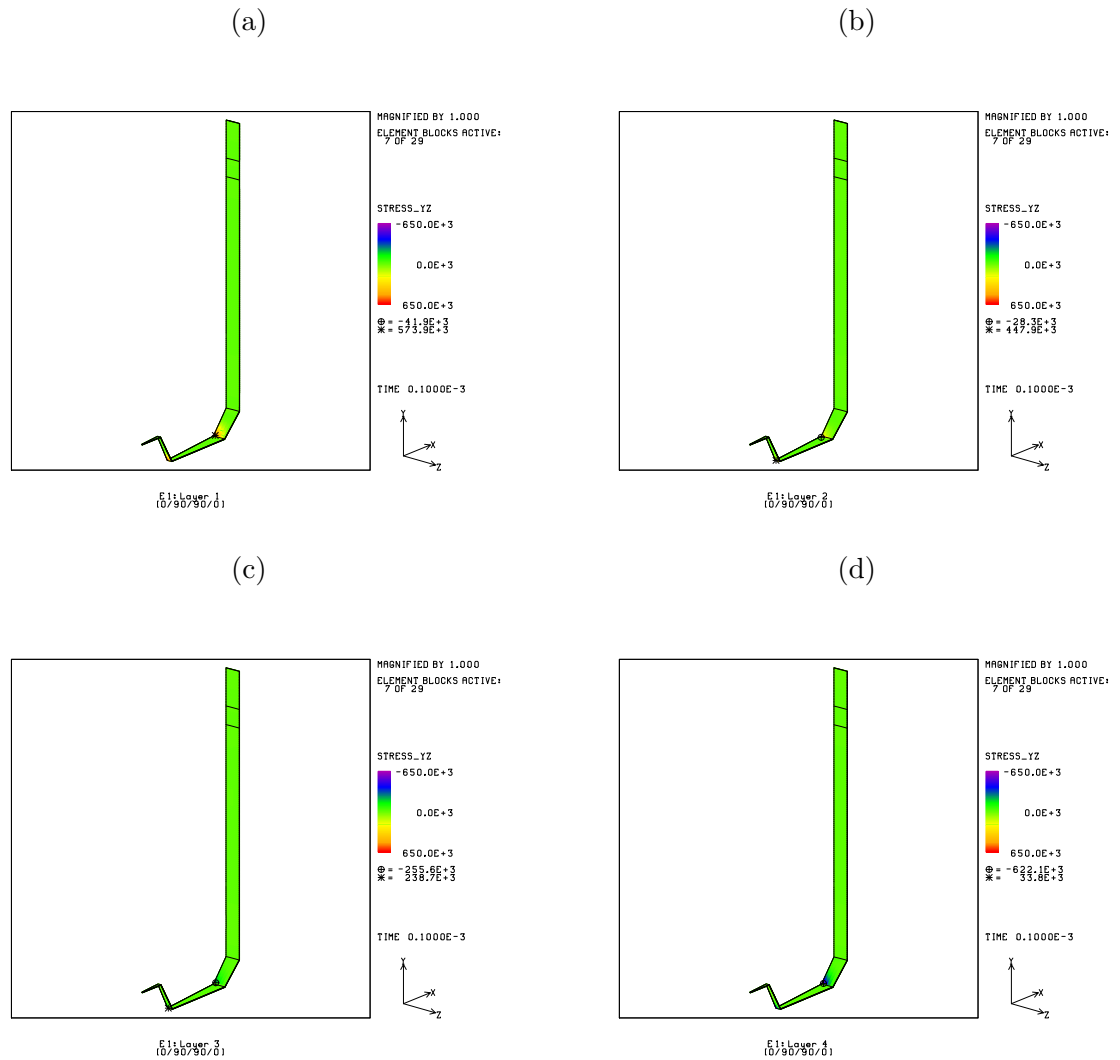
Figure 4.13: Negative of axial-circumferential shear stresses due to internal pressurization for the [0/90/90/0] container modeled using only continuum elements: (a) layer 1 (outermost layer); (b) layer 2; (c) layer 3; (d) layer 4 (innermost layer).
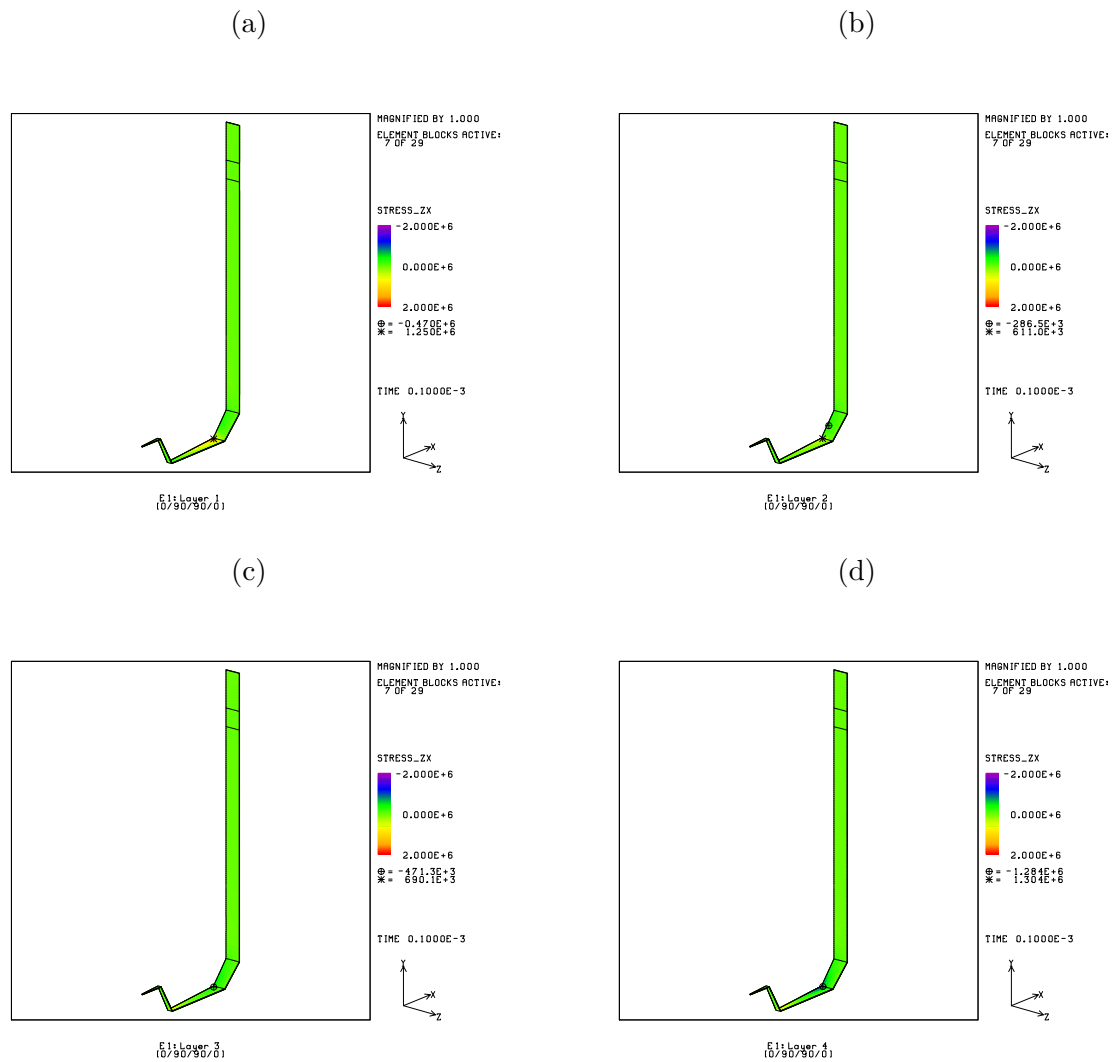
Figure 4.14: Negative of circumferential-radial shear stresses due to internal pressurization for the [0/90/90/0] container modeled using only continuum elements: (a) layer 1 (outermost layer); (b) layer 2; (c) layer 3; (d) layer 4 (innermost layer).

(a)   (b)

(c)   (d)
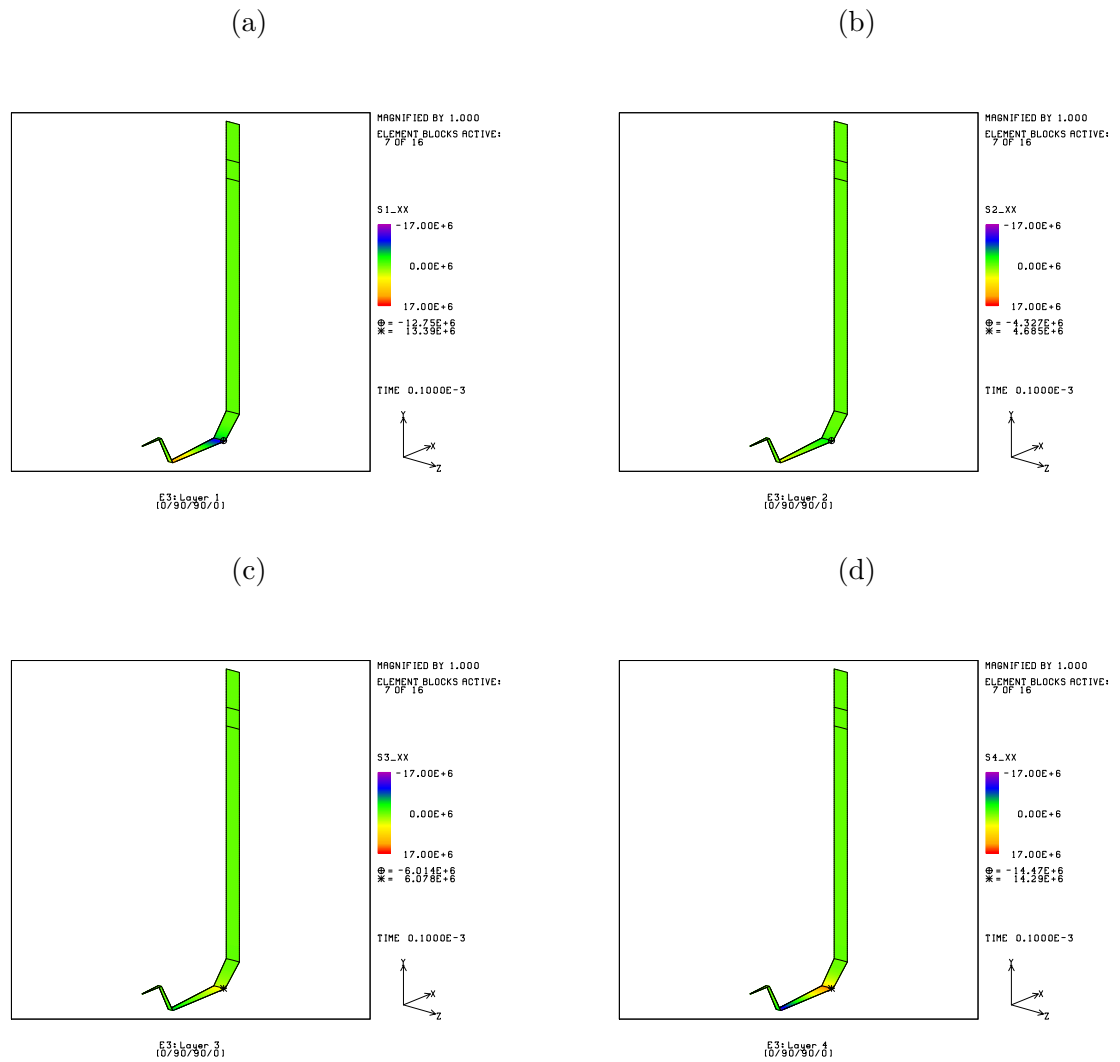
Figure 4.15: Radial stresses due to internal pressurization for the [0/90/90/0] container modeled using primarily shell elements: (a) layer 1 (outermost layer); (b) layer 2; (c) layer 3; (d) layer 4 (innermost layer).

(a)   (b)

(c)   (d)
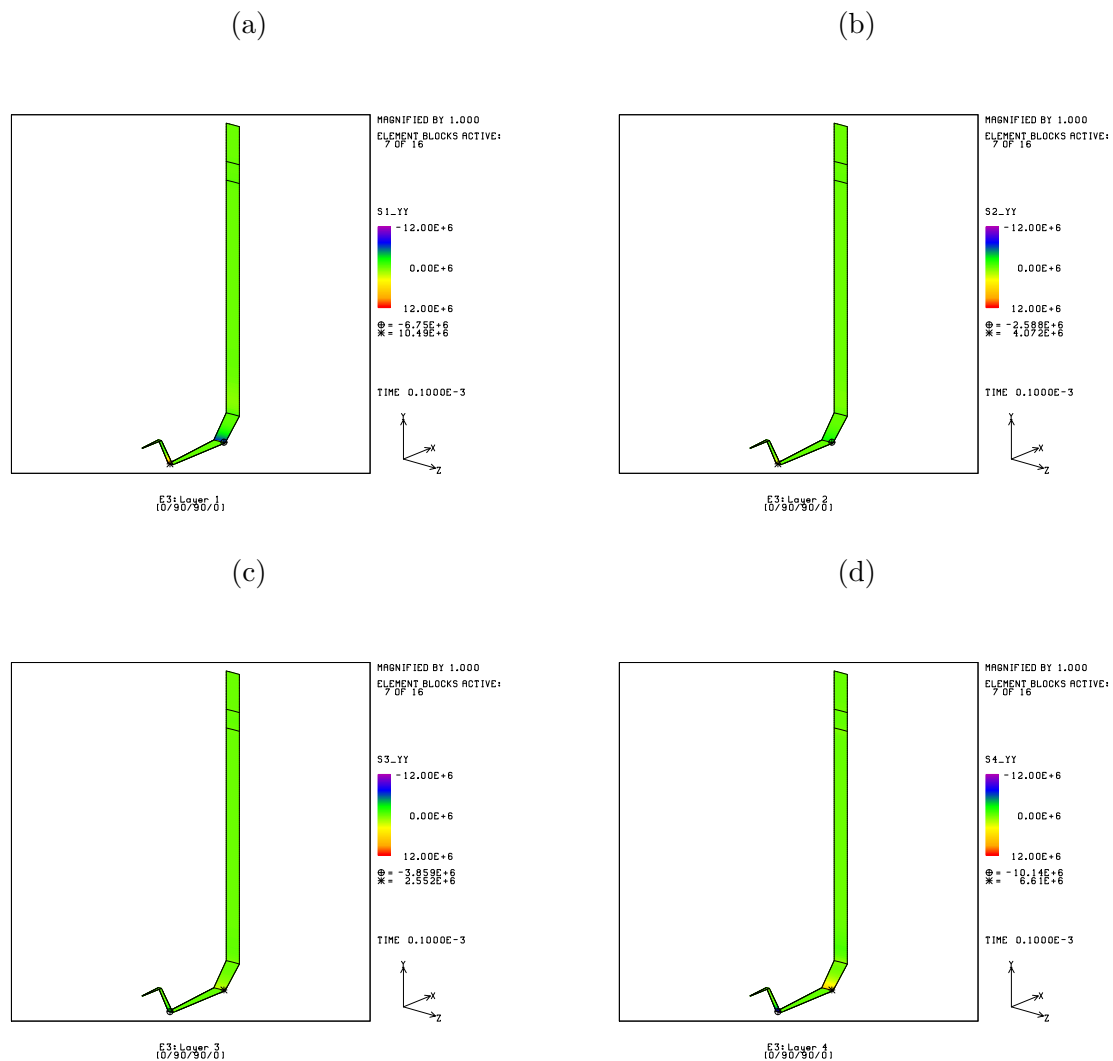
Figure 4.16: Axial stresses due to internal pressurization for the [0/90/90/0] container modeled using primarily shell elements: (a) layer 1 (outermost layer); (b) layer 2; (c) layer 3; (d) layer 4 (innermost layer).

(a)

(b)

(c)

(d)
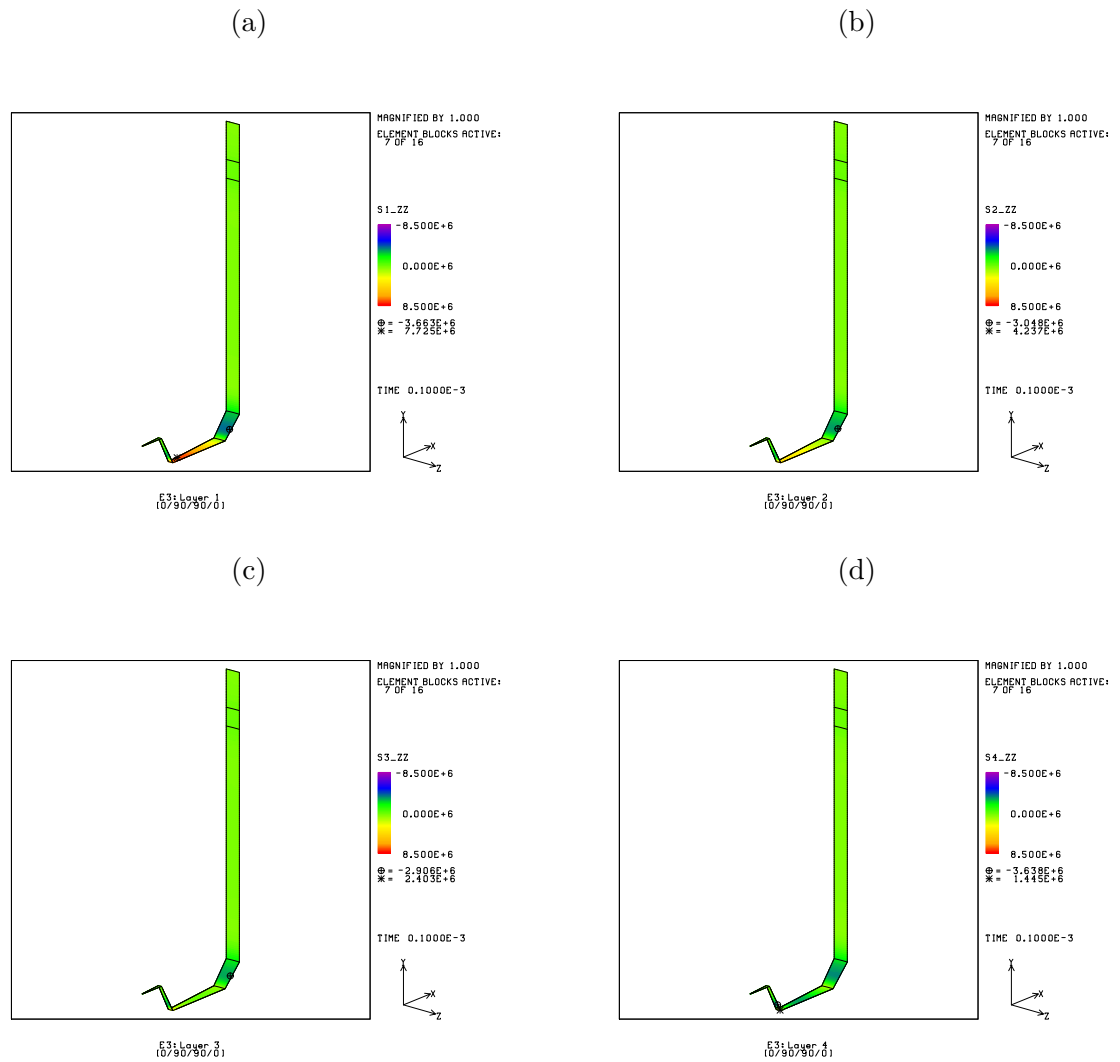
Figure 4.17: Circumferential stresses due to internal pressurization for the [0/90/90/0] container modeled using primarily shell elements: (a) layer 1 (outermost layer); (b) layer 2; (c) layer 3; (d) layer 4 (innermost layer).

(a)

(b)

(c)

(d)
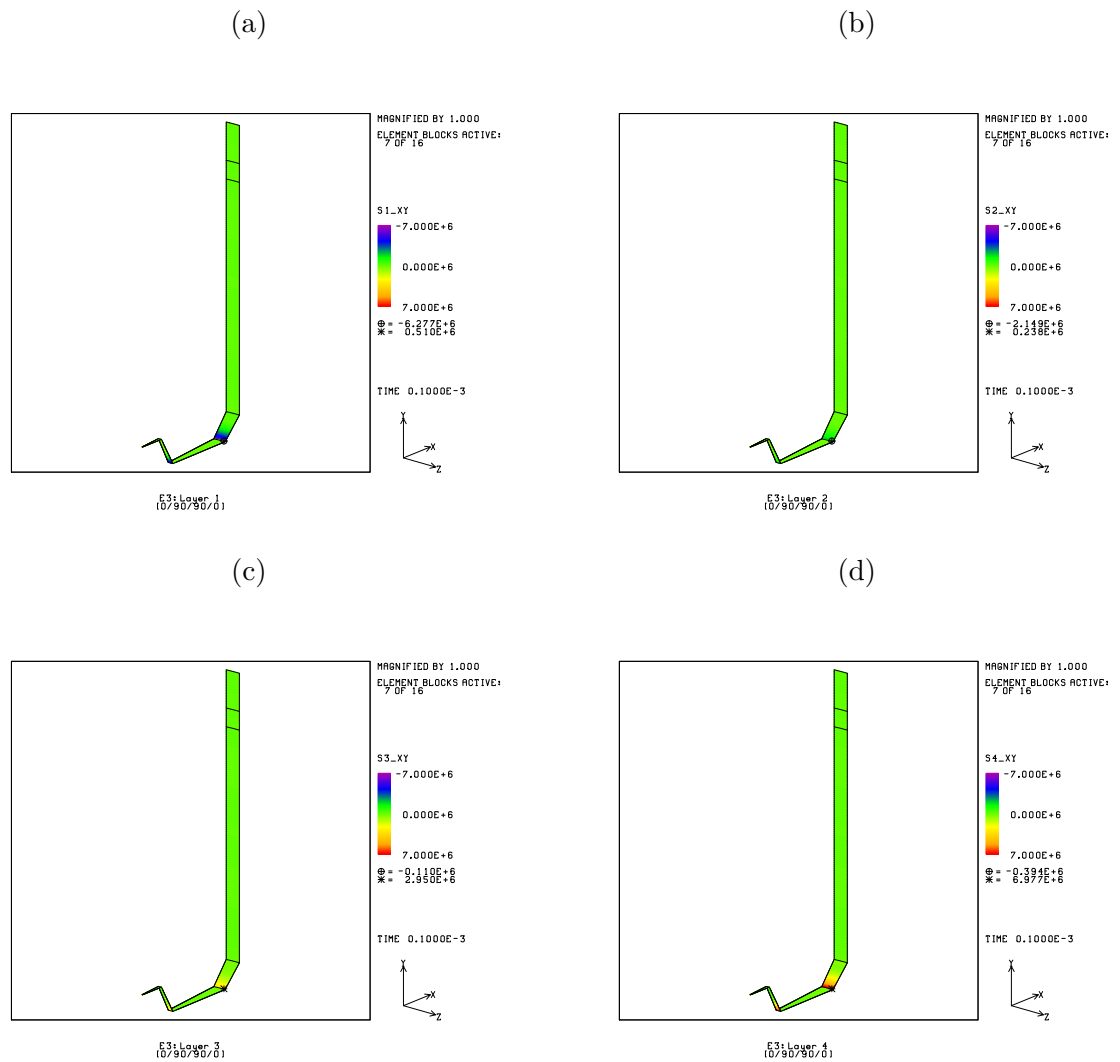
Figure 4.18: Radial-axial shear stresses due to internal pressurization for the [0/90/90/0] container modeled using primarily shell elements: (a) layer 1 (outermost layer); (b) layer 2; (c) layer 3; (d) layer 4 (innermost layer).

(a) (b)

(c) (d)
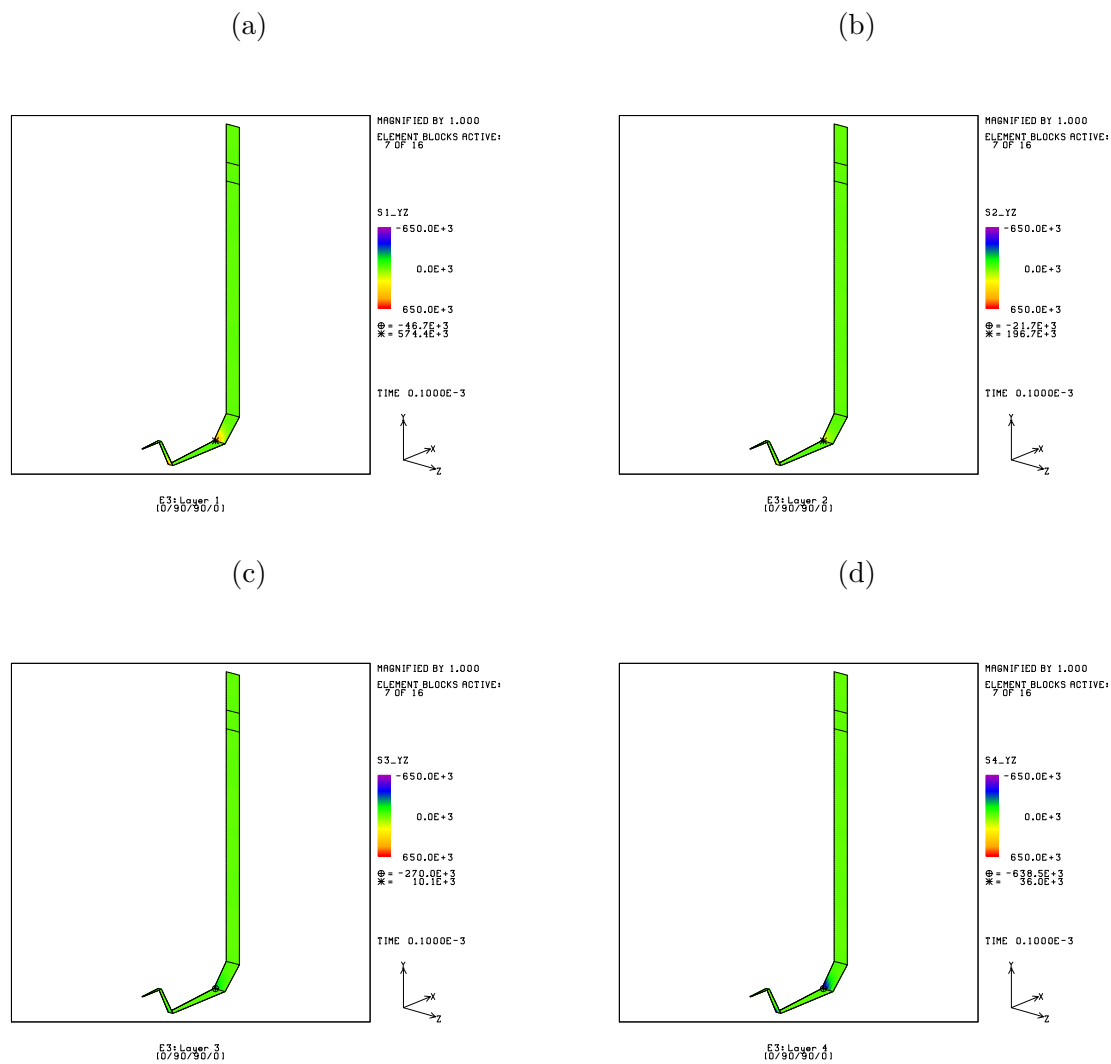
Figure 4.19: Negative of axial-circumferential shear stresses due to internal pressurization for the [0/90/90/0] container modeled using primarily shell elements: (a) layer 1 (outermost layer); (b) layer 2; (c) layer 3; (d) layer 4 (innermost layer).

(a)   (b)

(c)   (d)
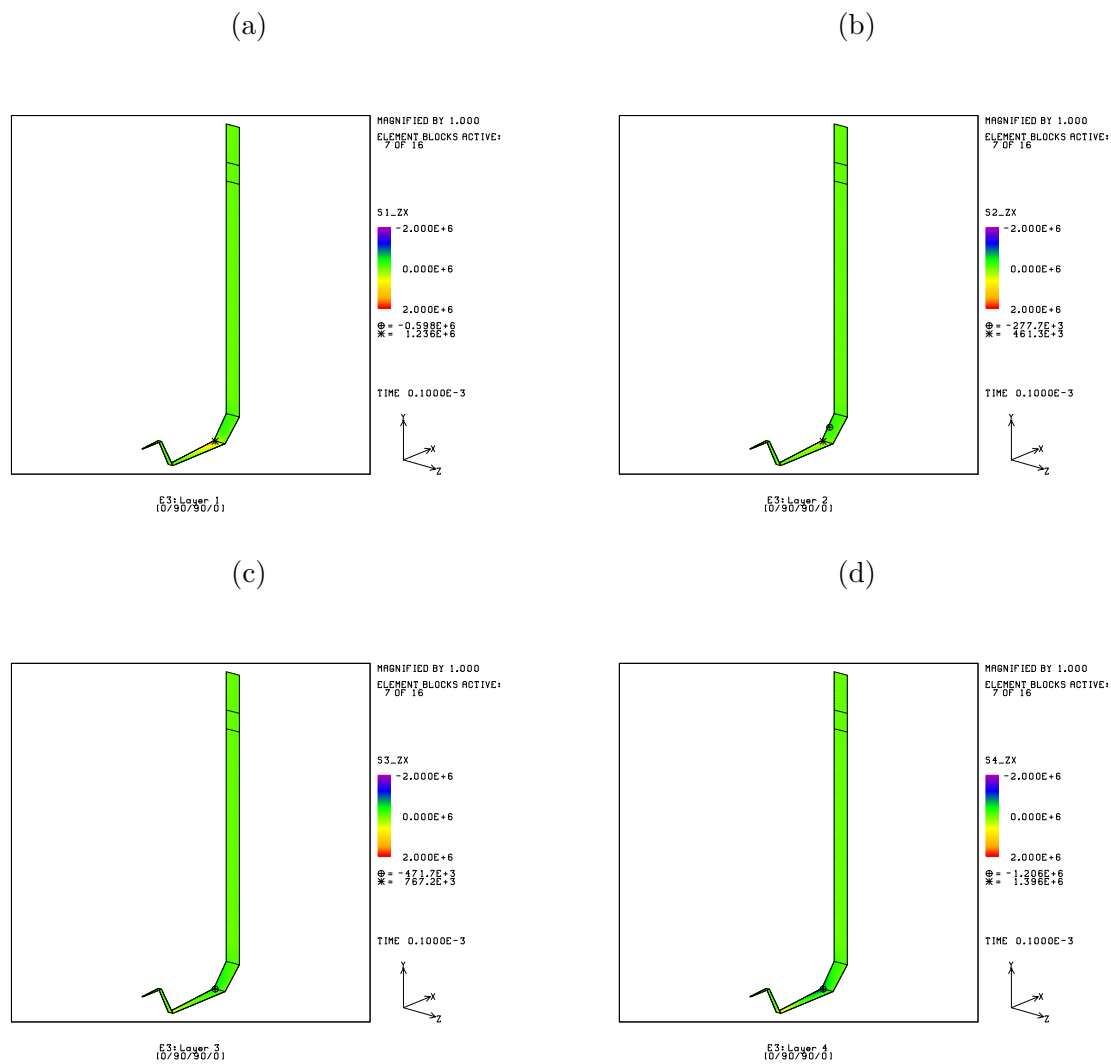
Figure 4.20: Negative of circumferential-radial shear stresses due to internal pressurization for the [0/90/90/0] container modeled using primarily shell elements: (a) layer 1 (outermost layer); (b) layer 2; (c) layer 3; (d) layer 4 (innermost layer).

5   Comparison of Shell and Continuum Element Approaches for Composite Modeling

In many cases of finite element analysis, using shell elements to model composite structures is more convenient and efficient compared to using continuum elements. First of all, in the model creation stage, it is easier to create meshes where a single shell element is used in the thickness direction to represent a laminated structure than to have to create separate element blocks for each layer as is required for a continuum approach. However, the specification of the resulting material model for the shell case requires careful attention in the case of non-symmetric laminates for which the sign of the entries in the extensional-bending coupling stiffness matrix $[B]$ is tied to the direction of the shell normal. That is, in such cases, it is necessary to compute $[B]$ with the stacking sequence specified with the top layer corresponding to the side of shell element defined by the positive element normal. Recall from basic composite theory that the signs of entries in the extensional stiffness matrix $[A]$ and the bending stiffness matrix $[D]$ do not depend on which side of the laminate is specified as the top for non-symmetric lay-ups. The same holds true for the transverse shear stiffness matrix $[A_{ts}]$. If the stacking sequence used in computing $[B]$ is inadvertently the reverse of what it should be (e.g., $[10/20/30/40]$ instead of $[40/30/20/10]$), the magnitudes of the entries in $[B]$ will be correct, but the signs will be the opposite of what is required. Such a mistake will likely lead to erroneous results for the integrated force and force-couple resultants in addition to the layerwise stresses, depending on the exact load applied and the non-symmetric stacking sequence being examined. Hence, care must be taken in such cases to match the sign of the entries in $[B]$ to the direction of the positive normal of shell elements in question. On the other hand, since the principal material directions are directly specified for each layer in the continuum approach, it is less likely that a mistake will be made in reversing the stacking sequence for the case of a non-symmetric laminate.

Another difference between the two approaches in ADAGIO/PRESTO concerns the results output. For the case where continuum elements are used, the layerwise stresses are directly available, but the integrated force and force-couple resultants must be calculated in a post-processing stage, if they are desired. In most cases, the layerwise

stress distribution is of more interest. However, for the current shell element approach in ADAGIO/PRESTO, the reverse situation results where the integrated force and force-couple resultants are directly available and the layerwise stress distribution must be determined using ALGEBRA or another post-processing program. At present, an alternative layered shell approach is being implemented in ADAGIO/PRESTO where layerwise stresses will be directly available.

In some cases, the kinematic assumptions in the Mindlin shell theory used in ADAGIO are invalid for the problem at hand. It is quite possible that the normal to the laminate midplane in the undeformed configuration will not remain a straight line as the structure deforms. In most situations this will not be the case, but the user should always remain cognizant of the fact that Mindlin and other shell theories always incorporate more restrictive deformation assumptions than a general three-dimensional continuum theory. Whether the shell kinematic constraints are appropriate or not are, of course, problem dependent and sometimes not known *a priori.*

Another potential issue with using shell elements to represent a composite structure results from the fact that traditional shell elements are of zero thickness, regardless of the material model being employed. For the current input interface available for the composite shell model in ADAGIO, the $[A]$, $[A_{ts}]$, $[B]$, and $[D]$ matrices which correspond to pre-integrating the material response through the thickness direction are input directly. In many cases, the structure being analyzed is purely a single laminated composite structure for which the fact that traditional shell elements have zero thickness is not an issue. However, this may not be the case if a structure is being analyzed where a composite laminate is sandwiched between other materials, especially if continuum elements are used for those other materials. In such situation, using a zero thickness shell element will result in the surrounding materials having the incorrect thickness or wrong offset, either of which may or may not significantly affect the analysis results.

Next to accuracy of results and the time and effort required to create a model (i.e., the mesh and input deck generation), the biggest concern of an analyst is likely to be the computational effort required to achieve a solution. At a minimum, at least one hex element must be used per layer for the continuum modeling approach, whereas a single shell element can used through the thickness of a laminate. The shell and

hex elements typically used in ADAGIO/PRESTO each have a total of 24 degrees-of-freedom. Hence, for a multilayer composite, using a continuum element approach will result in a larger number of unknowns that need to be calculated. In some situations, it may be necessary to use even more than one hex element through the thickness of each composite layer. Exactly how many elements through the thickness of a layer are required is, of course, problem dependent. Thus, in many cases, the computational effort required for modeling composites using shell elements in ADAGIO is less than that required when hex/brick continuum elements are used. However, in some cases, ADAGIO has a much harder time converging, if at all, when shell elements are used.

Many problems of interest involve axisymmetric geometries. However, in analyzing these and other composite structures, analysts must be careful not to rely too much on intuition gained from isotropic analyses. For instance, in the case of an isotropic structure possessing axisymmetric geometry under axisymmetric loads, no circumferential displacements will occur. Rather, in such a case, the structure can only expand/contract along the radial and axial directions. Hence, such a situation can be modeled by considering only a small sector (pie cut) and applying boundary conditions on the circumferential edges specifying that no circumferential displacements occur. However, in the case of a laminated composite structure possessing axisymmetric geometry under axisymmetric loads, circumferential displacements may or may not occur depending on the laminate stacking sequence. Thus, when a small sector is modeled for a such composite structure, it is not correct to simply apply a condition of no circumferential displacements along the sector circumferential edges. Rather, true cyclic periodic boundary conditions must be used such that the sector modeled deforms in a way that the periodicity is preserved in the response. That is, the response is still axisymmetric in that it is independent of the angular position when expressed using an appropriate cylindrical coordinate system, even though it may involve circumferential displacements. For example, if a $10°$ sector is modeled, the deformations must be such that taking 36 of these deformed $10°$ sectors, the ends would still fit together to form a complete $360°$ ring with no gaps.

In general, continuum finite element modeling of composite structures appears to be more robust than shell finite element modeling in terms of determining the laminated behavior accurately and in achieving a solution using ADAGIO. However, the

price paid is that the model creation phase can be more time consuming for an analyst and the model solution phase can be more computationally expensive compared to a shell model which can achieve the same accuracy for many problems. Of course, many times a little bit of effort upfront can be used to create a model which is not needlessly larger than required. For instance, periodic boundary conditions can be used for axisymmetric structures. There is, however, a practical limit on how small such a sector can be in such a case. Regardless of whether continuum or shell elements are used, careful attention must be paid when creating and analyzing a composite model, as much of the intuition acquired from the analysis of isotropic structures cannot be used.

6 Summary

There have been several significant accomplishments over the course of this ASC AD project that are aligned with the general goals of Advanced Deployment projects:

1. A coding error was uncovered and corrected in the "nlve thermoset" model being employed in the ADAGIO computations.

2. For the first time, the isotropic nonlinear viscoelastic material model has been run in parallel using the SIERRA code.

3. A realistic DP application has been analyzed for a customer demonstrating new capabilities that are simply unavailable in commercial codes.

4. Additional flexibility was added to the orientation initialization routines of the orthotropic linear elastic model, based upon needs identified by the composite container analyses performed here.

5. The ability to analyze large composite problems using Sandia's SIERRA/ADAGIO code was successfully demonstrated. Previously, any such composite modeling at Sandia required the use of commercial codes which are limited in terms of problem size and in some cases by the unavailability of proper cyclic periodic boundary conditions.

6. A comparative study of modeling composites using continuum versus shell elements has been completed and the resulting general guidelines for analysts have been detailed herein.

7   References

[1] Hammerand, D.C., *Laminated Composites Modeling in ADAGIO/PRESTO*, Sandia Report SAND2004-2143, Sandia National Laboratories, Albuquerque, NM, May 2004.

8 Appendix A: ADAGIO Input Deck for the Adhesive Joint Problem

```
begin sierra nlve axisymmetric joint process

   title TEMPO analysis of bonded cylinder history


  ###  Problem units:  length=meters, stress=pascals, temp=Kelvin ###
  ###                  force=newtons                               ###
  ### Function definitions ###
  ###########################
###
### Define the temperature history for the problem
###
   begin definition for function TEMP_HIST_STAGE1
     type is piecewise linear
     ordinate is temperature
     abscissa is time
     begin values
          0.0     358.15   ###  85 C (start at Tref)   ###
       1500.0     333.15   ###  60 C (cool at 1 C/min) ###
       1680.0     318.15   ###  45 C (cool at 5 C/min) ###
       1980.0     293.15   ###  20 C (cool at 5 C/min) ###
       2000.0     293.15   ###  20 C (pre-load to 18000lbs) ###
       2500.0     318.15   ###  45 C (heat at 3 C/min + add preload @ 240 lbs/C) ###
       3000.0     343.15   ###  70 C (heat at 3 C/min + add preload @ 240 lbs/C) ###
      10200.0     343.15   ###  70 C (hold for 120 mins) ###
      10700.0     318.15   ###  45 C (cool at 3 C/min + reduce preload @ 240 lbs/C) ###
      11200.0     293.15   ###  20 C (cool at 3 C/min + reduce preload to 18000lbs) ###
      12700.0     218.15   ### -55 C (cool at 3 C/min) ###
      14200.0     293.15   ###  20 C (reheat at 3 C/min) ###
     end values
   end definition for function TEMP_HIST_STAGE1


###
### Define the axial pressure response to be applied to the inner cylinder
### Note pressures are applied to 1/4 cylinder  X-section      ###
###      (total load) = pressure x cross-sectional area         ###
###      for axicyl9045.g there are 45 elems and 184 nodes on load plane   ###
   begin definition for function apress
     type is piecewise linear
     ordinate is pressure
     abscissa is time
     begin values
          0.0        0.0  ###  85 C (start at Tref)   ###
       1500.0        0.0  ###  60 C (cool at 1 C/min) ###
       1680.0        0.0  ###  45 C (cool at 5 C/min) ###
       1980.0        0.0  ###  20 C (cool at 5 C/min) ###
       2000.0   56.034E6  ###  20 C (pre-load to 18000lbs=80067.6N for whole X-section)
       2500.0   74.712E6  ###  45 C (heat at 3 C/min + add preload @ 240 lbs/C) ###
       3000.0   93.390E6  ###  70 C (heat at 3 C/min + add preload @ 240 lbs/C) ###
      10200.0   93.390E6  ###  70 C (hold for 120 mins) ###
      10700.0   74.712E6  ###  45 C (cool at 3 C/min + reduce preload @ 240 lbs/C) ###
      11200.0   56.034E6  ###  20 C (cool at 3 C/min + reduce preload to 18000lbs) ###
      12700.0   15.565E6  ### -55 C (cool at 3 C/min and reduce preload to 5000 lbs) ###
      14200.0   56.034E6  ###  20 C (reheat at 3 C/min) ###
     end values
   end definition for function apress


###
```

```
### This defines a null function
###
   begin definition for function lzero
     type is piecewise linear
     ordinate is lzero
     abscissa is time
     begin values
        0.0     0.0
        1.0e+10  0.000
     end values
   end definition for function lzero


###
### Define the polymer thermal strain as a function of temperature.
###   This is merely a place holder to populate a SIERRA input.
###   The nonlinear viscoelastic thermoset model is thermodynamically consistent
###     for finite strains.
###   In finite strain mechanics, there is no thermal strain definition.
###   Rather the constitutive equation predicts a pressure corresponding
###     a temperature change.  SIERRA wants something anyway so here it is.
   begin definition for function ADH_THERMAL_STRAIN
     type is piecewise linear
     ordinate is strain
     abscissa is temperature
     begin values
       -1000.0   0.0
           0.0   0.0
        1000.0   0.0
     end values
   end definition for function ADH_THERMAL_STRAIN


###
###  This is the typical thermal strain definition as a function of temperature
###       for the metal.
   begin definition for function AL_THERMAL_STRAIN
     type is piecewise linear
     ordinate is strain
     abscissa is temperature
     begin values
       -100.0   -0.00234     ### 6061T6 Alum Linear CTE=2.34E-5/C ###
        500.0    0.0117
     end values
   end definition for function AL_THERMAL_STRAIN


  ### Direction definitions ###
  ###########################
  define direction x with vector 1.0 0.0 0.0
  define direction y with vector 0.0 1.0 0.0
  define direction z with vector 0.0 0.0 1.0


  ### Material definitions ###
  ###########################

  begin property specification for material ALuminum_6061T6
     density          = 2710.0
     thermal strain function = AL_THERMAL_STRAIN

     begin parameters for model elastic
       youngs modulus  = 6.9e+10
       poissons ratio  = 0.33
     end parameters for model elastic
```

```
end property specification for material ALuminum_6061T6


begin property specification for material ALuminum_1100
   density          = 2710.0
   thermal strain function = AL_THERMAL_STRAIN


   begin parameters for model elastic
     youngs modulus  = 6.9e+10
     poissons ratio  = 0.33
   end parameters for model elastic
end property specification for material ALuminum_1100



begin property specification for material ALuminum_1100soft
   density          = 2710.0
   thermal strain function = AL_THERMAL_STRAIN


   begin parameters for model elastic
     youngs modulus  = 1.0E+6
     poissons ratio  = 0.33
   end parameters for model elastic
end property specification for material ALuminum_1100soft


begin property specification for material black_adhesive
   density          = 1176.0
   thermal strain function = ADH_THERMAL_STRAIN


   begin parameters for model nlve_thermoset
     bulk modulus = 6.0e9
     shear modulus = 0.68e9
     1psi prony 1 = 0.0
     1psi prony 2 = 0.0
     1psi prony 3 = 0.0
     1psi prony 4 = 0.0
     1psi prony 5 = 0.0
     1psi prony 6 = 0.0
     1psi prony 7 = 0.0
     1psi prony 8 = 0.0
     1psi prony 9 = 0.0
     1psi prony 10 = 0.0
     1psi prony 11 = 0.0
     1psi prony 12 = 0.0
     1psi prony 13 = 0.0
     1psi prony 14 = 0.0
     1psi prony 15 = 0.0
     1psi prony 16 = 0.0
     1psi prony 17 = 0.0
     1psi prony 18 = 0.0
     1psi prony 19 = 0.0
     1psi prony 20 = 0.0
     1psi prony 21 = 0.0
     1psi prony 22 = 0.0
     1psi prony 23 = 0.0
     1psi prony 24 = 0.0
     1psi prony 25 = 0.0
     1psi prony 26 = 0.0
     1psi prony 27 = 0.0
     1psi prony 28 = 0.0
     1psi prony 29 = 0.0
     1psi prony 30 = 0.0
     2psi prony 1 =  0.0
```

```
2psi prony 2 =  0.0
2psi prony 3 =  0.0
2psi prony 4 =  0.0
2psi prony 5 =  0.0
2psi prony 6 =  0.0
2psi prony 7 =  0.0
2psi prony 8 =  0.0
2psi prony 9 =  0.0
2psi prony 10 = 0.0
2psi prony 11 = 0.0
2psi prony 12 = 0.0
2psi prony 13 = 0.0
2psi prony 14 = 0.0
2psi prony 15 = 0.0
2psi prony 16 = 0.0
2psi prony 17 = 0.0
2psi prony 18 = 0.0
2psi prony 19 = 0.0
2psi prony 20 = 0.0
2psi prony 21 = 0.0
2psi prony 22 = 0.0
2psi prony 23 = 0.0
2psi prony 24 = 0.0
2psi prony 25 = 0.0
2psi prony 26 = 0.0
2psi prony 27 = 0.0
2psi prony 28 = 0.0
2psi prony 29 = 0.0
2psi prony 30 = 0.0
3psi prony 1 = 0.0
3psi prony 2 = 0.0
3psi prony 3 = 0.0
3psi prony 4 = 0.0
3psi prony 5 = 0.0
3psi prony 6 = 0.0
3psi prony 7 = 0.0
3psi prony 8 = 0.0
3psi prony 9 = 0.0
3psi prony 10 = 0.0
3psi prony 11 = 0.0
3psi prony 12 = 0.0
3psi prony 13 = 0.0
3psi prony 14 = 0.0
3psi prony 15 = 0.0
3psi prony 16 = 0.0
3psi prony 17 = 0.0
3psi prony 18 = 0.0
3psi prony 19 = 0.0
3psi prony 20 = 0.0
3psi prony 21 = 0.0
3psi prony 22 = 0.0
3psi prony 23 = 0.0
3psi prony 24 = 0.0
3psi prony 25 = 0.0
3psi prony 26 = 0.0
3psi prony 27 = 0.0
3psi prony 28 = 0.0
3psi prony 29 = 0.0
3psi prony 30 = 0.0
4psi prony 1 = 0.0
4psi prony 2 = 0.0
```

```
4psi prony 3 = 0.0
4psi prony 4 = 0.0
4psi prony 5 = 0.0
4psi prony 6 = 0.0
4psi prony 7 = 0.0
4psi prony 8 = 0.0
4psi prony 9 = 0.0
4psi prony 10 = 0.0
4psi prony 11 = 0.0
4psi prony 12 = 0.0
4psi prony 13 = 0.0
4psi prony 14 = 0.0
4psi prony 15 = 0.0
4psi prony 16 = 0.0
4psi prony 17 = 0.0
4psi prony 18 = 0.0
4psi prony 19 = 0.0
4psi prony 20 = 0.0
4psi prony 21 = 0.0
4psi prony 22 = 0.0
4psi prony 23 = 0.0
4psi prony 24 = 0.0
4psi prony 25 = 0.0
4psi prony 26 = 0.0
4psi prony 27 = 0.0
4psi prony 28 = 0.0
4psi prony 29 = 0.0
4psi prony 30 = 0.0
1psi ref = 6.4042e+05
i1 deriv 1psi = 0.0
2psi ref = 5.6998e+05
t deriv 2psi = -1.2755e+03
3psi ref = 1.1684e+03
t deriv 3psi = -3.1239e+00
4psi ref = 7.2275e-01
t deriv 4psi = 6.9662e-04
t 2deriv 4psi = 4.3610e-06
reference temp = 358.15
reference density = 1176
wlf c1 = 10
wlf c2 = 67
b shift constant = 3.0706e+05
shift ref value = 3.1390e+04
wwbeta 1psi = 0.18
wwtau 1psi = 5
wwbeta 2psi = 0.18
wwtau 2psi = 0.00015
wwbeta 3psi = 0.18
wwtau 3psi = 5
wwbeta 4psi = 0.15
wwtau 4psi = 2
double integ factor = 0
rubbery bulk mod = 4800000000
i1 deriv r_bulk = 0
glassy bulk mod = 6000000000
i1 deriv g_bulk = 0
rubbery shear mod = 9700000
t deriv r_shear = 0
i2 deriv r_shear = 0
glassy shear mod = 680000000
t deriv g_shear = -1500000
```

```
rubbery vol cte = 0.00053
t deriv r_cte = 1e-7
glassy vol cte = 0.000195
t deriv g_cte = 0
rubbery hcapacity = 3020
t deriv r_hcapacity = 3
glassy hcapacity = 2420
t deriv g_hcapacity = 3
GLASS TRANSITION TEM = 358.15
PSI EQ 2I = 4.0761e+06
PSI EQ IT = -2.1633e+03
PSI EQ 2T = -7.2857e+00
PSI EQ 2H = 8.2483e+03
PSI EQ 3I = 0.0
PSI EQ 2IT = -9000.0
PSI EQ I2T = 1.0284e+01
PSI EQ 3T = 7.6802e-03
PSI EQ 2HT = 0.0
PSI EQ 4I = 0.0
PSI EQ 3IT = 0.0
PSI EQ 2I2T = 0.0
PSI EQ I3T = 0.0
PSI EQ 4T = -8.7074e-05
PSI EQ 4H = 0.0
PSI POT IT = -1.1684e+03
PSI POT 2T = -7.2275e-01
PSI POT 2IT = 0.0
PSI POT I2T = 6.2479e+00
PSI POT 3T = -2.0899e-03
PSI POT 4T = -2.6166e-05
relax time 1 =  1e-13
relax time 2 =  1e-12
relax time 3 =  1e-11
relax time 4 =  1e-10
relax time 5 =  1e-09
relax time 6 =  1e-08
relax time 7 =  1e-07
relax time 8 =  1e-06
relax time 9 =  3.16e-06
relax time 10 = 1.0e-05
relax time 11 = 3.16e-05
relax time 12 = 1.0e-04
relax time 13 = 3.16e-04
relax time 14 = 1.0e-03
relax time 15 = 3.16e-03
relax time 16 = 1.0e-02
relax time 17 = 3.16e-02
relax time 18 = 1.0e-01
relax time 19 = 3.16e-01
relax time 20 = 1.0
relax time 21 = 3.16
relax time 22 = 10.0
relax time 23 = 31.6
relax time 24 = 100
relax time 25 = 316
relax time 26 = 1000
relax time 27 = 3160
relax time 28 = 10000
relax time 29 = 31600
relax time 30 = 100000
end parameters for model nlve_thermoset
```

```
   end property specification for material black_adhesive


### BV Problem definitions ###
############################

 begin finite element model loading1

    Database Name = axicyl9045.g
    Database Type = exodusII

    begin parameters for block block_1
      material ALuminum_6061T6
      solid mechanics use model elastic
    end parameters for block block_1

    begin parameters for block block_2
      material black_adhesive
      solid mechanics use model nlve_thermoset
    end parameters for block block_2

    begin parameters for block block_3
      material ALuminum_6061T6
      solid mechanics use model elastic
    end parameters for block block_3

    begin parameters for block block_5
      material ALuminum_1100soft
      solid mechanics use model elastic
    end parameters for block block_5

 end finite element model loading1


 begin finite element model loading2

    Database Name = axicyl9045.g
    Database Type = exodusII

    begin parameters for block block_1
      material ALuminum_6061T6
      solid mechanics use model elastic
    end parameters for block block_1

    begin parameters for block block_2
      material black_adhesive
      solid mechanics use model nlve_thermoset
    end parameters for block block_2

    begin parameters for block block_3
      material ALuminum_6061T6
      solid mechanics use model elastic
    end parameters for block block_3

    begin parameters for block block_5
      material ALuminum_1100
      solid mechanics use model elastic
    end parameters for block block_5

 end finite element model loading2
```

```
begin adagio procedure stage1

   begin time control
      begin time stepping block p1
         start time =  0.0
          begin parameters for adagio region adagio
            time increment = 10.0
          end parameters for adagio region adagio
         end time stepping block p1

      begin time stepping block p2
         start time =  60.0
          begin parameters for adagio region adagio
            time increment = 30.0
          end parameters for adagio region adagio
         end time stepping block p2

      begin time stepping block p3
         start time =  1500.0
          begin parameters for adagio region adagio
            time increment = 12.0
          end parameters for adagio region adagio
         end time stepping block p3

      begin time stepping block p4
         start time =  1680.0
          begin parameters for adagio region adagio
            time increment = 25.0
          end parameters for adagio region adagio
         end time stepping block p4

         termination time = 1980.0

   end time control

   begin adagio region adagio
     use finite element model loading1
     options = thermalstrain

     prescribed nodal temperature using function TEMP_HIST_STAGE1

     ### output description ###

     begin results output output_adagio1
       Database Name = axicyl9045stage1p.e
       Database Type = exodusII
       element Variables = rotated_stress as stress
       element Variables = temperature as temp
       element Variables = MAT%nlve_thermoset(242|243|263|264|265|266|267|268)
       global Variables = timestep as timestep
       nodal Variables = force_external as f_ext
       nodal Variables = displacement as displ
#        nodal Variables = force_internal as f_int

       start time = 0.0
       at time      0.0 increment = 30.0
       at time     60.0 increment = 720.0
       at time   1500.0 increment =  60.0
       at time   1680.0 increment =  60.0
```

```
      at time   1980.0 increment =    2.0
      termination time = 1980.0


  end results output output_adagio1



  ### definition of BCs ###

  begin prescribed displacement
    node set = nodelist_20
    direction = z
    function = lzero
    scale factor = 0.0


  end prescribed displacement

  begin prescribed displacement
    node set = nodelist_21
    direction = x
    function = lzero
    scale factor = 0.0
  end prescribed displacement

  begin prescribed displacement
    node set = nodelist_8
    direction = y
    function = lzero
    scale factor = 0.0
  end prescribed displacement



  ####  Contacts  ######

  begin contact definition jstick1
    enforcement = tied
    contact surface surf_14 contains surface_14
    contact surface surf_15 contains surface_15

    begin interaction
      master = surf_14
      slave = surf_15
      normal tolerance = 1.0e-5
      tangential tolerance = 1.0e-5
      capture tolerance = 1.0e-7
#        tension release= 1.0E+25
    end interaction
  end contact definition jstick1

  begin contact definition sstick1
    enforcement = tied
    contact surface surf_16 contains surface_16
    contact surface surf_17 contains surface_17

    begin interaction
      master = surf_16
      slave = surf_17
      normal tolerance = 1.0e-5
      tangential tolerance = 1.0e-5
      capture tolerance = 1.0e-7
#        tension release= 1.0E+25
    end interaction
```

```
end contact definition sstick1


    ### -----------------###
    ### Solver definition ###
    ### -----------------###


    Loadstep predictor using line search type secant

      begin adagio solver cg
        Target Relative Residual = 1.0e-6
        Target Residual = 0.008  during p1
        Target Residual = 0.008  during p2
        Target Residual = 0.008  during p3
        Target Residual = 0.008  during p4
        Maximum Iterations = 30000
        Minimum Iterations = 10
        Orthogonality measure for reset = 0.20
        Line Search type secant
        iteration print = 50
        nodal preconditioning type = elastic
      end adagio solver cg


    predictor scale factor = 1.0 during p1
    predictor scale factor = 1.0 during p2
    predictor scale factor = 1.0 during p3
    predictor scale factor = 1.0 during p4


  end adagio region adagio

end adagio procedure stage1

#############################################################################

  begin adagio procedure stage2

    begin procedural transfer AgioToAgio
      include variables from region adagio in block block_1
      include variables from region adagio in block block_2
      include variables from region adagio in block block_3
      include variables from region adagio in block block_5
    end procedural transfer AgioToAgio

    begin time control
      begin time stepping block p5
        start time =  1980.0
        begin parameters for adagio region adagio
          time increment = 0.1
        end parameters for adagio region adagio
      end time stepping block p5

      begin time stepping block p6
        start time =  1981.0
        begin parameters for adagio region adagio
          time increment = 0.25
        end parameters for adagio region adagio
      end time stepping block p6

      begin time stepping block p7
        start time =  2000.0
        begin parameters for adagio region adagio
```

```
      time increment = 25.0
      end parameters for adagio region adagio
    end time stepping block p7


  begin time stepping block p8
      start time =  2500.0
      begin parameters for adagio region adagio
        time increment = 20.0
      end parameters for adagio region adagio
    end time stepping block p8


  begin time stepping block p9
      start time =  3000.0
      begin parameters for adagio region adagio
        time increment = 5
      end parameters for adagio region adagio
    end time stepping block p9


  begin time stepping block p10
      start time =  3100.0
      begin parameters for adagio region adagio
        time increment = 50
      end parameters for adagio region adagio
    end time stepping block p10


  begin time stepping block p11
      start time =  10200.0
      begin parameters for adagio region adagio
        time increment = 20.0
      end parameters for adagio region adagio
    end time stepping block p11


  begin time stepping block p12
      start time =  10700.0
      begin parameters for adagio region adagio
        time increment = 25.0
      end parameters for adagio region adagio
    end time stepping block p12


  begin time stepping block p13
      start time =  11200.0
      begin parameters for adagio region adagio
        time increment = 25.0
      end parameters for adagio region adagio
    end time stepping block p13


  begin time stepping block p14
      start time =  12700.0
      begin parameters for adagio region adagio
        time increment = 25.0
      end parameters for adagio region adagio
    end time stepping block p14


    termination time = 14200.0

end time control

begin adagio region adagio
  use finite element model loading2
  options = thermalstrain
```

```
prescribed nodal temperature using function TEMP_HIST_STAGE1

### output description ###

begin results output output_adagio2
  Database Name = axicyl9045stage2.e
  Database Type = exodusII
  element Variables = rotated_stress as stress
  element Variables = temperature as temp
  element Variables = MAT%nlve_thermoset(242|243|263|264|265|266|267|268)
  global Variables = timestep as timestep
  nodal Variables = force_external as f_ext
  nodal Variables = displacement as displ
#    nodal Variables = force_internal as f_int

  start time = 1980.0
  at time  1980.0 increment =   2.0
  at time  2000.0 increment = 100.0
  at time  2500.0 increment = 100.0
  at time  3000.0 increment = 1000.0
  at time 10200.0 increment = 100.0
  at time 10700.0 increment = 100.0
  at time 11200.0 increment = 300.0
  at time 12700.0 increment = 300.0
  termination time = 14200.0

end results output output_adagio2

### definition of BCs ###

begin prescribed displacement
  node set = nodelist_20
  direction = z
  function = lzero
  scale factor = 0.0
end prescribed displacement

begin prescribed displacement
  node set = nodelist_21
  direction = x
  function = lzero
  scale factor = 0.0
end prescribed displacement

begin prescribed displacement
  node set = nodelist_8
  direction = y
  function = lzero
  scale factor = 0.0
end prescribed displacement

begin pressure
  surface = surface_13
  function = apress
  scale factor = -1.0
end pressure


####  Contacts  ######

begin contact definition jstick2
```

```
          enforcement = tied
          contact surface surf_14 contains surface_14
          contact surface surf_15 contains surface_15

          begin interaction
            master = surf_14
            slave = surf_15
            normal tolerance = 1.0e-5
            tangential tolerance = 1.0e-5
            capture tolerance = 1.0e-7
#             tension release= 1.0E+25
          end interaction
        end contact definition jstick2

      begin contact definition sstick2
          enforcement = tied
          contact surface surf_16 contains surface_16
          contact surface surf_17 contains surface_17

          begin interaction
            master = surf_16
            slave = surf_17
            normal tolerance = 1.0e-5
            tangential tolerance = 1.0e-5
            capture tolerance = 1.0e-7
#             tension release= 1.0E+25
          end interaction
        end contact definition sstick2

      ### -----------------###
      ### Solver definition ###
      ### -----------------###

      Loadstep predictor using line search type secant

        begin adagio solver cg
          Target Relative Residual = 1.0e-4
          Target Residual         = 0.00001
          Maximum Iterations = 25000
#           Minimum Iterations = 1
          Orthogonality measure for reset = 0.2
          Line Search type secant
          iteration print = 50
          nodal preconditioning type = elastic
        end adagio solver cg
#       End adagio multilevel solver MLcontact

        predictor scale factor = 1.0 during p5
        predictor scale factor = 1.0 during p6
        predictor scale factor = 1.0 during p7
        predictor scale factor = 1.0 during p8
        predictor scale factor = 0.0 during p9
        predictor scale factor = 1.0 during p10
        predictor scale factor = 1.0 during p11
        predictor scale factor = 1.0 during p12
        predictor scale factor = 1.0 during p13
        predictor scale factor = 1.0 during p14

    end adagio region adagio
```

```
   end adagio procedure stage2


end sierra nlve axisymmetric joint process
```

9 Appendix B: ADAGIO Input Deck for [30/60/50/10] Ring B Modeled Using Continuum Elements

```
begin sierra ring

  begin definition for function delta
    type is piecewise linear
    abscissa is time
    ordinate is delta
    begin values
      0.0  0.0
      1.0  1.0
    end values
  end definition for function delta

  begin definition for function zero
    type is constant
    begin values
      0.0
    end values
  end definition for function zero

  begin definition for function CTE11
    type is piecewise linear
    ordinate is CTE11
    begin values
      250.0  0.0
      450.0  111.111e-6
    end values
  end definition for function CTE11

  begin definition for function CTE22
    type is piecewise linear
    ordinate is CTE22
    begin values
      250.0  0.0
      450.0  111.111e-6
    end values
  end definition for function CTE22

  begin definition for function CTE33
    type is piecewise linear
    ordinate is CTE33
    begin values
      250.0  0.0
      450.0  333.333e-5
    end values
  end definition for function CTE33

  begin definition for function pressure
    type is piecewise linear
    ordinate is pressure
    abscissa is time
    begin values
      0.0     0.0
      0.0001  0.01
      0.001  1.0
    end values
  end definition for function pressure
```

```
define point pt0 with coordinates 0.0 0.0 0.0
define point ptZ with coordinates 0.0 1.0 0.0
define point ptXZ with coordinates 1.0 0.0 0.0


define coordinate system sysC cylindrical with point pt0 point ptZ point ptXZ


define coordinate system sysR rectangular with point pt0 point ptZ point ptXZ


define direction Axis with vector 0.0 1.0 0.0
define point PointOnAxis with coordinates 0.0 0.0 0.0

begin property specification for material ring1
  density = 0.000140426

  begin parameters for model elastic_3d_orthotropic
    youngs modulus     = 9.28691e6
    shear modulus      = 3.56366e6
    youngs modulus aa = 9.28691e6
    youngs modulus bb = 8.04972e6
    youngs modulus cc = 1.41849e6
    poissons ratio ab = 0.081
    poissons ratio bc = 0.303
    poissons ratio ca = 0.0462805
    shear modulus ab  = 0.645428e6
    shear modulus bc  = 0.645428e6
    shear modulus ca  = 0.645428e6
    coordinate system = sysC
    direction for rotation = 2
    alpha             = 90.0
    second direction for rotation = 3
    second alpha = 120.0
    thermal strain aa function = CTE11
    thermal strain bb function = CTE22
    thermal strain cc function = CTE33
  end parameters for model elastic_3d_orthotropic

  begin parameters for model elastic
     youngs modulus = 9.28691e6
     shear modulus = 3.56366e6
  end parameters for model elastic

end property specification for material ring1



begin property specification for material ring2
  density = 0.000140426

  begin parameters for model elastic_3d_orthotropic
    youngs modulus     = 9.28691e6
    shear modulus      = 3.56366e6
    youngs modulus aa = 9.28691e6
    youngs modulus bb = 8.04972e6
    youngs modulus cc = 1.41849e6
    poissons ratio ab = 0.081
    poissons ratio bc = 0.303
    poissons ratio ca = 0.0462805
    shear modulus ab  = 0.645428e6
    shear modulus bc  = 0.645428e6
    shear modulus ca  = 0.645428e6
    coordinate system = sysC
```

```
        direction for rotation = 2
        alpha             = 90.0
        second direction for rotation = 3
        second alpha = 150.0
        thermal strain aa function = CTE11
        thermal strain bb function = CTE22
        thermal strain cc function = CTE33
      end parameters for model elastic_3d_orthotropic

    begin parameters for model elastic
        youngs modulus = 9.28691e6
        shear modulus = 3.56366e6
      end parameters for model elastic

end property specification for material ring2


begin property specification for material ring3
    density = 0.000140426

    begin parameters for model elastic_3d_orthotropic
        youngs modulus     = 9.28691e6
        shear modulus      = 3.56366e6
        youngs modulus aa = 9.28691e6
        youngs modulus bb = 8.04972e6
        youngs modulus cc = 1.41849e6
        poissons ratio ab = 0.081
        poissons ratio bc = 0.303
        poissons ratio ca = 0.0462805
        shear modulus ab  = 0.645428e6
        shear modulus bc  = 0.645428e6
        shear modulus ca  = 0.645428e6
        coordinate system = sysC
        direction for rotation = 2
        alpha             = 90.0
        second direction for rotation = 3
        second alpha = 140.0
        thermal strain aa function = CTE11
        thermal strain bb function = CTE22
        thermal strain cc function = CTE33
      end parameters for model elastic_3d_orthotropic

    begin parameters for model elastic
        youngs modulus = 9.28691e6
        shear modulus = 3.56366e6
      end parameters for model elastic

end property specification for material ring3


begin property specification for material ring4
    density = 0.000140426

    begin parameters for model elastic_3d_orthotropic
        youngs modulus     = 9.28691e6
        shear modulus      = 3.56366e6
        youngs modulus aa = 9.28691e6
        youngs modulus bb = 8.04972e6
        youngs modulus cc = 1.41849e6
        poissons ratio ab = 0.081
        poissons ratio bc = 0.303
```

```
      poissons ratio ca = 0.0462805
      shear modulus ab  = 0.645428e6
      shear modulus bc  = 0.645428e6
      shear modulus ca  = 0.645428e6
      coordinate system = sysC
      direction for rotation = 2
      alpha             = 90.0
      second direction for rotation = 3
      second alpha = 100.0
      thermal strain aa function = CTE11
      thermal strain bb function = CTE22
      thermal strain cc function = CTE33
    end parameters for model elastic_3d_orthotropic

    begin parameters for model elastic
       youngs modulus = 9.28691e6
       shear modulus = 3.56366e6
    end parameters for model elastic

end property specification for material ring4




begin finite element model mesh1
  Database Name = wedge.g
  Database Type = exodusII

  begin parameters for block block_1
    material ring1
    solid mechanics use model elastic_3d_orthotropic
    hourglass stiffness = 0.05
  end parameters for block block_1

  begin parameters for block block_2
    material ring2
    solid mechanics use model elastic_3d_orthotropic
    hourglass stiffness = 0.05
  end parameters for block block_2

  begin parameters for block block_3
    material ring3
    solid mechanics use model elastic_3d_orthotropic
    hourglass stiffness = 0.05
  end parameters for block block_3

  begin parameters for block block_4
    material ring4
    solid mechanics use model elastic_3d_orthotropic
    hourglass stiffness = 0.05
  end parameters for block block_4

end finite element model mesh1


begin adagio procedure load

  begin time control
    begin time stepping block p1
      start time = 0.0
      begin parameters for adagio region contain_region
```

```
      number of time steps = 10
    end parameters for adagio region contain_region
  end time stepping block p1

  termination time = 1.e-3

end time control

begin adagio region contain_region

  use finite element model mesh1




  begin results output ring_output
    Database Name = wedge.e
    Database Type = exodusII
    nodal variables = displacement as displ
    element variables = rotated_stress as stress
    element variables = cstress as cstress
    element variables = ax
    element variables = ay
    element variables = az
    element variables = bx
    element variables = by
    element variables = bz
    element variables = cx
    element variables = cy
    element variables = cz
  end results output ring_output

  begin user output
    block = block_1 block_2 block_3 block_4
    transform element variable rotated_stress to coordinate system sysC as cstress
  end user output

  begin user variable cstress
   type = element sym_tensor length = 1
   initial value = 0.0 0.0 0.0 0.0 0.0 0.0
  end user variable cstress



  # inside surface: pressure loading
   begin pressure
     surface = surface_100
     function = pressure
   end pressure

  # cyclic symmetry
   begin periodic
     master = nodelist_5
     slave = nodelist_6
     search tolerance = 1.e-6
     reference axis = Axis
     point on axis = PointOnAxis
     theta = 0.5
   end periodic


  Loadstep predictor using line search type secant
```

```
    Begin adagio solver cg
       target relative residual = 1.0e-5
       acceptable relative residual = 5.e-3
       Maximum Iterations = 10000
       Minimum Iterations = 0
       Line Search type secant
       iteration print = 1
       preconditioner = probe
    end   adagio solver cg


  end adagio region contain_region

end adagio procedure load


end sierra ring
```

10 Appendix C: ADAGIO Input Deck for [30/60/50/10] Ring B Modeled Using Shell Elements

```
begin sierra wedge

  begin definition for function delta
    type is piecewise linear
    abscissa is time
    ordinate is delta
    begin values
      0.0  0.0
      1.0  1.0
    end values
  end definition for function delta

  begin definition for function zero
    type is constant
    begin values
      0.0
    end values
  end definition for function zero


  begin definition for function pressure
    type is piecewise linear
    ordinate is pressure
    abscissa is time
    begin values
      0.0     0.0
      0.0001  0.01
      0.001   1.0
    end values
  end definition for function pressure

  begin definition for function fnth11
    type is piecewise linear
    abscissa is temperature
    ordinate is Nth11
    begin values
      300.0  0.0
      400.0  5.2742
    end values
  end definition for function fnth11

  begin definition for function fnth22
    type is piecewise linear
    abscissa is temperature
    ordinate is Nth22
    begin values
      300.0  0.0
      400.0  5.1418
    end values
  end definition for function fnth22

  begin definition for function fnth12
    type is piecewise linear
    abscissa is temperature
    ordinate is Nth12
    begin values
```

```
       300.0   0.0
       400.0   0.264331
    end values
end definition for function fnth12


begin definition for function fmth11
    type is piecewise linear
    abscissa is temperature
    ordinate is Mth11
    begin values
       300.0   0.0
       400.0  -0.000177736
    end values
end definition for function fmth11


begin definition for function fmth22
    type is piecewise linear
    abscissa is temperature
    ordinate is Mth22
    begin values
       300.0   0.0
       400.0 0.000177736
    end values
end definition for function fmth22


begin definition for function fmth12
    type is piecewise linear
    abscissa is temperature
    ordinate is Mth12
    begin values
       300.0   0.0
       400.0 0.000156975
    end values
end definition for function fmth12


define point pt0 with coordinates 0.0 0.0 0.0
define point ptZ with coordinates 0.0 1.0 0.0
define point ptXZ with coordinates 1.0 0.0 0.0


define coordinate system sysC cylindrical with point pt0 point ptZ point ptXZ


define coordinate system sysR rectangular with point pt0 point ptZ point ptXZ


define direction Axis with vector 0.0 1.0 0.0
define point PointOnAxis with coordinates 0.0 0.0 0.0


define direction deg10 with vector 0.984807753 0.0 0.173648177


define direction deg100 with vector -0.173648177 0.0 -0.984807753


begin property specification for material wedge1
  density = 0.000140426

    thermal strain function = zero

    begin parameters for model elastic_laminate
      youngs modulus = 9.28691e6
      shear modulus = 3.56366e6
      a11 =  664.752e2
      a12 =  284.527e2
      a16 =   36.5165e2
```

```
        a22 =  640.923e2
        a26 =   11.0592e2
        a66 =  283.494e2
        a44 =  645.428e1
        a45 =     0.0
        a55 =  645.428e1
        b11 = -20.9654
        b12 =  17.7664
        b16 =   2.18347
        b22 = -14.5674
        b26 =   0.641858
        b66 =  17.7664
        d11 =  619.621e-3
        d12 =  191.989e-3
        d16 =   99.168e-3
        d22 =  558.677e-3
        d26 =  -65.7699e-3
        d66 =  191.128e-3
        coordinate system = sysC
        direction for rotation = 1
        alpha = 0.0
        theta = 0.0
        nth11 function = fnth11
        nth22 function = fnth22
        nth12 function = fnth12
        mth11 function = fmth11
        mth22 function = fmth22
        mth12 function = fmth12
      end parameters for model elastic_laminate


      begin parameters for model elastic
        youngs modulus = 9.28691e6
        shear modulus = 3.56366e6
      end parameters for model elastic

  end property specification for material wedge1

  begin shell section shell_1
     thickness scale factor = 0.01
  end shell section shell_1

  begin finite element model mesh1
    Database Name = wedge.g
    Database Type = exodusII

      begin parameters for block block_1
        material wedge1
        solid mechanics use model elastic_laminate
        section = shell_1
      end parameters for block block_1

  end finite element model mesh1


  begin adagio procedure load

    begin time control
      begin time stepping block p1
        start time = 0.0
        begin parameters for adagio region contain_region
          number of time steps = 10
```

```
      end parameters for adagio region contain_region
    end time stepping block p1


    termination time = 1.e-3


  end time control


  begin adagio region contain_region

    use finite element model mesh1

    begin results output wedge_output
      Database Name = wedge.e
      Database Type = exodusII
      nodal variables = displacement as displ
      element Variables = memb_stress as stress_memb
      element Variables = top_stress as stress_top
      element Variables = bottom_stress as stress_bot
      element Variables = cm_stress
      element Variables = ct_stress
      element Variables = cb_stress
      element Variables = element_thickness as thick
      element Variables = element_area as area
      element Variables = axis1_dir as axis1
      element Variables = axis2_dir as axis2
    end results output wedge_output

    begin user output
      block = block_1
      transform element variable memb_stress to coordinate system sysC as cm_stress
    end user output

    begin user variable cm_stress
     type = element sym_tensor length = 1
     initial value = 0.0 0.0 0.0 0.0 0.0 0.0
    end user variable cm_stress

    begin user output
      block = block_1
      transform element variable top_stress to coordinate system sysC as ct_stress
    end user output

    begin user variable ct_stress
     type = element sym_tensor length = 1
     initial value = 0.0 0.0 0.0 0.0 0.0 0.0
    end user variable ct_stress

    begin user output
      block = block_1
      transform element variable bottom_stress to coordinate system sysC as cb_stress
    end user output

    begin user variable cb_stress
     type = element sym_tensor length = 1
     initial value = 0.0 0.0 0.0 0.0 0.0 0.0
    end user variable cb_stress


    # inside surface: pressure loading
     begin pressure
       surface = surface_100
```

```
      function = pressure
      scale factor = -1.0
    end pressure


    # cyclic symmetry
     begin periodic
       master = nodelist_5
       slave = nodelist_6
       search tolerance = 1.e-6
       reference axis = Axis
       point on axis = PointOnAxis
       theta = 0.5
     end periodic


    Loadstep predictor using line search type secant


    Begin adagio solver cg
      target relative residual = 1.0e-5
      Maximum Iterations = 10000
      Minimum Iterations = 0
      Line Search type secant
      iteration print = 1
      preconditioner = probe
    end   adagio solver cg


  end adagio region contain_region

 end adagio procedure load


end sierra wedge
```

Distribution:

1	0196	Rouse, Jerry, 1524
1	0372	Bishop, Joseph E., 1527
1	0372	Breivik, Nicole L., 1526
1	0372	Dempsey, Frank, 1526
1	0372	Dion, Kristin, 1526
1	0372	Duong, Henry, 1527
1	0372	Gruda, Jeffrey D., 1526
1	0372	Gwinn, Kenneth W., 1526
1	0372	Harding, David, 1526
1	0372	Hinnerichs, Terry D., 1526
1	0372	Holland, John, 1527
1	0372	Jones, Timothy C., 1526
1	0372	Jung, Joseph, 1527
1	0372	Kmetyk, Luba, 1527
1	0372	Longcope, Donald B., 1527
1	0372	May, Rodney A., 1526
1	0372	Metzinger, Kurt E., 1526
1	0372	Neidigk, Matthew, 1526
1	0372	Ostien, Jakob T., 1527
1	0372	Skousen, Troy J., 1527
1	0372	Wellman, Gerald W., 1527
1	0376	Adams, Charlie R., 1525
1	0376	Arguello, J. G. Lupe, 1526
1	0376	Rath, Jonathan S., 1527
1	0376	Stone, C. Mike, 1527
1	0380	Blanford, Mark L., 1542
1	0380	Crane, Nathan K., 1542
1	0380	Gilmartin, William, 1542
1	0380	Gullerud, Arne, 1542
1	0380	Hales, Jason D., 1542

1	0380	Heinstein, Martin W., 1542
1	0380	Key, Samuel W., 1542
1	0380	Koteras, J. Richard, 1542
1	0380	Perschbacher, Brent, 1542
1	0380	Pierson, Kendall H., 1542
1	0380	Porter, Vicki, 1542
1	0380	Reese, Garth M., 1542
1	0380	Spencer, Benjamin, 1542
1	0380	Walsh, Timothy F., 1542
1	0380	Wilson, Christopher Riley, 1542
1	0553	Bateman, Vesta I., 1526
1	0553	Smallwood, David O., 1524
1	0555	Garrett, Mark S., 1522
1	0555	Nelson, Curtis F., 1524
1	0555	Stasiunas, Eric C., 1524
1	0557	Baca, Thomas J., 1525
1	0557	C de Baca, John, 1527
1	0557	Cap, Jerome S., 1527
1	0557	Carne, Thomas G., 1524
1	0557	Dorrell, Larry, 1525
1	0557	Edwards, Timothy, 1527
1	0557	Epp, David S., 1525
1	0557	Griffith, D. Todd, 1524
1	0557	Martinez, Dominic, 1525
1	0557	Mayes, Randall L., 1525
1	0557	O'Gorman, Christian C., 1525
1	0557	Roberts, Nathaniel D., 1525
1	0557	Simmermacher, Todd W., 1524
1	0615	Roach, Dennis P., 6252
1	0835	Naething, Richard M., 1542
1	0836	Shumacher, Shane C., 1516

1	0847	Bitsie, Fernando, 1524
1	0847	Dohrmann, Clark, 1524
1	0847	Field, Richard V., Jr., 1524
1	0847	Holzmann, Wil A., 1525
1	0847	Miller, A. Keith, 1525
1	0847	Redmond, James M., 1524
1	0847	Rice, Amy E., 1525
1	0847	Segalman, Daniel J., 1524
1	0847	Simmons, Leslie, 1525
1	0847	Starr, Michael J., 1524
1	0847	Tipton, D. Gregory, 1525
1	0847	Walther, Howard P., 1527
1	0847	Wilson, Peter J., 1520
1	0888	Adolf, Douglas B., 1821
1	0888	Clough, Roger L., 1821
1	0893	Chambers, Robert S., 1523
1	0893	Chaplya, Pavel, 1523
1	0893	Cox, James V., 1523
10	0893	Hammerand, Daniel, 1523
1	0893	Lavin, Colby, 1523
1	0893	Lo, David, 1523
1	0893	Neilsen, Mike K., 1523
1	0893	Pott, John, 1523
1	0893	Reedy, E. Dave, 1523
1	0893	Scherzinger, William, 1523
1	0893	File Copy, 1523
1	0902	Allen, Matthew Scott, 1524
1	0902	Fulcher, Clay W. G., 1527
1	1310	Massad, Jordan E., 1524
1	1310	Sumali, Anton, 1524

6	9042	Brown, Arthur A., 8763
1	9042	Chen, Er-Ping, 8770
1	9042	Kwon, Davina M., 8774
1	9042	Ohashi, Yuki, 8774
1	9403	Foulk, James W., 8763
1	9403	Shepodd, Timothy J., 8762
1	0899	Technical Library, 9616
1	9018	Central Technical Files, 8945-1